MECHANISTIC STUDIES OF THE E3 UBIQUITIN LIGASES SCF^{Fbx4} AND PARKIN

by

JUNGLIM LEE

B.S. / M.S., University of Arizona at Tucson, 2008

A thesis submitted to the

Faculty of the Graduate School of the

University of Colorado in partial fulfillment

of the requirements for the degree of

Doctor of Philosophy

Department of Chemistry and Biochemistry

2014

This thesis entitled:
Mechanistic Studies of the E3 Ubiquitin Ligases SCF^{Fbx4} and Parkin
written by Junglim Lee
has been approved for the Department of Chemistry and Biochemistry

_____
Prof. Xuedong Liu

_____
Prof. Hang Yin

Date_____

The final copy of this thesis has been examined by the signatories, and we find that both the content and the form meet acceptable presentation standards of scholarly work in the above mentioned discipline.

Lee, Junglim (Ph.D., Biochemistry)

Mechanistic Studies of the E3 Ubiquitin Ligases SCF^{Fbx4} and Parkin

Thesis directed by Professor Xuedong Liu

The ubiquitination pathway is linked to a growing number of diseases including cancer and Parkinson's disease. Previously, the absence of robust functional assays had posed challenges in exploiting E3 ligases as therapeutic targets. The aim of this study was to use *in vitro* reconstituted ubiquitination systems to explore the therapeutic potential of targeting E3 ligases, in addition to gaining insight into how E3 ligases are regulated.

Telomerase activation is a rate-limiting step in carcinogenesis. However, attempts to target telomerase have been mostly unsuccessful. Thus, we targeted TRF1 - a protein that represses telomere elongation by preventing telomerase from accessing the telomeres. In Chapter 2, a reconstituted *in vitro* ubiquitination assay involving the E3 ligase SCF^{Fbx4} and its substrate TRF1 was used to develop highly specific peptide inhibitors. In particular, a structure-based computational approach was used to rationally design peptides that can disrupt the E3 ligase (SCF^{Fbx4}) - substrate (TRF1) binding interface and subsequent ubiquitination. Characterization of the inhibitors demonstrates that our sequence-optimization protocol results in an increase in peptide-TRF1 affinity without compromising peptide-protein specificity.

Since it was revealed that Parkin exists in an auto-inhibited conformation, the question of how Parkin becomes activated has been under investigation. In Chapter 4, an *in vitro* ubiquitination assay involving the Parkin E3 ligase and the anti-apoptotic protein Bcl2 has been developed to gain insight into the activation mechanism of Parkin. We have demonstrated that

phosphorylation of Parkin unlocks the auto-inhibited state of the E3 ubiquitin ligase, allowing both self-ubiquitination of Parkin and mono-ubiquitination of its substrate Bcl2.

Acknowledgements

I would like to thank my advisor, Dr. Xuedong Liu, for the years of support and guidance. His optimism and passion for science has encouraged me throughout the years. I am deeply grateful. I thank my committee members Drs. Natalie Ahn, Hang Yin, Johannes Rudolph, and Ding Xue for their support, guidance, and input regarding the direction of my research. I thank Dr. Margaret Asirvatham for teaching support. I would like to express my thanks to my colleagues in the Liu laboratory. In particular, I thank Conggang Zhang - a fellow member of the Liu laboratory. Your work ethic is unparalleled, and you have always been available for whomever needs help. I am deeply appreciative of your support. A special thanks to Dr. Deanne Sammond for scientific guidance. Your kind professionalism is unmatched. I would like to thank Dr. Myeongseon Lee for offering much needed scientific advice. I thank Huan-Wei Tseng, Tianjing Hu, Yinghua Peng, Akiko Tanimoto, Youngshun Huang, Sarah McQuate, and Wei Wang for your friendship. Graduate school wouldn't have been so much fun without you. I would like to thank our undergraduate research assistant Timothy Kopper for his assistance. I thank my parents, Hwajin Lee and Dongho Lee. I thank my sister Ada Younglim Lee. Last but not least, I thank my husband John Y. Kim for always being on my side.

TABLE OF CONTENTS

Chapter 1: Introduction

1.1 Discovery of the Ubiquitin System…….....1

1.2 The Ubiquitination Pathway……2

1.3 Classification of E3 Ubiquitin Ligases……5

1.4 E3 Ubiquitin Ligases from a Clinical Perspective…….…..7

1.5 Research Topics……...8

1.6 References……..10

Chapter 2: TRF1 as a Molecular Target for Cancer Therapeutics: Developing Peptide Inhibitors of TRF1 Proteolysis

2.1 Introduction……12

2.1.1 Telomere Regulation and TRF1…….12

2.1.2 Regulation of TRF1 degradation by the Ubiquitin-Proteasome Pathway……..14

2.1.3 Disrupting Protein-Protein Interactions using Computationally Designed Peptides …….16

2.2 Materials and Methods……...18

2.3 Results……25

2.3.1 Peptide Design and Synthesis……25

2.3.2 IC_{50} Determination of Peptide Inhibitors using *in vitro* Ubiquitination Assay……..30

2.3.3 K_D Determination of Inhibitors using Fluorescence Polarization Assay...33

2.3.4 Inhibitors do not disrupt p27 Ubiquitination……..38

2.4 Discussion……..39

2.5 References……41

Chapter 3: Kinetic Analysis of Parkin Phosphorylation by PINK1

3.1 Introduction……45

3.1.1 Mitochondrial Quality Control and Parkinson's Disease……..45

3.1.2 Clinical Importance of PINK1 and Parkin……46

3.1.3 PINK1-Parkin Pathway promotes Mitophagy……...49

3.2 Materials and Methods……...50

3.3 Results……52

3.3.1 PINK1 phosphorylates Parkin *in vitro*……52

3.3.2 Kinetic Studies of Parkin Phosphorylation by PINK1……...…57

3.4 Discussion……..…62

3.5 References……66

Chapter 4: Phosphorylation causes Allosteric Activation of Parkin

4.1 Introduction……70

4.1.1 Role of Parkin in Parkinson's Disease……...70

4.1.2 Parkin is a RING-between-RING E3 Ligase……71

4.1.3 Interaction Partners of Parkin……....73

4.1.4 Parkin, Bcl2, Mitophagy, and Cellular Autophagy……74

4.2 Materials and Methods……...76

4.3 Results……80

4.3.1 Reconstitution of *in vitro* Ubiquitination Assays using Non-phosphorylated Parkin……...80

4.3.2 Phosphorylation of Parkin results in its Allosteric Activation in *cis*…....86

4.3.3 Phosphorylation of Parkin results in its Allosteric Activation in *trans*….91

4.4 Discussion……93

4.5 References……....95

Chapter 5: Conclusions and Future Directions

5.1 Conclusions and Future Directions……..…101

5.2 References……...105

Appendix: Characterization of Small Molecule Inhibitors that disrupt the Skp2-CKS1 Interaction

A.1 Introduction……..106

A.2 Materials and Methods…….108

A.3 Results……..108

A.4 Discussion……110

A.5 References……....113

Tables

Table 2.1: Analytical ultracentrifugation…….……...29

Table 2.2: Experimental characterization of peptides……..40

Table 3.1: Kinetic parameters for TcPINK1……....64

Table 4.1: List of proteins used in this study……...79

Table A.1: Structure activity relationship of Skp2-Cks1 inhibitors……109

Figures

Figure 1.1: The ubiquitination pathway…….....3

Figure 1.2: Different types of ubiquitination…….....6

Figure 2.1: Structure of the $TRF1_{TRFH}$-$Fbx4_G$ complex…….……..15

Figure 2.2: Peptide inhibitor design…….17

Figure 2.3: Peptide synthesis……...……23

Figure 2.4: Optimizing the anti-TRF1 peptide inhibitor……..……26

Figure 2.5: Peptides inhibit poly-ubiquitination *in vitro*…….……32

Figure 2.6: K_D determination of peptide inhibitors……..34

Figure 2.7: Wild-type and designed peptides do not bind to $TRF1_{TRFH}^{L115R}$ or $TRF1_{TRFH}^{L120R}$ ……...……...35

Figure 2.8: CD Spectroscopy of wild-type and mutant $TRF1_{TRFH}$ proteins……...…37

Figure 2.9: A recombinant assay system was employed to evaluate the specificity of the rationally optimized peptide inhibitors…….38

Figure 3.1: Parkin is phosphorylated by PINK1 at Ser^{65}…….……....48

Figure 3.2: Time course experiment……53

Figure 3.3: Michaelis-Menten kinetics experiment to determine k_{cat} and K_M for substrate ATP…….……54

Figure 3.4: Data analysis……...……..55

Figure 3.5: TcPINK1 phosphorylates wild-type rParkin using ATP as a substrate…...…….56

Figure 3.6: Time course experiment……..……..58

Figure 3.7: Michaelis-Menten kinetics experiment to determine k_{cat} and K_M for substrate wild-type rParkin……..59

Figure 3.8: Data analysis……60

Figure 3.9: TcPINK1 phosphorylates wild-type rParkin using wild-type rParkin as a substrate……...…….61

Figure 4.1: Domain organization of Parkin……72

Figure 4.2: Proteins involved in ubiquitination *in vitro*……..……..81

Figure 4.3: *In vitro* ubiquitination of Bcl2……..…….83

Figure 4.4: Time dependent ubiquitination of Bcl2…….…….…..……..85

Figure 4.5: Time course of auto-ubiquitination of Parkin *in vitro*…..…..……87

Figure 4.6: Time course of auto-ubiquitination of Parkin *in vitro*…..…..……88

Figure 4.7: UbcH7~Ub thioester discharge assays…….…..……..……..90

Figure 4.8: *In vitro* ubiquitination of Bcl2 using phosphorylated Parkin species…..……..92

Figure A.1: AlphaScreen assay to detect Skp2-Cks1 interactions…….…...…….107

Figure A.2: Counterscreen of hits identified by the primary screen……..…….112

CHAPTER 1

INTRODUCTION

1.1 Discovery of the ubiquitin system

It was suggested as early as 1953 that intracellular protein degradation requires intracellular energy (Simpson 1953). In 1971, tyrosine aminotransferase was proposed to be degraded in an ATP-dependent manner (Hershko and Tomkins 1971). In 1975, Goldstein and colleagues isolated a 8.5 kilodalton "polypeptide" from bovine thymus that induced T and B lymphocyte differentiation *in vitro*, and generated an antibody against it (Goldstein et al. 1975). They noted that the polypeptide was detected in a variety of tissues in various organisms. The following was their conclusion. "That UBIP should have been so rigorously conserved throughout this immense evolutionary timespan suggests a function vital to the living organism" (Goldstein et al. 1975). In 1977, a Y-shaped DNA-associated protein with one C-terminus but two N-termini was discovered by Goldknopf and Busch (Goldknopf and Busch 1977). The short arm of the branched structure was soon identified as ubiquitin (Hunt and Dayhoff 1977). This protein was identical to the polypeptide described by Goldstein and colleagues. A cell-free, ATP-dependent protein degradation system using rabbit reticulolysates that functioned optimally at pH 7.8 was developed in the same year (Etlinger and Goldberg 1977). In 1978, Ciechanover, Hershko, and colleagues discovered that covalent conjugation of ubiquitin preceded the degradation of the protein that they were monitoring (Ciechanover et al. 1978). A highly complex, temporally controlled, and tightly regulated ATP dependent process known as the ubiquitination pathway was characterized in the following years (Glickman and Ciechanover 2002).

1.2 The ubiquitination pathway

The ubiquitination pathway is characterized by the covalent attachment of a small 76 amino acid protein, ubiquitin, to one or more lysine side chains of a generally larger target protein. Ubiquitin is a highly conserved protein that is only found in eukaryotic organisms. However, the protein is ubiquitous in the case of eukaryotes. It is found in the cytosol and nucleus of nearly all eukaryotic cells. Proteins targeted by the ubiquitin-proteasome system are often mis-folded. However, intact proteins can also be regulated via the ubiquitin-proteasome pathway. For a given protein, proper synthesis and degradation rates must be achieved for the cell to carry out its biological functions.

The ubiquitination pathway signals or regulates various eukaryotic proteins – markedly by degradation through the 26S proteasome. In eukaryotes, the vast majority of intracellular proteins are degraded by the ubiquitin proteasome system (Rock et al. 1994). However, it is important to note that post-translational modification of a target protein through attachment of ubiquitin does not always lead to the proteasomal degradation of the target protein. A variety of non-proteolytic processes such as the cell cycle, protein trafficking, endocytosis, autophagy, transcriptional modulation, and DNA repair can also be regulated through ubiquitination (Glickman and Ciechanover 2002; Hershko and Ciechanover 1998; Kirkin et al. 2009; Pickart 1997).

The transfer of ubiquitin to its target substrate is carried out by a sequence of three classes of enzymes – E1 (ubiquitin activating enzyme), E2 (ubiquitin conjugating enzyme), and E3 (ubiquitin ligase) (Pickart 2001). The E1 enzyme activates the C-terminus of the ubiquitin moiety by covalently attaching ubiquitin to its active site cysteine residue. This first step is

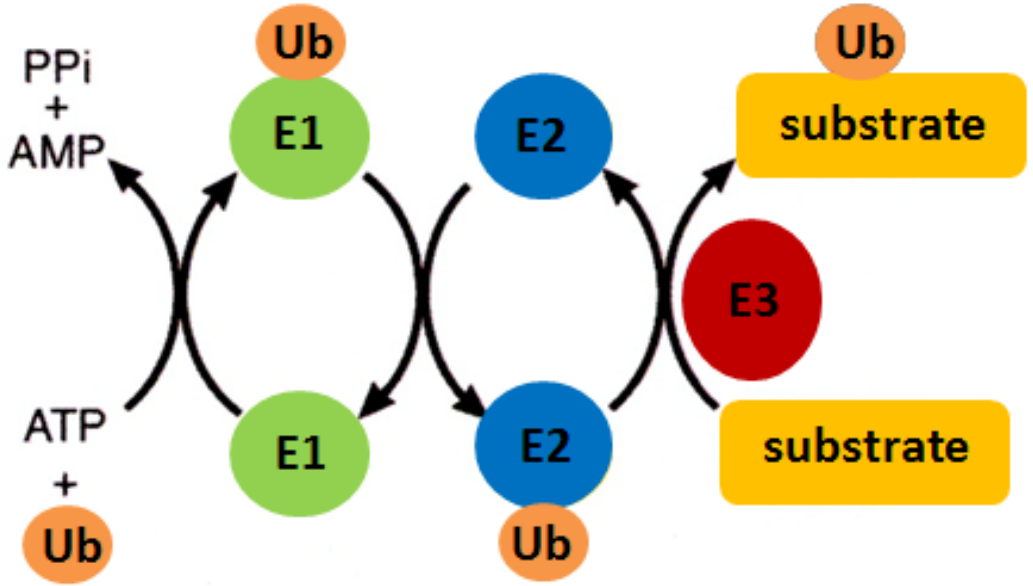

Figure 1.1: The ubiquitination pathway. The ubiquitination cascade consists of a ubiquitin activating enzyme (E1), a ubiquitin conjugating enzyme (E2), and a ubiquitin ligase enzyme (E3).

dependent on ATP hydrolysis. The activated ubiquitin is then transferred to a cysteine residue on the E2 ubiquitin-conjugating enzyme. The third ubiquitination step is carried out by the ubiquitin ligase (E3) that binds to both the charged E2 and substrate. In this final step, ubiquitin is transferred to either a lysine side chain ε-amino group on the substrate, or to the end of a growing polyubiquitin chain. In humans, there are two known E1 enzymes, roughly 60 E2 enzymes, and 600-1000 E3 enzymes (Rape 2009). It is the E3 ubiquitin ligase that determines the specificity of a given ubiquitination process (Dye and Schulman 2007; Kerscher et al. 2006; Pickart and Eddins 2004).

Protein ubiquitination can be induced by a large variety of upstream signaling events. For instance, extracellular ligands can stimulate cell surface receptors to become ubiquitinated (Hicke and Dunn 2003). In the case of many cytosolic and nuclear proteins, although not universally required, post-translational modifications such as phosphorylation may precede ubiquitination (Di Fiore et al. 2003; Muratani and Tansey 2003). Such modifications allow precise spatial and temporal targeting via ubiquitination. Like phosphorylation, ubiquitination is reversible – ubiquitin can be rapidly removed via deubiquitylating enzymes (DUBs) that serve as on/off switches or cause shifting between different modifications on the same lysine residue (Hershko and Ciechanover 1998).

Ubiquitination can occur in three different modes. Substrates can be mono-ubiquitinated by a single ubiquitin molecule. Target substrates can be sequentially ubiquitinated to form polyubiquitin chains – one ubiquitin molecule at a time. Preformed poly-ubiquitin chains can also be transferred to a target substrate. Ubiquitin has seven lysine residues – Lys^{6}, Lys^{11}, Lys^{27}, Lys^{29}, Lys^{33}, Lys^{48}, and Lys^{63}. Poly-ubiquitin chains are formed by creating isopeptide bonds between the preceding ubiquitin lysine residue (ε-aminogroup) and the C-terminal glycine on the

incoming ubiquitin molecule. Ubiquitination can function as a signaling module, where the signal transmitted depends on the characteristics of the modification (mono or poly-ubiquitination) (Di Fiore et al. 2003). To be degraded by the 26S proteasome, a protein must be linked to a chain of four or more ubiquitin moieties. One can argue that the primary difference between ubiquitination and phosphorylation is the structural complexity of the ubiquitin molecule – ubiquitin has a highly complex surface structure that a phosphate group lacks. The fact that ubiquitin can form structurally diverse chains further increases this complexity.

1.3 Classification of E3 ubiquitin ligases

The E3 ubiquitin ligases are a large and diverse group of enzymes (Ardley and Robinson 2005). There are several distinct families of E3 ligases that are each characterized by a defining motif (Deshaies and Joazeiro 2009). The RING (really interesting new gene), U-box (a variation of the RING motif that lacks the zinc-chelating cysteine and histidine residues), HECT (homologous to E6-associated protein C-terminus), and RBR (RING-between-RING) families are among the most well-known. The HECT and RBR E3 ligases have a catalytic cysteine residue that is responsible for the formation of a covalent thioester intermediate. The RING and U-box proteins are thought to function in a scaffold-like fashion, facilitating the transfer of ubiquitin from E2 to target substrate. The RING E3s are the largest class, comprising approximately 90% of known E3 ligases. This family of ligases can be further divided into single subunit E3 ligases and multimeric complexes.

Although some E3 ligases function alone, the vast majority of them form large multi-protein complexes. All in all, it is the E3 ligases that provide the specificity required for

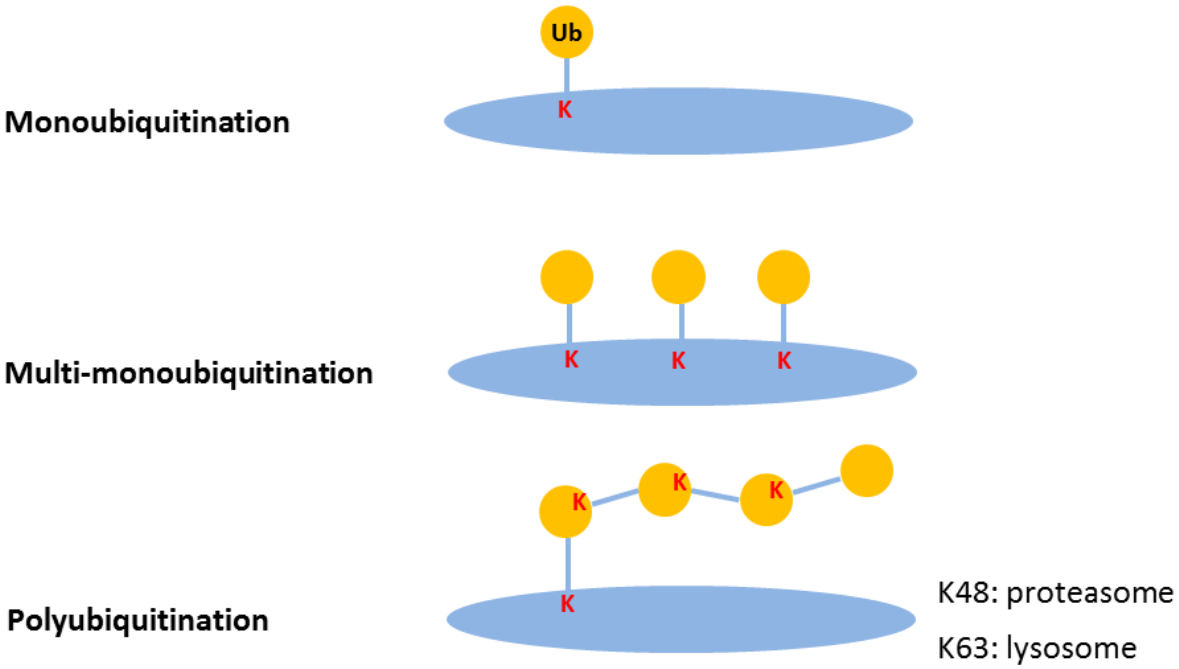

Figure 1.2: Different types of ubiquitination. Attachment of a single ubiquitin molecule to a single lysine residue leads to mono-ubiquitination. Addition of several single ubiquitin molecules to different lysine residues results in multi-mono-ubiquitination. Poly-ubiquitination occurs when a chain of ubiquitin molecules is attached to one or more lysine residues.

the selective post-translational modifications that are required for regulating complex signaling pathways. The significance of E3 ligases is highlighted by their variety, and by the number of biological processes they regulate.

1.4 E3 ubiquitin ligases from a clinical perspective

In the last decade, there has been a surge in interest in the ubiquitination pathway. What was formerly regarded as a simple protein degradation signal has emerged as a regulator of various complex signaling networks. Therefore, it is not surprising that deregulation of ubiquitin signaling systems can be associated with the initiation and progression of many human diseases. In fact, mutations of E1, E2s, E3s, DUBs, ubiquitin, and substrates have all been found in human disorders (Jiang and Beaudet 2004). As mentioned in previous sections, the enzymes of the ubiquitination system are tightly controlled by post-translational modifications or processes such as compartmentalization and oligomerization (Dikic et al. 2003; Thien and Langdon 2001). Due to such precise regulation, proteins involved in the ubiquitination pathway are expected to be among the most promising drug targets.

So far, there has been some success in targeting E1 enzymes. Bortezomib is a proteasome inhibitor used for treating multiple myeloma and mantle-cell lymphoma. Following the success of bortezomib, several other proteasome inhibitors including carfilzomib, Ritonavir, Salinosporamide A, CEP-18770, PR-957 have shown promise (Ruschak et al. 2011). However, the lack of diversity of E1 enzymes may confer a lack of specificity. While E2 enzymes are slightly more diverse than E1 enzymes, they are evolutionarily highly conserved. The structural similarities between the different E2 enzymes would also impose challenges related to selectivity.

Since the specificity of the ubiquitination system primarily resides in the E3 ligases, these least promiscuous enzymes may prove to be the most ideal targets for therapeutic intervention.

As a matter of fact, E3 ubiquitin ligases are linked to a growing number of diseases including neurodegenerative diseases, cancer, diabetes, chronic inflammation, HIV, and muscular diseases. SCF-I2, thalidomide, and lenalidomide are compounds that are known to target this class of enzymes. SCF-I2 is an allosteric inhibitor of substrate recognition that binds to the WD40 domain containing yeast F-box protein Cdc4. Studies have shown that the compound inhibits the ubiquitination of SCF^{Cdc4} substrates. Thalidomide, a drug initially introduced as a sedative, is believed to bind and inactivate the RING finger E3 ligase Cereblon. Cereblon forms an E3 ligase complex with damaged DNA binding protein 1 (DDB1), Cullin-4A (CUL4A), and regulator of cullins 1 (ROC1) (Angers et al. 2006).

Therapeutic agents that target the ubiquitination system may show severe side effects in some cases. The side effects may be due to the inherent complexity of the ubiquitination system. The components required for ubiquitination are diverse and varied, and oftentimes little is known about how the process is regulated. Only further insights to this complicated system will allow us to develop highly specific drugs.

1.5 Research topics

In the past, the lack of robust functional assays had posed challenges in exploiting E3 ubiquitin ligases as therapeutic targets. The focus of this thesis is to use *in vitro* reconstituted ubiquitination systems to explore the therapeutic potential of targeting E3 ligases, in addition to gaining insight into how ubiquitin E3 ligases are regulated. To reconstitute E3 ubiquitin ligase

pathways, recombinant proteins involved in several biologically significant pathways have been expressed and purified.

In Chapter 2, a reconstituted *in vitro* ubiquitination assay involving the E3 ligase SCF^{Fbx4} and the telomere regulating TRF1 protein was used to develop highly specific peptide inhibitors that may potentially target cancer cells. A structure-based computational approach was applied to rationally design peptide inhibitors that disrupt the TRF1 (substrate) - SCF^{Fbx4} (E3 ligase) interface and subsequent ubiquitination.

In Chapter 4, a robust *in vitro* ubiquitination assay involving the Parkin E3 ligase and the anti-apoptotic protein Bcl2 has been developed to gain insight into how post-translational modifications can affect E3 ligase activity. Literature in the field indicates that both Parkin and Bcl2 may be involved in the development of Parkinson's disease.

1.6 References

Angers S., Li T., Yi X., MacCoss M.J., Moon R.T., Zheng N. (2006) Molecular architecture and assembly of the DDB1-CUL4A ubiquitin ligase machinery. Nature ***443***, 590-593.

Ardley H.C., Robinson P.A. (2005) E3 ubiquitin ligases. Essays Biochem. ***41***, 15-30.

Ciehanover A., Hod Y., Hershko A. (1978) A heat-stable polypeptide component of an ATP-dependent proteolytic system from reticulocytes. Biochem. Biophys. Res. Commun. ***81***, 1100-1105.

Deshaies R.J., Joazeiro C.A. (2009) RING domain E3 ubiquitin ligases. Annu. Rev. Biochem. ***78***, 399-434.

Di Fiore P.P., Polo S., Hofmann K. (2003) When ubiquitin meets ubiquitin receptors: a signalling connection. Nat. Rev. Mol. Cell Biol. ***4***, 491-497.

Dikic I., Szymkiewicz I., Soubeyran P. (2003) Cbl signaling networks in the regulation of cell function. Cell Mol. Life Sci. ***60***, 1805–1827.

Dye B.T., Schulman B.A. (2007) Structural mechanisms underlying posttranslational modification by ubiquitin-like proteins. Annu. Rev. Biophys. Biomol. Struct. ***36***, 131-150.

Etlinger J.D., Goldberg A.L. (1977) A soluble ATP-dependent proteolytic system responsible for the degradation of abnormal proteins in reticulocytes. Proc. Natl. Acad. Sci. USA ***74***, 54-58.

Glickman M.H., Ciechanover A. (2002) The ubiquitin-proteasome proteolytic pathway: destruction for the sake of construction. Physiol. Rev. ***82***, 373-428.

Goldknopf I.L., Busch H. (1977) Isopeptide linkage between nonhistone and histone 2A polypeptides of chromosomal conjugate-protein A24. Proc. Natl. Acad. Sci. USA. ***74***, 864-868.

Goldstein G., Scheid M., Hammerling U., Schlesinger D.H., Niall H.D., Boyse E.A. (1975) Isolation of a polypeptide that has lymphocyte-differentiating properties and is probably represented universally in living cells. Proc. Natl. Acad. Sci. USA ***72***, 11-15.

Hershko A., Ciechanover A. (1998) The ubiquitin system. Annu. Rev. Biochem. ***67***, 425-479.

Hershko A., Tomkins G.M. (1971) Studies on the degradation of tyrosine aminotransferase in hepatoma cells in culture. Influence of the composition of the medium and adenosine triphosphate dependence. J. Biol. Chem. ***246***, 710-714.

Hicke L., Dunn R. (2003) Regulation of membrane protein transport by ubiquitin and ubiquitin-binding proteins. Annu. Rev. Cell Dev. Biol. ***19***, 141-172.

Hunt L.T., Dayhoff M.O. (1977) Amino-terminal sequence identity of ubiquitin and the nonhistone component of nuclear protein A24. Biochem. Biophys. Res. Commun. ***74***, 650-655.

Jiang Y.H., Beaudet A.L. (2004) Human disorders of ubiquitination and proteasomal degradation. Curr. Opin. Pediatr. ***16***, 419-426.

Kerscher O., Felberbaum R., Hochstrasser M. (2006) Modification of proteins by ubiquitin and ubiquitin-like proteins. Annu. Rev. Cell Dev. Biol. ***22***, 159-180.
Kirkin V., McEwan D.G., Novak I., Dikic I. (2009) A role for ubiquitin in selective autophagy. Mol. Cell ***34***, 259-269.

Muratani M., Tansey W.P. (2003) How the ubiquitin-proteasome system controls transcription. Nat. Rev. Mol. Cell Biol. ***4***, 192-201.

Pickart C.M. (1997) Targeting of substrates to the 26S proteasome. FASEB J. ***111***, 1055-1066.

Pickart C.M. (2001) Mechanisms underlying ubiquitination. Annu Rev Biochem. ***70***, 503-533.

Pickart C.M., Eddins M.J. (2004) Ubiquitin: structures, functions, mechanisms. Biochim. Biophys. Acta. ***1695***, 55-72.

Rape M. (2009) Ubiquitin, infinitely seductive. Symposium on the many faces of ubiquitin. EMBO Rep. ***10***, 558–562.

Rock K.L., Gramm C., Rothstein L., Clark K., Stein R., Dick L., Hwang D., Goldberg A.L. (1994) Inhibitors of the proteasome block the degradation of most cell proteins and the generation of peptides presented on MHC class I molecules. Cell ***78***, 761-771.

Ruschak A.M., Slassi M., Kay L.E., Schimmer A.D. (2011) Novel proteasome inhibitors to overcome bortezomib resistance. J. Natl. Cancer Inst. ***103***, 1007-1017.

Simpson M.V. (1953) The release of labeled amino acids from the proteins of rat liver slices. J. Biol. Chem. ***201***, 143-154.

Thien C.B., Langdon W.Y. (2001) Cbl: many adaptations to regulate protein tyrosine kinases. Nat. Rev. Mol. Cell Biol. ***2***, 294–307

CHAPTER 2

TRF1 AS A MOLECULAR TARGET FOR CANCER THERAPEUTICS: DEVELOPING PEPTIDE INHIBIHTORS OF TRF1 PROTEOLYSIS

2.1 Introduction

2.1.1 Telomere regulation and TRF1

Telomerase is a reverse transcriptase that maintains telomere length (Feng et al. 1995). However, its activity is suppressed in somatic cells such that telomere attrition triggers replicative senescence or apoptosis (Schmitt 2003). In cancer cells, telomerase is up-regulated or reactivated, effectively making the cell immortal (Kim et al. 1994). Previous studies have shown that telomerase activity positively correlates with unfavorable cancer prognosis (Shay 1998). Since it was discovered that telomerase activation is a rate-limiting step in carcinogenesis, telomerase has gained much interest as a drug target. Both screening and structure-based methods have been extensively employed to identify small-molecule leads that can selectively disrupt telomerase activity. Strategies commonly used to target telomerase activity include targeting the reverse transcriptase subunit of telomerase (BIBR1532 and nucleoside analogues) (Murakami et al. 1999; Pascolo et al. 2002; Strahl and Blackburn 1994), inhibiting hTERT phosphorylation by using inhibitors of protein kinase C (Chang et al. 2006), targeting the RNA component of telomerase (peptide nucleic acids, antisense oligonucleotides—GRN163L) (Djojosubroto et al. 2005; Shammas et al. 1999), stabilizing G-quadruplex structures (Read et al. 2001), and using T-oligos that mimic the end of human telomeres to induce a DNA-damage response (Rankin et al. 2008). Nonetheless, with the exception of GRN163L, which has recently entered phase III clinical trials, attempts at clinically targeting telomerase activity by using classic small-molecule derivatives have largely been unsuccessful.

An alternative strategy is to target the proteins involved in telomere protection and maintenance. Telomeres are coated and maintained by a network of sequence-specific DNA-binding factors that tightly control telomerase activity, including TRF1, TRF2, tankyrases, and TIN2. In particular, TRF1 acts in *cis* at chromosome ends to repress telomere elongation by preventing telomerase from accessing the telomeres (Smogorzewska 2000). Increasing TRF1 levels will cause telomere shortening followed by replicative senescence or apoptosis (van Steensel and de Lange 2000). Previous studies have shown that overexpression of TRF1 results in gradual telomere shortening (Ancelin et al. 2002; Smogorzewska 2000; van Steensel and de Lange 1997), whereas overexpression of dominant-negative mutants leads to telomere elongation in cells (Karlseder et al. 1999; Smogorzewska and de Lange 2002; van Steensel and de Lange 1997).

A variety of factors contribute to telomere-bound TRF1 levels. Currently, two E3 ligases are known to mediate the ubiquitination and degradation of TRF1. The RING H2 zinc finger protein RLIM binds to a site adjacent to the myb domain of TRF1, and localizes to the nucleus upon binding with TRF1 (Her and Chung 2009). Studies have shown that overexpression of RLIM decreases the level of TRF1, and that shRNA knockdown of RLIM increases the level of TRF1 leading to telomere shortening and impaired cell growth (Her and Chung 2009). SCF^{Fbx4}, on the other hand, binds to the TRFH domain of TRF1 through an atypical small GTPase domain and localizes to the cytoplasm upon binding with its substrate (Zeng et al. 2010). Zeng et al. showed that TRF1 has a higher binding affinity to TIN2 than to Fbx4 (Zeng et al. 2010), and crystal structures indicate that the Fbx4–TRF1 binding interface overlaps with the TIN2–TRF1 interface; this might allow TIN2 to sequester TRF1 from Fbx4 *in vivo*. Studies have also shown that nucleostemin (NS) and guanine nucleotide binding protein-like 3 (GNL3L), GTP-binding

proteins that shuttle between the nucleolar–nuclear compartments, bind to TRF1 (Tsai et al. 2009). GNL3L has been shown to stabilize TRF1, whereas NS has been shown to enhance the degradation of TRF1 (Zhu et al. 2006; Zhu et al. 2009). Despite the complexity involved in TRF1 regulation, blocking TRF1 ubiquitination should theoretically lead to increased levels of TRF1, gradual shortening of telomeres, and replicative senescence or apoptosis.

2.1.2 Regulation of TRF1 degradation by the ubiquitin-proteasome pathway

Fbx4 functions as the substrate-specific adaptor subunit of SCF^{Fbx4} that recognizes both TRF1 and cyclin D1 as substrates (Lee et al. 2006). The interaction between TRF1 and Fbx4 was initially discovered from a two-hybrid screen (Zhou and Lu 2001). It was later found that overexpression of Fbx4 reduces endogenous TRF1 levels and causes the telomeres to lengthen progressively (Lee et al. 2006). Inhibition of Fbx4 by RNA interference (RNAi), on the other hand, stabilizes TRF1 and promotes telomere shortening, and this ultimately impairs cell growth (Lee et al. 2006). RNAi studies demonstrated that knockdown expression of Fbx4 stabilizes TRF1 (Zeng et al. 2010; Zhou and Lu 2001). Furthermore, disabling the binding interaction between TRF1 and Fbx4 abrogates TRF1 ubiquitination both *in vitro* and *in vivo* (Zeng et al. 2010).

In this study, we directly targeted the E3 ligase (SCF^{Fbx4})–substrate (TRF1) interface by using computationally enhanced peptide inhibitors derived from the $TRF1_{TRFH}$–$Fbx4_G$ crystal structure (PDB ID: 3L82; Figure 2.1) (Zeng et al. 2010). The approach was based on the hypothesis that TRF1 binding peptides optimized *in silico* will prevent ubiquitination — a critical step in regulating TRF1 levels, which are controlled by sequential post-translational modifications and subsequent degradation. ADP-ribosylation of TRF1 by tankyrase 1 releases

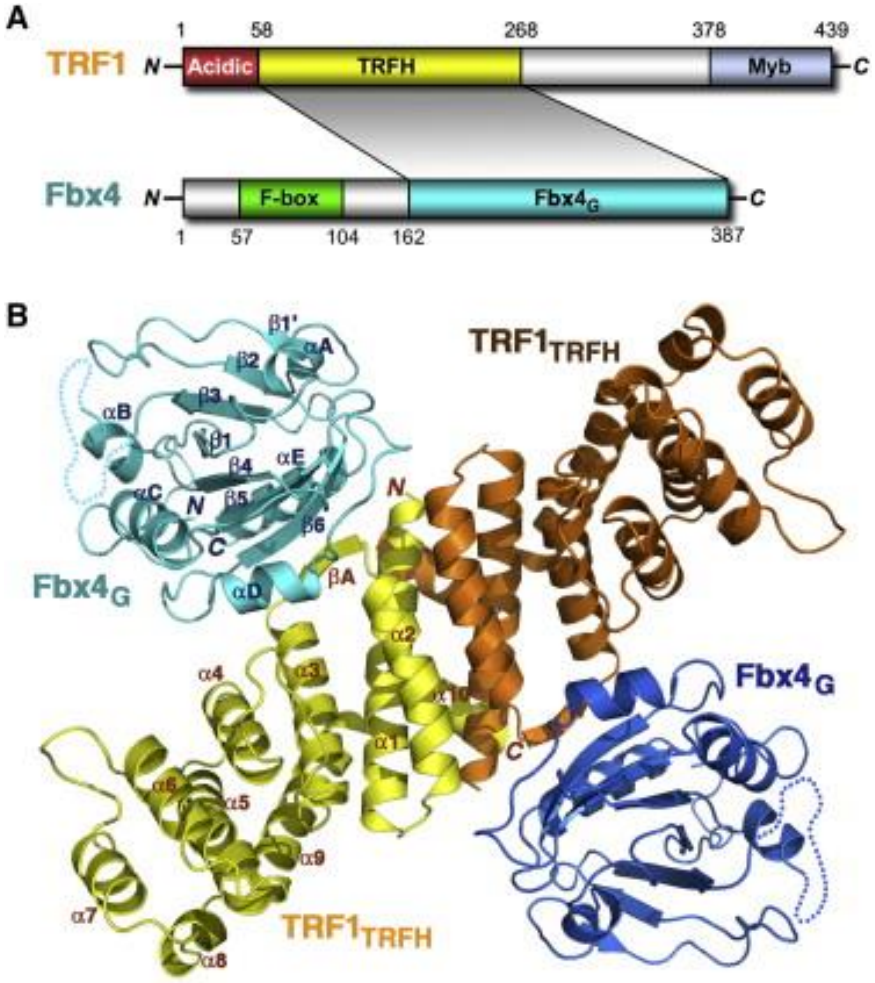

Figure 2.1: Structure of the $TRF1_{TRFH}$-$Fbx4_G$ complex. (A) Schematic representation of TRF1 and Fbx4 polypeptide chains. TRF1-Fbx4 interaction is mediated by $TRF1_{TRFH}$ and $Fbx4_G$ domains. (B) Ribbon diagram of the dimeric $TRF1_{TRFH}$-$Fbx4_G$ complex adapted from Zeng et al. (Zeng et al. 2010).

TRF1 from telomeres, and ubiquitination of TRF1 is achieved through an enzymatic cascade involving a series of cooperative protein–protein interactions (Chang et al. 2003). In principle, each step is susceptible to specific inhibition. In particular, the specificity-conferring nature of E3 ligase–substrate interactions makes them prime candidates as targets for cancer therapy. However, only a few inhibitors that exploit E3 ligase–substrate interfaces are known up to this date - the Nutlins being the most thoroughly characterized among them. In the case of Nutlins, a crystal structure determined by Pavletich et al., prior to the small-molecule screen, revealed a deep hydrophobic pocket located at the interface of MDM2 and p53 (Kussie et al. 2006; Vassilev et al. 2004). Such well-defined cavities have not been documented for RING domain E3s and their substrates, including and Fbx4 and TRF1. In recent years, peptides that disrupt protein–protein interactions have been emerging as modulators of signaling pathways. For instance, both natural and unnatural peptide inhibitors that disrupt the MDM2–p53 interaction were identified (Kritzer et al. 2005; Kritzer et al. 2006; Liu et al. 2010). However, using rationally designed, short peptides that possess a high degree of conformational freedom to target protein–protein interfaces remains a challenge.

2.1.3 Disrupting protein-protein interactions using computationally designed peptides

The 2.4 Å-resolution crystal structure determined by Zeng et al. reveals the molecular basis by which Fbx4 recognizes TRF1 (Zeng et al. 2010). In particular, the αD helix of $Fbx4_G$ reinforces the formation of the $TRF1_{TRFH}$–$Fbx4_G$ complex through extensive van der Waals interactions with $TRF1_{TRFH}$. This short helix packs against a slightly indented hydrophobic area that spans the surface of both molecules. Mutations on both sides of the interface are sufficient to abolish $TRF1_{TRFH}$–$Fbx4_G$ binding *in vitro* and *in vivo* (Zeng et al. 2010), thus suggesting that

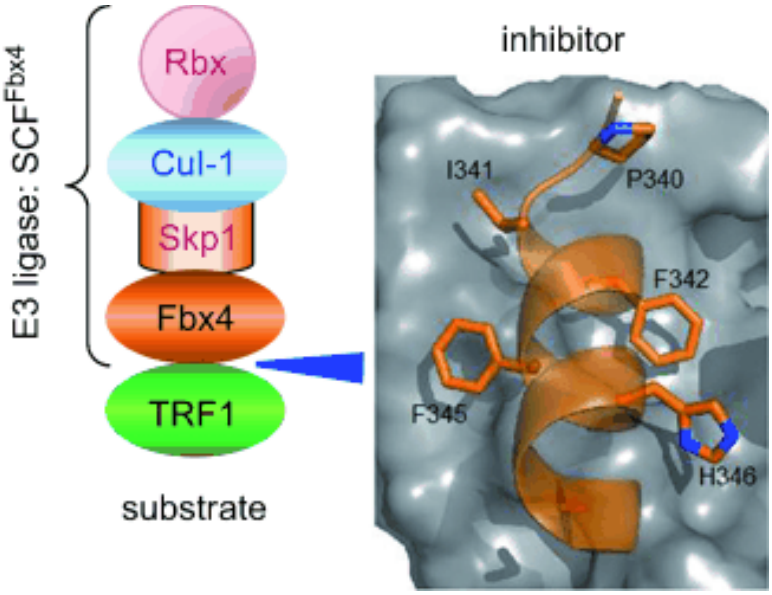

Figure 2.2: Peptide inhibitor design. A structure-based computational approach was used to rationally design peptide inhibitors that can target an E3 ligase (SCF^{Fbx4})–substrate (TRF1) interface and subsequent ubiquitination. Characterization of the inhibitors demonstrates that our sequence-optimization protocol results in an increase in peptide–TRF1 affinity without compromising peptide–protein specificity.

it is possible to target the $TRF1_{TRFH}$–$Fbx4_G$ interface by using peptides. London et al. examined 151 protein–protein structures as starting points for the derivation of high-affinity peptide segments that could be extracted from one binding partner, and used as inhibitors against the wild-type interaction (London et al. 2010). Their results indicate that short linear segments contribute most of the binding energy for more than 50 % of the examined protein–protein interactions. Evaluating the $TRF1_{TRFH}$–$Fbx4_G$ interface shows that the short helical segment of $Fbx4_G$ comprising residues 339–348 contributes more than half (689 $Å^2$) of the total buried surface area at the interface (1371 $Å^2$), and buries numerous hydrophobic residues. Hence, we believed that this segment was likely to provide a good starting point.

2.2 Materials and Methods

Inhibitory peptide design: The backbone coordinates for sequence positions 339 to 347 (MPCFYLAHE) were isolated from F-box-only protein 4 ($Fbx4_G$) in the $TRF1_{TRFH}$–$Fbx4_G$ complex (PDB ID: 3L82) for inhibitor peptide Design 1. The helical region was extended in the C-terminal direction in an effort to stabilize the bound peptide conformation and thus limit the configurational entropy loss. Helix extension was achieved by aligning an α-helix from the $TRF1_{TRFH}$ binding partner with the isolated $Fbx4_G$ helix. As a result, four additional positions were added to the helix, although the three C-terminal positions do not make contact with the target protein, $TRF1_{TRFH}$, in the model structure. The first four N—H groups and the last four C═O groups of an α-helix lack intrahelical hydrogen bond partners, and this potentially destabilizes the helical secondary structure. N- and C-terminal helix-capping motifs have been identified in both proteins and peptides, and are thought to provide a mechanism to stabilize the helical secondary structure (Aurora and Rose 1998). A glycine–threonine–glycine motif was

appended to the C-terminus of the inhibitor peptide design to act as a C-terminal helix cap. Sequence positions that had been buried in the globular Fbx4 structure became solvent exposed in the inhibitor peptide, and thus these positions were redesigned to allow exposure of only polar or charged amino acids. Previous work had shown that increasing the buried hydrophobic surface area could be an effective approach in enhancing protein–protein binding affinity (Sammond et al. 2007). Thus, positions that were buried or peripheral to the interface between the inhibitor peptide and the target protein were redesigned. Three positions from the precursor Fbx4 sequence were retained. The N-terminal position, Pro^{340}, was not altered so as to conserve the ϕ–ψ dihedral angles that might play a role in the interaction between the proline residue and the target protein TRF1. The position Met^{339} was also retained. His^{346} was retained because it forms a hydrogen bond with a target protein tyrosine residue (Tyr^{124}). Sequence design and structural optimization were performed with the molecular modeling program Rosetta (Rohl et al. 2004). A version of the Rosetta energy function with a dampened Lennard–Jones repulsion potential was used (Dantas et al. 2007).

Peptide synthesis: Solid-phase synthesis of peptides was carried out using Fmoc protected amino acids and Rink amide SS resin (200–400 mesh, Nova Biochem) on a CEM Liberty automated microwave peptide synthesizer (CEM Corporation, Matthews, NC). Dried resin was swelled in CH_2Cl_2 (30 min). The Fmoc group was removed by using a solution of 20 % piperidine in dimethylformamide (DMF). The deprotected resin was then suspended in a solution containing Fmoc-protected amino acid (5 equiv), 2-(1*H*-benzotriazole-1-yl)-1,1,3,3-tetramethyluronium hexafluorophosphonate (HATU; 5 equiv), *N*,*N*-diisopropylethylamine (DIPEA; 10 equiv), and DMF (4 mL). Couplings were performed in duplicate. Deprotection and coupling were repeated until all residues were incorporated according to the peptide design.

The fluorophore-labeled peptides were prepared on solid phase by using 7-hydroxycoumarin-3-carboxylic acid (AnaSpec, Inc., Fremont, CA) following the coupling conditions described above. The resulting peptides, with amidated C-termini and free amino N-termini, were cleaved from the resin and side-chain-protecting groups were removed with trifluoroacetic acid/water/ethane-1,2-dithiol/triisopropylsilane (94:2.5: 2.5:1, *v*/*v*/*v*/*v*) at room temperature (2 hours). The crude peptides were collected by precipitation with cold diethyl either (Sigma–Aldrich). The peptides were purified by using a 1200 series semipreparative reversed-phase HPLC system (Agilent) with an Agilent Zorbax 300 SB-C8 column and a linear gradient of buffer A (water/acetonitrile 9:1, *v*/*v*) and buffer B (acetonitrile), followed by lyophilization to dryness. The peptides were characterized by MALDI-TOF spectrometry on a Voyager DE-STR biospectrometry workstation (Applied Biosystems).

Protein expression and purification: For the fluorescence polarization assays, $TRF1_{TRFH}$ (residues 58–268) fused to a SUMO protein and N-terminal His_6 tag was expressed in *E. coli*. After 6 hours of induction with isopropyl-β-D-thiogalactopyranoside (IPTG; 0.1 mM) at 25 °C, the cells were harvested by centrifugation (4000 *g*). The harvested cell pellets were resuspended in lysis buffer (50 mM NaH_2PO_4, pH 8.0, 300 mM NaCl, 10 mM imidazole, 1 mM phenylmethylsulfonyl fluoride (PMSF), 1 mM dithiothreitol (DTT)) and lysed by sonication. The lysates were cleared by ultracentrifugation (200 000 *g*), and the resulting supernatant was incubated with Ni-NTA agarose beads for 1 hour at 4°C. The beads were then washed with imidazole (20 mM) before $TRF1_{TRFH}$ was eluted with imidazole (250 mM). The resulting $TRF1_{TRFH}$ was further purified on a HiLoad Superdex 200 column (GE Healthcare) after the His_6-Sumo tag had been cleaved off by using Ulp1 protease. For the *in vitro* ubiquitination assays, the TRF1 deletion mutant TRF1ΔMyb was expressed in *E. coli* and purified according to

Wild-Type: MPCFYLAHEL

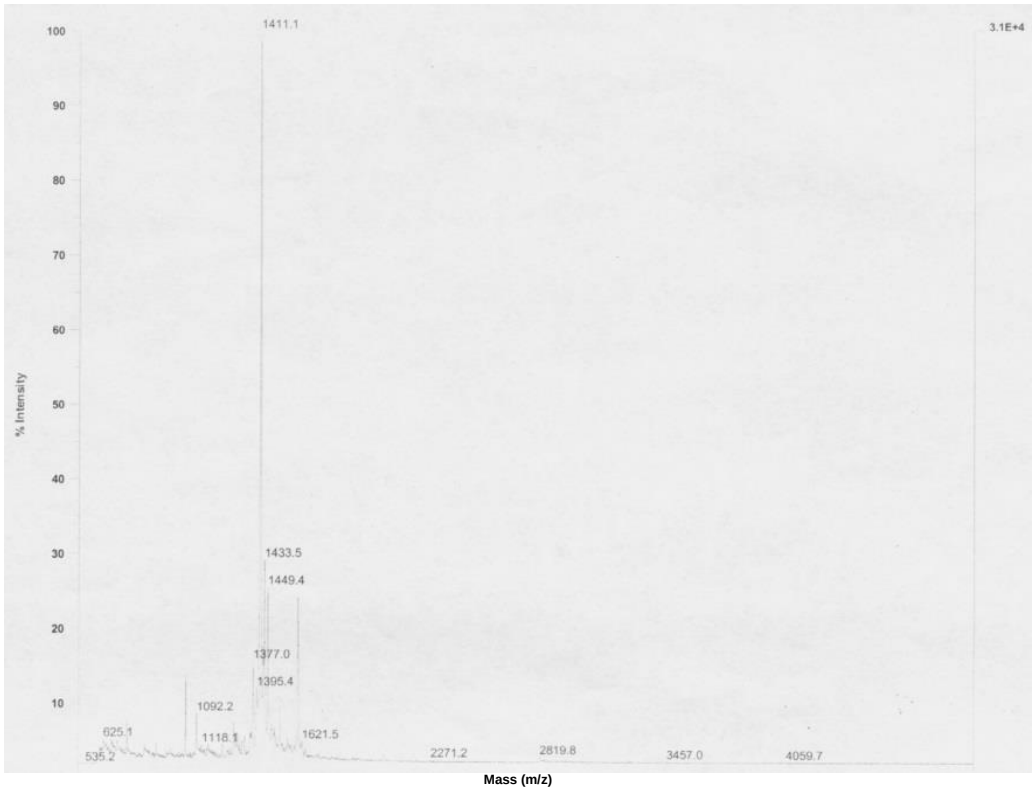

Design 1: MP<u>F</u>WK<u>F</u>HRMSKMGTG

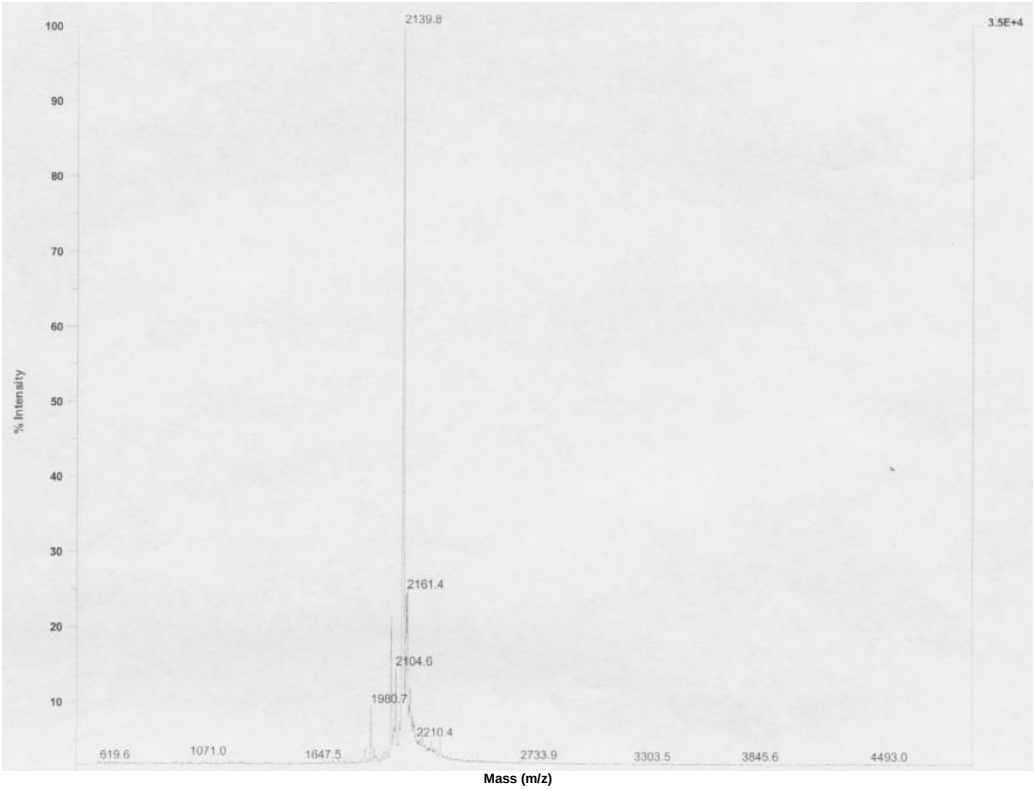

Design 2: MPAWKFHRMSKMGTG

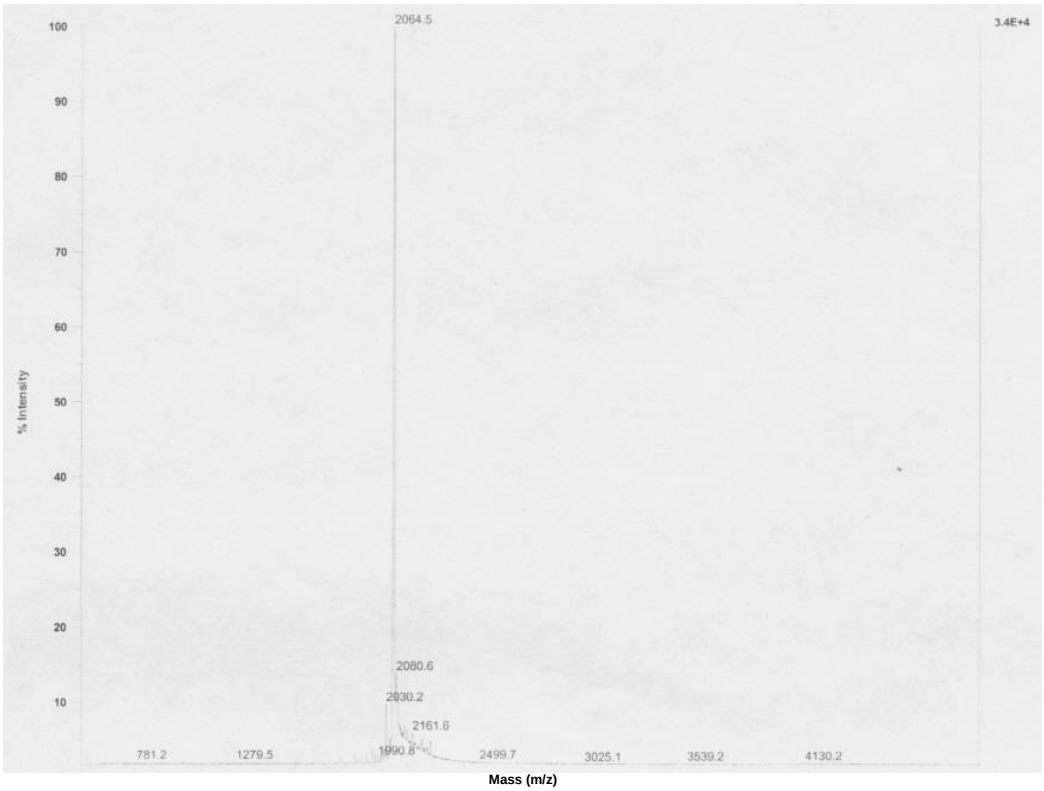

Design 3: MPFWKAHRMSKMGTG

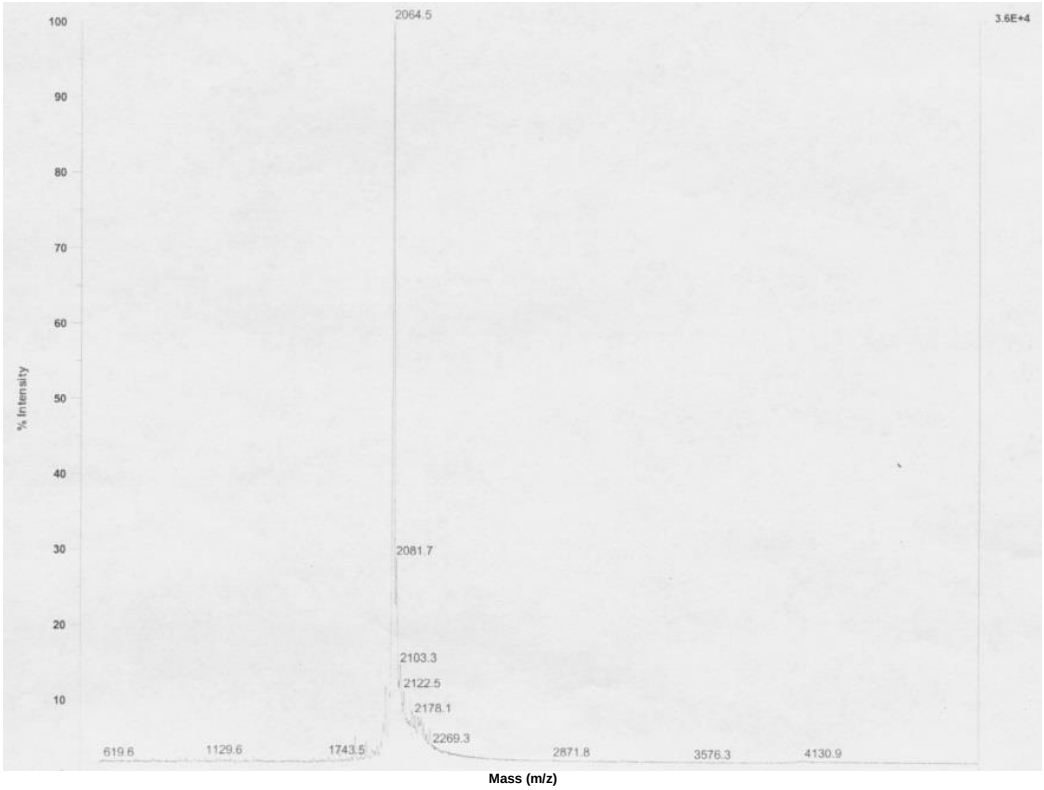

Figure 2.3: Peptide synthesis. Mass spectra of the peptide inhibitors measured by MALDI-TOF-MS. The measured molecular masses corresponding to the m/z signals were 1411.1 Da, 2139.8 Da, 2064.5 Da, and 2064.5 Da, and the theoretical calculated molecular masses were 1411.53 Da, 2142.53 Da, 2066.43 Da, and 2066.43 Da.

the same procedure as for $TRF1_{TRFH}$, with the addition of two affinity purification steps on Mono Q and Mono S ion exchange columns (GE Healthcare). GST-tagged Fbx4 with two deletions (residues 1–54 and 150–170) was coexpressed with truncated Skp1 (Schulman et al. 2000) in *E. coli* as a dicistronic message for 6 hours at 25°C by using IPTG (0.1 mM). The harvested cell pellets were resuspended in NETN buffer (Tris base, pH 7.5, 150 mM NaCl, 1 mM EDTA, 0.5 % NP40, 1 mM DTT). After the cells had been lysed by sonication, the cell debris was removed by ultracentrifugation (200 000 *g*), and the supernatant was mixed with glutathione Sepharose beads (Qiagen) for 1 hour at 4°C before elution with glutathione (20 mM). The complex was then further purified by gel filtration chromatography on the HiLoad Superdex 200 column. E1, UbcH5a (E2), Cul1-Rbx1, and Skp1-Skp2 were expressed and purified as described (Chen et al. 2008; Hao et al. 2005).

Fluorescence polarization assay: Fluorescence-polarization experiments were conducted on a Fluorolog-3 spectrofluorometer (Horiba Jobin Yvon, Inc). Coumarin-labeled peptides were dissolved into buffer (200 mM NaCl, 10 mM DTT, 25 mM Tris, pH 8.0). $TRF1_{TRFH}$ protein (up to 250 μM) was titrated into peptide solutions (100 nM). An excitation wavelength of 302 nm and an emission wavelength of 448 nm were used. Spectra were measured at 25°C by using 7.0 nm slit widths. Curve fitting and regression analysis were performed by using Sigma Plot 10.0 (SPSS Inc.). Data were fit to a quadratic single-site-binding equation (Equation 1), which was incorporated into Equation 2 to account for the observed polarization:

$$[\mathrm{A:B}] = \frac{[\mathrm{A_t}] + [\mathrm{B_t}] + K_\mathrm{D} - \sqrt{([\mathrm{A_t}] + [\mathrm{B_t}] + K_\mathrm{D})^2 - 4[\mathrm{A_t}][\mathrm{B_t}]}}{2} \quad (1)$$

$$P_\mathrm{obs} = \frac{(P_\mathrm{max} - P_\mathrm{o})[\mathrm{A:B}]}{[\mathrm{A_t}]} + P_0 \quad (2)$$

Here, [A:B] is the concentration of coumarin-labeled peptide and the $\mathrm{TRF1_{TRFH}}$ protein complex formed, $[\mathrm{A_t}]$ is the total concentration of coumarin-labeled peptide, $[\mathrm{B_t}]$ is the concentration of $\mathrm{TRF1_{TRFH}}$ protein, P_max is the maximum polarization observed when all coumarin-labeled peptide is bound to $\mathrm{TRF1_{TRFH}}$ protein, and P_obs is the measured polarization at a given concentration of $\mathrm{TRF1_{TRFH}}$ protein. The obtained fitted parameters were for K_D, P_max, and P_o.

***In vitro* TRF1 ubiquitination assay:** [γ-^{33}P]-labeled TRF1 proteins (4 mM) were generated by incubating TRF1 with GST–cyclin B/Cdk1 (0.1 mM) in a buffer composed of Tris (50 mM, pH 8.0), $\mathrm{MgCl_2}$ (10 mM), ATP (10 mM), and [γ-^{33}P]ATP (2 μCi) for 1 hour. GST-cyclin B/Cdk1 was removed from the phosphorylated TRF1 by means of glutathione affinity chromatography. Ubiquitination assays were performed by incubating the phosphorylated TRF1 with E1 (0.5 mM), UbcH5a (E2; 5 mM), $\mathrm{SCF^{Fbx4}}$ complex (E3; 1 mM), ubiquitin (5 mM), methylated ubiquitin (100 mM), and 20X energy regeneration system (1 μL; 10 mM ATP, 20 mM HEPES, pH 7.4, 10 mM MgOAc, 300 mM creatine phosphate, and 0.5 mg $\mathrm{mL^{-1}}$ creatine phosphokinase) in a final volume of 15 μL. The reaction mixtures were incubated at 30°C for 2.5 hours, and the reactions were terminated by boiling after addition of Laemmli sample buffer. The proteins were separated by SDS-PAGE, and the resulting gels were dried prior to phosphoimaging analysis.

CD spectroscopy: Spectra were recorded on a Chirascan-plus CD Spectrometer (Applied Photophysics) by using a protein concentration of 12 μM (0.1 cm path length). Protein

concentrations were determined by UV absorbance at 280 nm. Sixteen scans from 195 to 260 nm were averaged. All spectra were measured at 25.8°C. Results were recorded in millidegrees.

Analytical ultracentrifugation: The hydrodynamic properties of peptide Designs 1–3 were analyzed by analytical ultracentrifugation using sedimentation velocity (55 000 *g*). The experiments were performed in a Beckman XL-I analytical ultracentrifuge (Beckman Coulter, CA) at 25°C. $S_{20,w}$ values and frictional ratios (f/f_0) were determined by using Ultrascan III software with 2D spectrum analysis and a genetic algorithm (Demeler 2005).

***In vitro* p27 ubiquitination assay:** [γ-^{33}P]-labeled p27 proteins were generated by incubating the p27 with GST-cyclin E/Cdk2 (0.1 mM) in a buffer composed of Tris (50 mM, pH 8.0), $MgCl_2$ (10 mM), ATP (10 mM), and [γ-^{33}P]ATP (2 μCi) for 1 hour. The ubiquitination reaction was carried out by incubating the phosphorylated [γ-^{33}P]-labeled p27 with E1 (0.5 mM), Cdc34 (E2; 5 mM), SCF^{Skp2} complex (E3; 1 mM), Cks1 (1 mM), ubiquitin (5 mM), methylated ubiquitin (100 mM), and 20X energy regeneration system (1 μL) for 2 hours in a reaction volume of 15 μL at 30°C. The proteins were analyzed by SDS-PAGE and phosphorimaging.

2.3 Results

2.3.1 Peptide design and synthesis

The short peptide does in fact act as an inhibitor of the wild-type interaction, with a moderate IC_{50} of 205.9 μM (obtained from *in vitro* ubiquitination assays). Fluorescence polarization experiments show that the selected peptide binds to $TRF1_{TRFH}$ with a K_D of 41.8 μM (Table 2.2). Although the initial peptide displays promising results, we sought to enhance its inhibition of the $TRF1_{TRFH}$–$Fbx4_G$ interaction through rational peptide design.

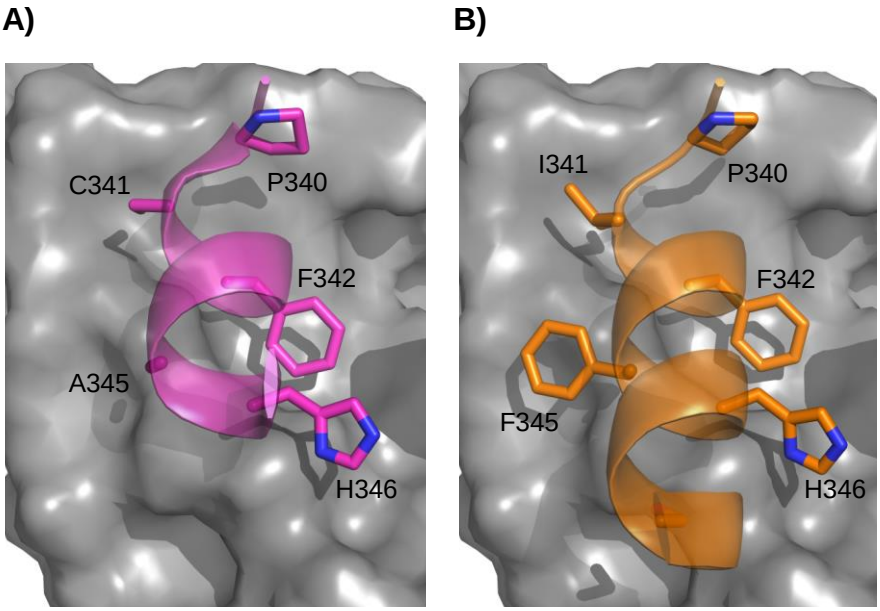

Figure 2.4: Optimizing the anti-TRF1 peptide inhibitor. (A) The peptide segment selected from the Fbx4 structure, shown bound to the TRF1 protein target based on the TRF1-Fbx4 crystal structure (Zeng et al. 2010). (B) Model of the rationally optimized peptide inhibitor. Both the original inhibitor peptide and the rationally optimized inhibitor are shown with the same binding mode as the peptide segment (residues 339-348) cut from the Fbx4 protein. The peptides are shown in cartoon representation with side chains located at key positions of the interface shown and labeled. The target protein, TRF1, is shown in surface representation.

A structure-based design protocol (Fleishman et al 2011; Sammond et al. 2007) using Rosetta (Rohl et al. 2004) was employed to enhance the affinity for TRF1 of a nine-residue linear segment (^{339}MPCFYLAHE^{347}) that spans the length of the αD helix of $Fbx4_G$. Previous work found that protein–protein interactions can be reliably enhanced by increasing the buried hydrophobic surface area at the interface (Sammond et al. 2007). Two candidates for the introduction of larger hydrophobic residues were identified, C341I and A345F. Solubility was a concern when isolating the segment from a larger globular protein. In addition, increasing the hydrophobicity of the extracted peptide in an effort to enhance binding affinity can lead to a further decrease in solubility. Thus, we replaced a solvent-exposed leucine residue with lysine, L344K, and added two hydrophilic residues, Ser^{349} and Lys^{350}, to the C-terminus of the peptide (Design 1, Table 2.2). Finally, we sought to stabilize the short helical peptide by adding a C-terminal capping motif. We anticipated that these affinity-enhancing measures would provide a large contribution to the overall affinity of the peptide–TRF1 complex. In addition, we generated two alanine substitution variants (Designs 2 and 3) to further assess the importance of the two key interface residues (Phe^{342} and Phe^{345}, underlined).

To address the issues of peptide solubility, we performed analytical ultracentrifugation (AUC). Examination of the AUC data shows that Designs 1–3 do not self-associate and are monomers in solution (Table 2.1). However, the data also suggest that Designs 1 and 2 sample multiple conformations (Table 2.1).

Design 1: MPFWKFHRMSKMGTG

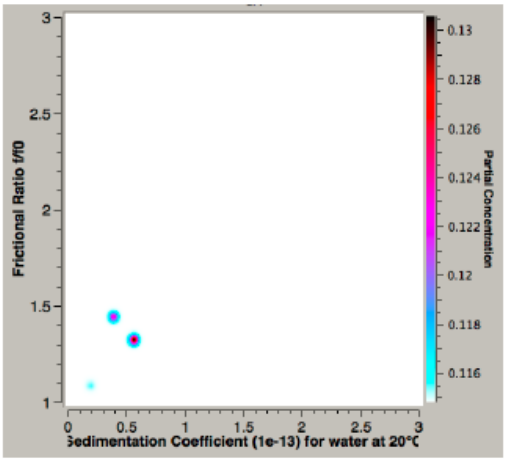

Design 2: MPAWKFHRMSKMGTG

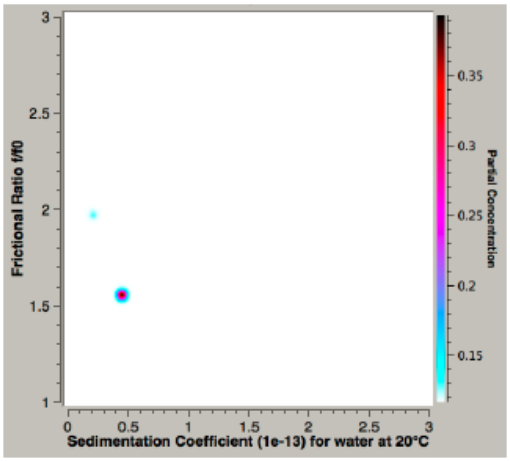

Design 3: MPFWKAHRMSKMGTG

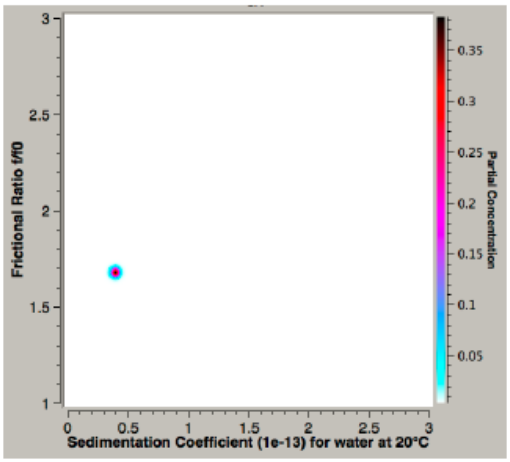

Peptide	$S_{20,w}$ ($10e^{-13}$)	f/f_o	Relative concentration (%)
Design 1	0.17	2.983	20.07
	0.43	1.001	33.13
	0.57	1.285	46.81
Design 2	0.21	1.972	22.90
	0.48	1.557	77.10
Design 3	0.42	1.471	100

Table 2.1: Analytical ultracentrifugation. Graphical representation of species detected by genetic algorithm $S_{20,w}$ and frictional ratios represented in pseudo-3D plots. The hydrodynamic properties of peptides, Design 1, Design 2 and Design 3, were analyzed using analytical ultracentrifugation using sedimentation velocity. $S_{20,w}$ values and frictional ratios (f/f_0) were determined using Ultrascan III software using 2-D spectrum analysis and a genetic algorithm. AUC data suggests that Design 1 samples multiple conformations.

2.3.2 IC_{50} Determination of peptide inhibitors using *in vitro* ubiquitination assay

To examine the biological activity of the peptide designs, we reconstituted Fbx4-dependent TRF1 ubiquitination *in vitro*. Although phosphorylation is not a prerequisite for ubiquitination (Zeng et al. 2010), wild-type TRF1 was first phosphorylated by using cyclin B-Cdk1 in the presence of ^{33}P-γ-ATP to allow quantitative detection. We then incubated TRF1 with recombinant ubiquitin, E1, E2 (UbcH5a), and the SCF^{Fbx4} complex. Increasing amounts of coumarin-labeled peptide inhibitors were added to the reaction mixture, and the relative effectiveness of the peptide inhibitors was determined by measuring the disruption of polyubiquitination, from which the IC_{50} values were generated. The tested peptides showed a range of inhibitory effects from none to more potent. The rationally optimized peptide inhibitor (Design 1) showed enhanced inhibitory activity, with an IC_{50} that is decreased by more than sixfold (31.3 μM), thus showing robust inhibition of polyubiquitination compared to the minimally sized wild-type peptide lacking the modifications (IC_{50}=205.9 μM). Both alanine substitution variants, Designs 2 and 3, lost inhibitory activity compared to Design 1 (IC_{50}=270.6 and 95.8 μM, respectively) in the *in vitro* ubiquitination experiments. In contrast, control peptides 1 and 2 showed little or no inhibitory activity. However, the variation in Hill coefficients suggests that the mechanism of inhibition might be slightly different for each peptide design (Figure 2.5). In summary, although all three peptides derived from the αD helix of Fbx4 showed inhibition in the micromolar range, the inhibitory potency varied, with IC_{50} values ranging from 31.3 to 270.6 μM.

A)

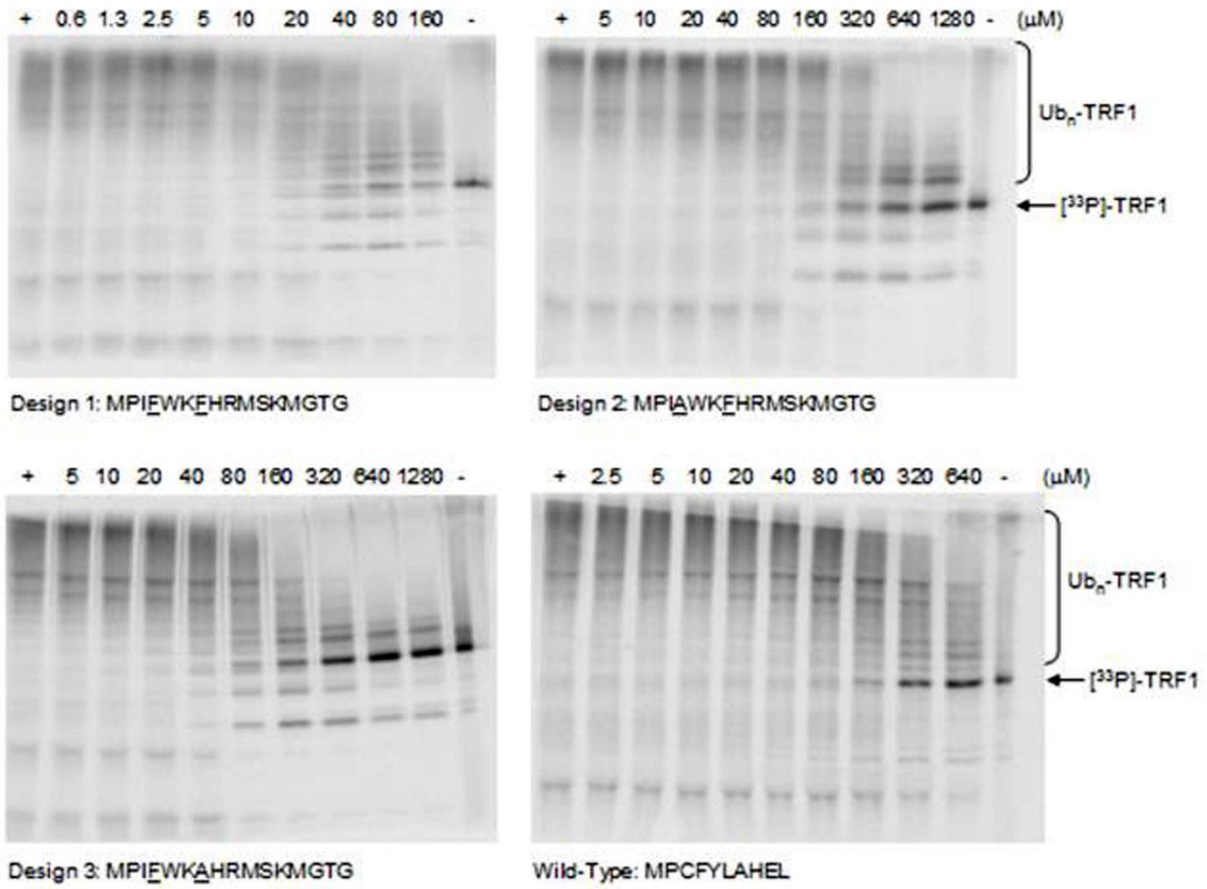
+ 0.6 1.3 2.5 5 10 20 40 80 160 -
+ 5 10 20 40 80 160 320 640 1280 - (μM)
Ub$_n$-TRF1
[^{33}P]-TRF1
Design 1: MPIEWKEHRMSKMGTG
Design 2: MPIAWKEHRMSKMGTG
+ 5 10 20 40 80 160 320 640 1280 -
+ 2.5 5 10 20 40 80 160 320 640 - (μM)
Ub$_n$-TRF1
[^{33}P]-TRF1
Design 3: MPIEWKAHRMSKMGTG
Wild-Type: MPCFYLAHEL

B)

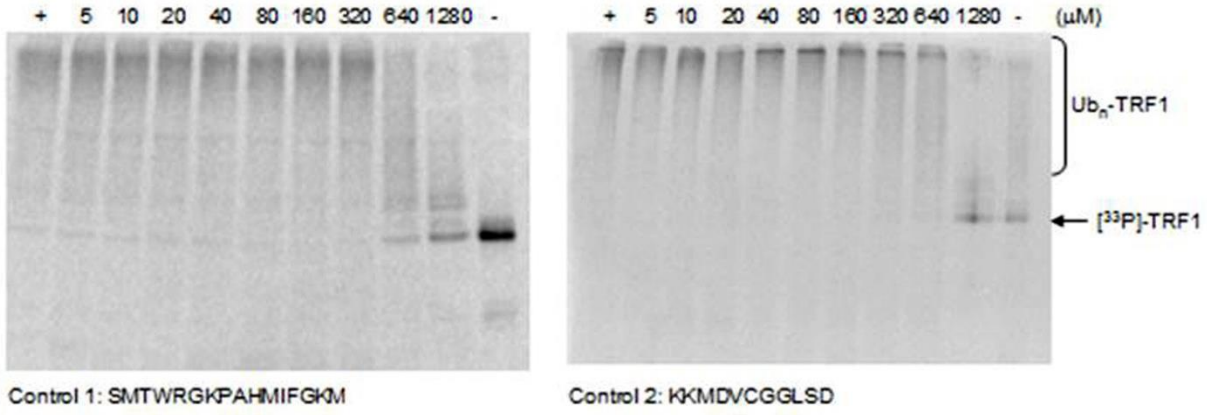
+ 5 10 20 40 80 160 320 640 1280 -
+ 5 10 20 40 80 160 320 640 1280 - (μM)
Ub$_n$-TRF1
[^{33}P]-TRF1
Control 1: SMTWRGKPAHMIFGKM
Control 2: KKMDVCGGLSD

C)

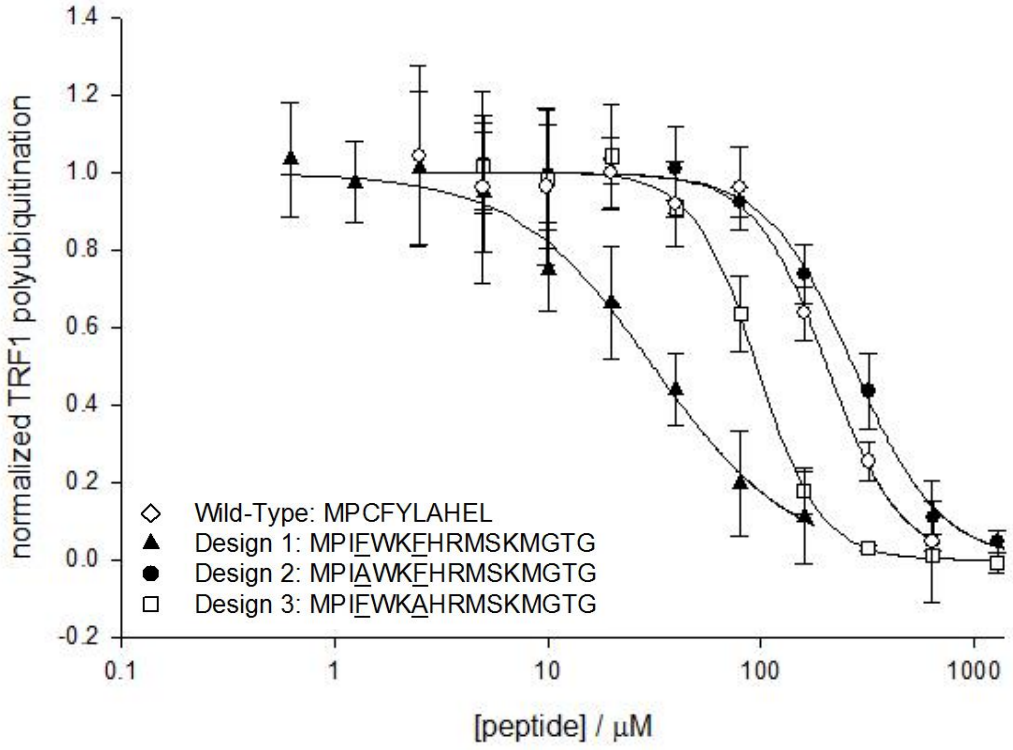

Figure 2.5: Peptides inhibit poly-ubiquitination *in vitro*. (A) Inhibition profiles of computationally enhanced peptide inhibitors. (B) Inhibition profiles of control peptides. (C) Normalized IC_{50} curves that represent the potency of the peptide designs. ImageJ was used to quantify the disruption of poly-ubiquitination. Measurements represent the mean ± standard deviation from three replicates.

2.3.3 K_D determination of inhibitors using fluorescence polarization assay

We then tested our computationally enhanced peptide inhibitor (Design 1) and their alanine variants (Designs 2 and 3) in a fluorescence-polarization binding assay to directly determine their binding affinities to $TRF1_{TRFH}$, and further assess the predicted binding mode. Peptides were labeled with 7-hydroxycoumarin as the fluorophore. Holding the peptide concentration at 0.1 μM, we added increasing concentrations of $TRF1_{TRFH}$ (up to 80 μM), measured the polarization values, and generated equilibrium binding isotherms (Figure 2.6). The dissociation constants (K_D) were determined to be 23.3, 47.8, 17.3, and 41.8 μM for Designs 1–3, and wild-type, respectively (Table 2.2). The increase in binding affinity for the computationally enhanced peptides with respect to wild-type was thus 1.8 or 2.4-fold - only Design 2 showed a slight decrease in affinity. The affinity enhancement for Design 3 suggests that the first phenylalanine residue of Design 1 contributes to binding. The role of the second phenylalanine residue in Design 1 is less clear. The negative controls, by contrast, could not be saturated within the same range of concentrations of $TRF1_{TRFH}$, or even exhibited nonspecific binding. The fluorescence-polarization experiments show that, in general, the designed peptides have lower K_D values than the control peptides; this is consistent with their potency observed in the *in vitro* ubiquitination assays. These results suggest that differences in binding affinity between peptides and $TRF1_{TRFH}$ largely account for the differences in the biological activities of the peptide inhibitors, although there are rare exceptions to this correlation.

It is important to note that the peptide that exhibited the lowest IC_{50} value (Design 1) did not show the highest affinity for $TRF1_{TRFH}$. An increase in binding affinity does not always directly translate into more favorable biological activity. The fact that our binding data do not completely correlate with our *in vitro* ubiquitination results is puzzling at first glance, but if we

consider the muti-step and muti-component nature of the ubiquitination process, this discrepancy might not be so surprising. The ubiquitin proteasome system contains a number of synergistic proteins that can potentially be influenced by distal binding events. Therefore, each component of the ubiquitination cascade can, in theory, be targeted by the peptide inhibitors: The inhibitors might be involved in nonspecific interactions at high micromolar concentrations, as implied by the *in vitro* ubiquitination control experiments (Figure 2.5). Explicitly, the discrepancies

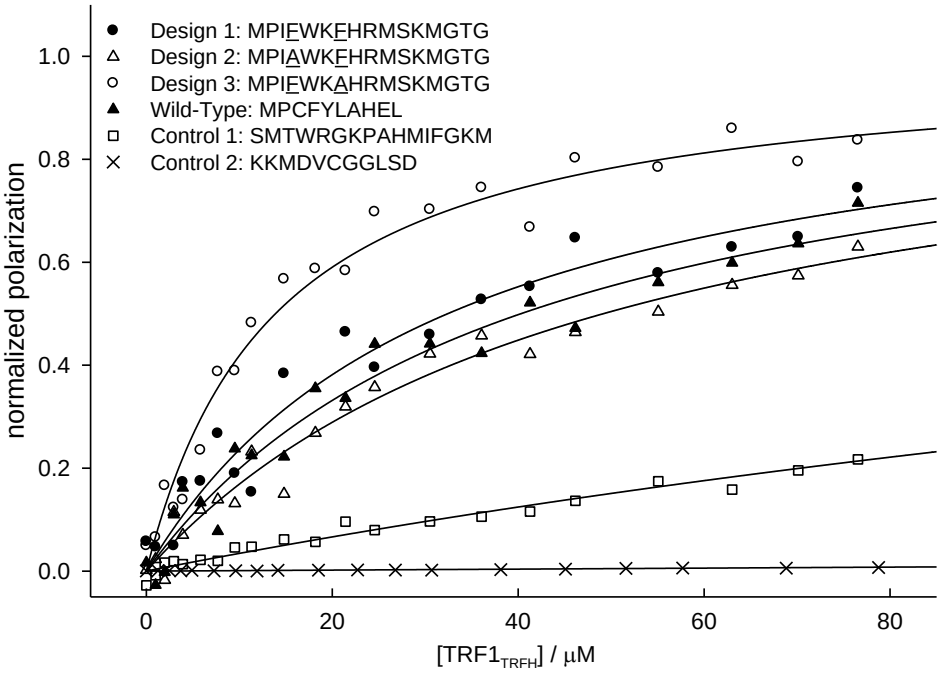

Figure 2.6: K_D determination of peptide inhibitors. Fluorescence polarization confirms that the wild-type and designed peptides bind to $TRF1_{TRFH}$.

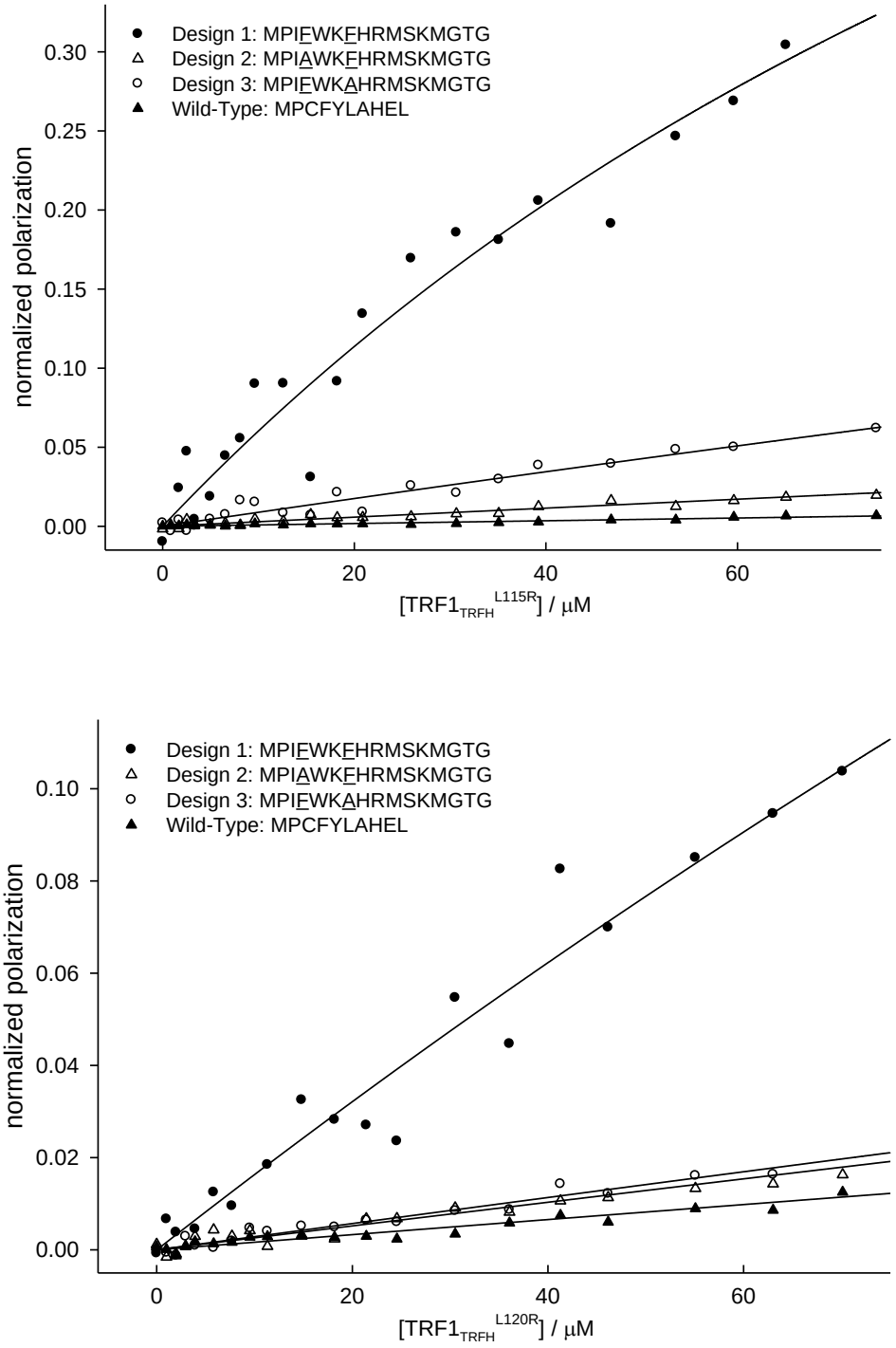

Figure 2.7: Wild-type and designed peptides do not bind to $TRF1_{TRFH}^{L115R}$ or $TRF1_{TRFH}^{L120R}$. Mutation of Leu^{115} or Leu^{120} to arginine abrogates peptide–protein complex formation.

between the IC_{50} values, obtained from *in vitro* ubiquitination experiments in which multiple proteins are present, and the K_D values, with only the target protein and inhibitor peptide present, suggest that nonspecific and competing interactions are taking place with additional protein components. It is important to note that short peptides can adopt a number of conformations; this differs considerably from the behavior of typical globular proteins. The difficulty in predicting and controlling such conformations poses additional challenges in peptide inhibitor design.

To elucidate the mechanism of binding, we examined whether mutating residues located at the interface of $TRF1_{TRFH}$ could weaken or disrupt the peptide–$TRF1_{TRFH}$ interactions. The crystal structure determined by Zeng et al. (Zeng et al. 2010) shows that Leu^{115} and Leu^{120} of $TRF1_{TRFH}$, located at the interface, both directly interact with the αD helix of Fbx4. In fact, these point mutations have been shown to disrupt the interaction of $TRF1_{TRFH}$ with $Fbx4_G$ in both glutathione-S-transferase (GST) pull-down and yeast two-hybrid assays (Zeng et al. 2010). Therefore, we speculated that substituting these residues with positively charged bulkier arginine residues through site-directed mutagenesis would abrogate binding activity between the peptide inhibitor and $TRF1_{TRFH}$. The $TRF1_{TRFH}$ mutants L115R and L120R were expressed and purified, and similar fluorescence-polarization assays were carried out. As speculated, the fluorescence-polarization studies revealed that the mutations impair the interaction between $TRF1_{TRFH}$ and the peptides (Figure 2.7). The combined site-directed mutagenesis and peptide binding experiments suggest that certain hydrophobic interactions between the peptides and TRF1 are necessary for binding. The results of our assays also suggest that peptide–$TRF1_{TRFH}$ binding occurs in a non-promiscuous manner, and that the inhibitors act through a specific mechanism, in good agreement with the computational model.

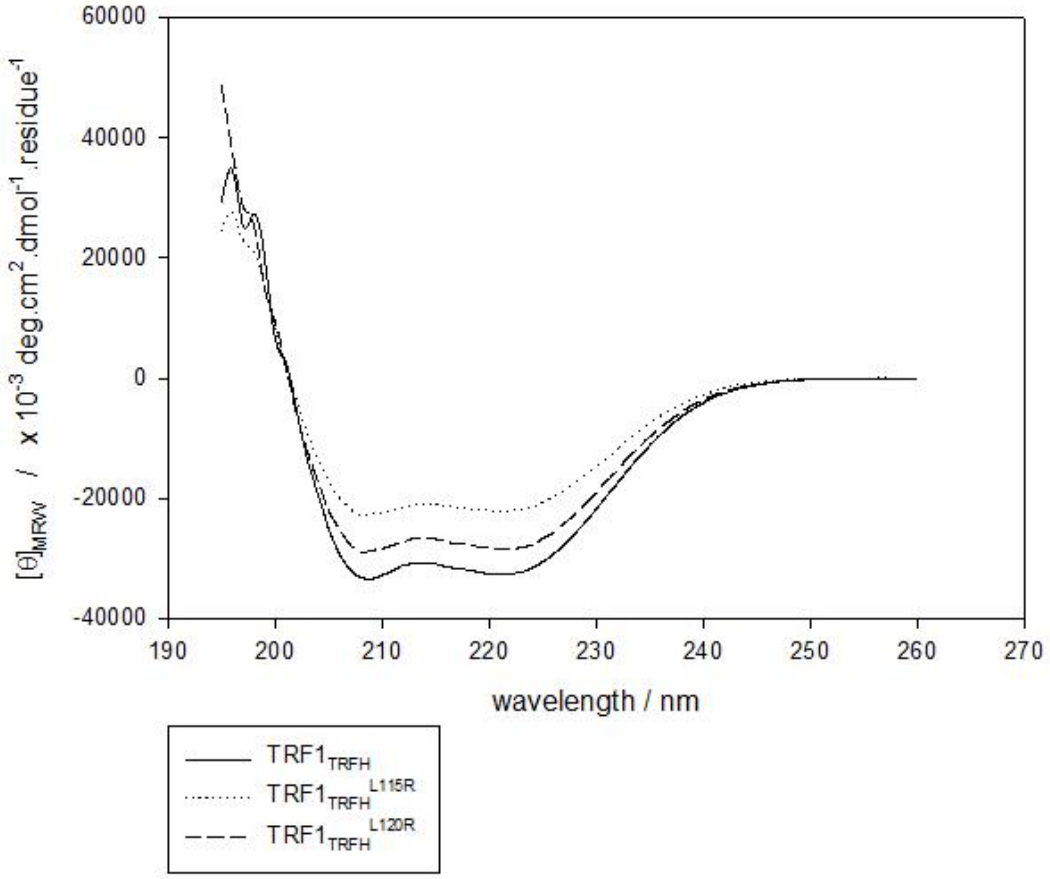

Figure 2.8: CD Spectroscopy of wild-type and mutant $TRF1_{TRFH}$ proteins. Circular dichroism spectra demonstrate the helicity of each protein.

2.3.4 Inhibitors do not disrupt p27 ubiquitination

The specificity of the designed peptides was further evaluated by assessing their effects on p27 ubiquitination. A recombinant assay system containing ubiquitin, E1, E2 (hCdc34), Cks1, p27 phosphorylated by cyclin E-Cdk2, and the SCF^{Skp2} complex was used. The SCF complex of this system is equivalent to SCF^{Fbx4} except for the fact that Fbx4 is switched out for Skp2, which plays the critical role of specifically recognizing its substrate p27. Skp2 and Fbx4, which both belong to the F-box family, share very limited homology (Cenciarelli et al. 1999). Our *in vitro* ubiquitination assays revealed that the computationally enhanced peptide inhibitor has no effect on the ubiquitination of p27 (Figure 2.9).

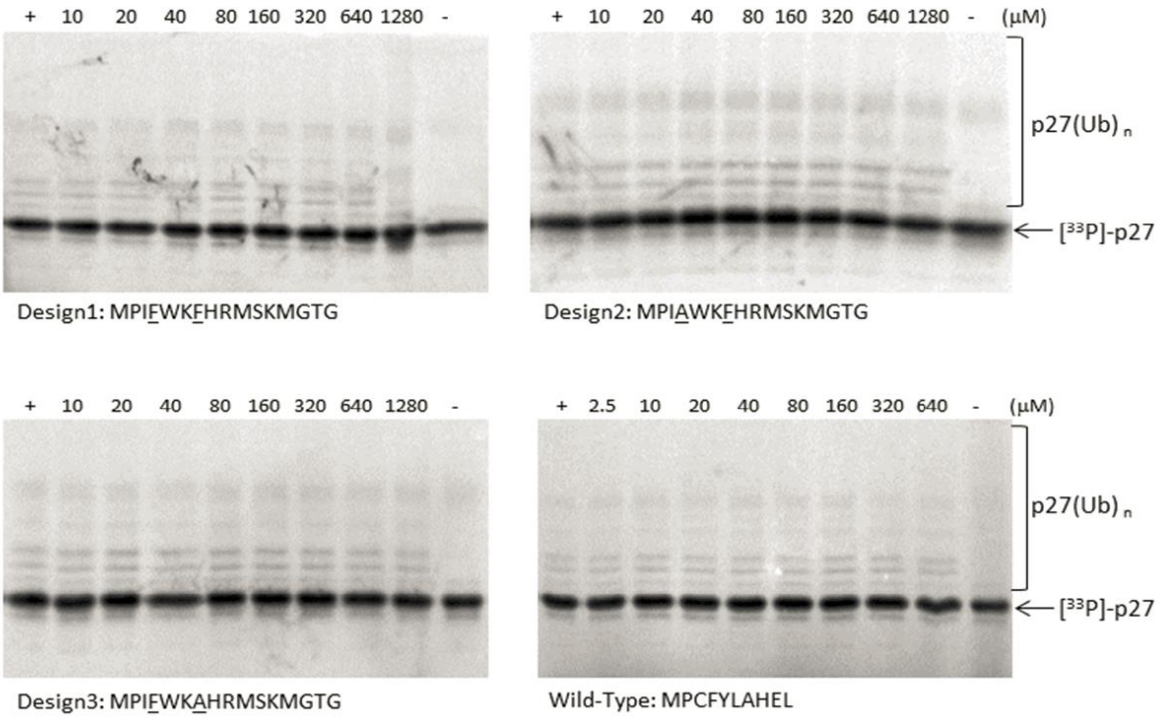

Figure 2.9: A recombinant assay system was employed to evaluate the specificity of the rationally optimized peptide inhibitors. Input p27 was phosphorylated by cyclin E-Cdk2 and was either left untreated or treated with a ubiquitination cocktail containing ubiquitin, E1, E2 (hCdc34), Cks1, and the SCF^{Skp2} complex. The proteins were resolved via SDS-PAGE and p27 was detected by phosphorimaging analysis.

2.4 Discussion

Taken together, the biochemical and biophysical data demonstrate that the computationally designed peptide inhibitors specifically disrupt the $TRF1_{TRFH}$–$Fbx4_G$ interaction. The fact that Fbx4 recognizes both TRF1 and cyclin D1 makes TRF1 a slightly less than ideal target from a clinical standpoint. Both substrates are involved in the regulation of cell growth and proliferation. However, ubiquitination of cyclin D1 requires the presence of the adaptor αB-crystallin and phosphorylation at Thr^{286} (Lin et al. 2006). Ubiquitination of TRF1, on the other hand, does not require an adaptor protein. Neither is phosphorylation of TRF1 necessary for its association with Fbx4. This implies that there could be some structural differences between the TRF–Fbx4 interaction and the Fbx4–αB-crystallin–cyclin D1 interaction. In addition, studies have shown that TIN2 and Fbx4 have overlapping TRF1-binding interfaces (Zeng et al. 2010). This suggests that TIN2 might block TRF1 recognition by Fbx4, thereby preventing SCF^{Fbx4}-mediated ubiquitination and degradation. Recently, it has been shown that telomerase-negative cancer cells are capable of maintaining their telomeres by a mechanism known as alternative lengthening of telomeres (ALT). Evidence also suggests that TRF1 might have a role outside of telomere maintenance (Tsai 2009), and this could lead to further complications. These factors are likely to influence the practicality of targeting TRF1 degradation from a clinical standpoint, but the efficacy of the approach remains to be determined, as it was for the case of the FDA-approved proteasome inhibitor bortezomib (Richardson et al. 2003). It is also important to note that F142, located in the TRFH domain of TRF1, serves as a docking site for the FxLxP-motif-containing proteins TIN2, PINX1, ATM, BLM, and DNA-PKcs, but does not play a significant role in the binding interaction between $TRF1_{TRFH}$ and Fbx4, which lacks the FxLxP motif. This

mechanistic difference in binding could potentially be exploited in enhancing inhibitor specificity.

In summary, our studies have validated the feasibility of designing peptides that selectively disrupt E3 ligase–substrate interactions, in the absence of large binding pockets, by rationally targeting specific regions of the interface. We have also demonstrated the applicability of our *in silico* Rosetta protocol in increasing peptide–protein affinities. Such inhibitors have the potential to be used as drug precursors that can aid the mechanistic studies of disease-related protein–protein interactions.

Peptide	Sequence	IC_{50} [μM][(a)]	K_d [μM][(b)]
Wild-Type	MPCFYLAHEL	205.9 ± 47.7	41.8 ± 2.2
Design 1	MPIFWKFHRMSKMGTG	31.3 ± 10.9	23.3 ± 12.8
Design 2	MPIAWKFHRMSKMGTG	270.6 ± 28.7	47.8 ± 1.8
Design 3	MPIFWKAHRMSKMGTG	95.8 ± 6.6	17.3 ± 4.9
Control 1	SMTWRGKPAHMIFGKM	> 550	> 250
Control 2	KKMDVCGGLSD	> 4000	> 10 000

Table 2.2: Experimental characterization of peptides. (A) IC_{50} values were determined from the *in vitro* ubiquitination assays. (B) Peptide–$TRF1_{TRFH}$ complex K_D values were determined using fluorescence polarization. Data are expressed as mean ± standard deviation. Experiments were performed in triplicates.

2.5 References

Ancelin K., Brunori M., Bauwens S., Koering C.E., Brun C., Ricoul M., Pommier J.P., Sabatier L., Gilson E. (2002) Targeting assay to study the cis functions of human telomeric proteins: evidence for inhibition of telomerase by TRF1 and for activation of telomere degradation by TRF2. Mol. Cell. Biol. ***22***, 3474-3487.

Aurora R., Rose G.D. (1998) Helix capping. Protein Sci. ***7***, 21-38.

Cenciarelli C., Chiaur D.S., Guardavaccaro D., Parks W., Vidal M., Pagano M. (1999) Identification of a family of human F-box proteins. Curr. Biol. ***9***, 1177-1179.

Chang W., Dynek J.N., Smith S. (2003) TRF1 is degraded by ubiquitin-mediated proteolysis after release from telomeres. Genes Dev. ***17***, 1328-1333.

Chang J.T., Lu Y.C., Chen Y.J., Tseng C.P., Chen Y.L., Fang C.W., Cheng A.J. (2006) hTERT phosphorylation by PKC is essential for telomerase holoprotein integrity and enzyme activity in head neck cancer cells. Br. J. Cancer ***94***, 870-878.

Chen Y., Yang Y., van Overbeek M., Donigian J.R., Baciu P., de Lange T., Lei M. (2008) A shared docking motif in TRF1 and TRF2 used for differential recruitment of telomeric proteins. Science ***319***, 1092-1096.

Dantas G., Corrent C., Reichow S.L., Havranek J.J., Eletr Z.M., Isern N.G., Kuhlman B., Varani G., Merritt E.A., Baker D. (2007) High-resolution structural and thermodynamic analysis of extreme stabilization of human procarboxypeptidase by computational protein design. J. Mol. Biol. ***366***, 1209-1221.

Demeler B. (2005) In Analytical Ultracentrifugation: Techniques and Methods (Eds.: D. J. Scott, S. E. Harding, A. J. Rowe), Royal Society of Chemistry, Cambridge, pp. 210–229.

Djojosubroto M.W., Chin A.C., Go N., Schaetzlein S., Manns M.P., Gryaznov S., Harley C.B., Rudolph K.L. (2005) Telomerase antagonists GRN163 and GRN163L inhibit tumor growth and increase chemosensitivity of human hepatoma. Hepatology ***42***, 1127-1136.

Feng J., Funk W.D., Wang S.S., Weinrich S.L., Avilion A.A., Chiu C.P., Adams R.R., Chang E., Allsopp R.C., Yu J. et al. (1995) The RNA component of human telomerase. Science ***269***, 1236-1241.

Fleishman S.J., Whitehead T.A., Ekiert D.C., Dreyfus C., Corn J.E., Strauch E.M., Wilson I.A., Baker D. (2011) Computational design of proteins targeting the conserved stem region of influenza hemagglutinin. Science ***332***, 816-821.

Hao B., Zheng N., Schulman B.A., Wu G., Miller J.J., Pagano M., Pavletich N.P. (2005) Structural basis of the Cks1-dependent recognition of p27Kip1 by the SCF^{Skp2} ubiquitin ligase. Mol. Cell ***20***, 9-19.

Her Y.R., Chung I.K. (2009) Ubiquitin Ligase RLIM Modulates Telomere Length Homeostasis through a Proteolysis of TRF1. J. Biol. Chem. ***284***, 8557-8566.

Karlseder J., Broccoli D., Dai Y., Hardy S., de Lange T. (1999) p53- and ATM-dependent apoptosis induced by telomeres lacking TRF2. Science ***283***, 1321-1325.

Kim N.W., Piatyszek M.A., Prowse K.R., Harley C.B., West M.D., Ho P.L., Coviello G.M., Wright W.E., Weinrich S.L., Shay J.W. (1994) Specific association of human telomerase activity with immortal cells and cancer. Science. ***266***, 2011-2015.

Kritzer J.A., Hodsdon M.E., Schepartz A. (2005) J. Solution Structure of a β-Peptide Ligand for hDM2. Am. Chem. Soc. ***127***, 4118-4119.

Kritzer J.A., Zutshi R., Cheah M., Ran F.A., Webman R., Wongjirad T.M., Schepartz A. (2006) Miniature protein inhibitors of the p53-hDM2 interaction. ChemBioChem ***7***, 29-31.

Kussie P.H., Gorina S., Marechal V., Elenbaas B., Moreau J., Levine A.J., Pavletich N.P. (1996) Structure of the MDM2 oncoprotein bound to the p53 tumor suppressor transactivation domain. Science ***274***, 948-953.

Lee T.H., Perrem K., Harper J.W., Lu K.P., Zhou X.Z. (2006) The F-box protein FBX4 targets PIN2/TRF1 for ubiquitin-mediated degradation and regulates telomere maintenance. J. Biol. Chem. ***281***, 759-768.

Lin D.I., Barbash O., Kumar K.G., Weber J.D., Harper J.W., Klein-Szanto A.J., Rustgi A., Fuchs S.Y., Diehl J.A. (2006) Phosphorylation-dependent ubiquitination of cyclin D1 by the SCFFBX4-aBcrystallin complex. Mol. Cell ***24***, 355-366.

Liu M., Li C., Pazgier M., Li C., Mao Y., Lv Y., Gu B., Wei G., Yuan W., Zhan C., Lu W.Y., Lu W. (2010) D-peptide inhibitors of the p53-MDM2 interaction for targeted molecular therapy of malignant neoplasms. Proc. Natl. Acad. Sci. USA ***107***, 14321-14326.

London N., Raveh B., Movshovitz-Attias D., Schueler-Furman O. (2010) Can self-inhibitory peptides be derived from the interfaces of globular protein-protein interactions? Proteins Struct. Funct. Bioinf. ***78***, 3140-3149.

Murakami J., Nagai N., Shigemasa K., Ohama K. (1999) Inhibition of telomerase activity and cell proliferation by a reverse transcriptase inhibitor in gynaecological cancer cell lines. Eur. J. Cancer ***35***, 1027-1034.

Pascolo E., Wenz C., Lingner J., Hauel N., Priepke H., Kauffmann I., Garin-Chesa P., Rettig W.J., Damm K., Schnapp A. (2002) Mechanism of human telomerase inhibition by BIBR1532, a synthetic, non-nucleosidic drug candidate. J. Biol. Chem. ***277***, 15566-15572.

Rankin A.M., Faller D.V., Spanjaard R.A. (2008) Telomerase inhibitors and 'T-oligo' as cancer therapeutics: contrasting molecular mechanisms of cytotoxicity. Anti-Cancer Drugs 2008, ***19***, 329-338.

Read M., Harrison R.J., Romagnoli B., Tanious F.A, Gowan S.H., Reszka A.P., Wilson W.D., Kelland L.R., Neidle S. (2001) Structure-based design of selective and potent G quadruplex-mediated telomerase inhibitors. Proc. Natl. Acad. Sci. USA ***98***, 4844-4849.

Richardson P.G., Barlogie B., Berenson J., Singhal S., Jagannath S., Irwin D., Rajkumar S.V., Srkalovic G., Alsina M., Alexanian R., Siegel D., Orlowski R.Z., Kuter D., Limentani S.A., Lee S., Hideshima T., Esseltine D.L., Kauffman M., Adams J., Schenkein D.P., Anderson K.C. (2003) A phase 2 study of bortezomib in relapsed, refractory myeloma. N. Engl. J. Med. ***348***, 2609-2617.

Rohl C.A., Strauss C.E., Misura K.M., Baker D. (2004) Protein structure prediction using Rosetta. Methods Enzymol. ***383***, 66-93.

Sammond D.W., Eletr Z.M., Purbeck C., Kimple R.J., Siderovski d.P., Kuhlman B. (2007) Structure-based protocol for identifying mutations that enhance protein-protein binding affinities. J. Mol. Biol. ***371***, 1392-1404.

Schmitt C.A. (2003) Senescence, apoptosis and therapy--cutting the lifelines of cancer. Nat. Rev. Cancer ***3***, 286-295.

Schulman B.A., Carrano A.C., Jeffrey P.D., Bowen Z., Kinnucan E.R., Finnin M.S., Elledge S.J., Harper J.W., Pagano M., Pavletich N.P. (2000) Insights into SCF ubiquitin ligases from the structure of the Skp1-Skp2 complex. Nature ***408***, 381-386.

Shammas M.A., Simmons C.G., Corey D.R., Shmookler Reis R.J. (1999) Telomerase inhibition by peptide nucleic acids reverses 'immortality' of transformed human cells. Oncogene ***18***, 6191-6200.

Shay J.W. (1998) Telomerase in cancer: diagnostic, prognostic and therapeutic implications. Cancer J. Sci. Am. ***4***, S26-S34.

Smogorzewska A., de Lange T. (2002) Different telomere damage signaling pathways in human and mouse cells. EMBO J. ***21***, 4338-4348.

Smogorzewska A., van Steensel B., Bianchi A., Oelmann S., Schaefer M.R., Schnapp G., de Lange T. (2000) Control of human telomere length by TRF1 and TRF2. Mol. Cell. Biol. ***20***, 1659-1668.

van Steensel B., de Lange T. (1997) Control of telomere length by the human telomeric protein TRF1. Nature ***385***, 740-743.

Strahl C., Blackburn E.H. (1994) Effects of reverse transcriptase inhibitors on telomere length and telomerase activity in two immortalized human cell lines. Nucleic Acids Res. ***16***, 53-65.

Tsai R.Y. (2009) Nucleolar modulation of TRF1: a dynamic way to regulate telomere and cell cycle by nucleostemin and GNL3L. Cell Cycle ***8***, 2912-2016.

Vassilev L.T., Vu B.T., Graves B., Carvajal D., Podlaski F., Filipovic Z., Kong N., Kammlott U., Lukacs C., Klein C., Fotouhi N., Liu E.A. (2004) *In vivo* activation of the p53 pathway by small-molecule antagonists of MDM2. Science ***303***, 844-848.

Zeng Z., Wang W., Yang Y., Chen Y., Yang X., Diehl J.A., Liu X., Lei M. (2010) Structural Basis of Selective Ubiquitination of TRF1 by SCF^{Fbx4}. Dev. Cell ***18***, 214-225.

Zhou X.Z., Lu K.P. (2001) The prolyl isomerase PIN1: a pivotal new twist in phosphorylation signalling and disease. Cell ***107***, 347-316.

Zhu Q., Meng L., Hsu J.K., Lin T., Teishima J., Tsai R.Y. (2009) GNL3L stabilizes the TRF1 complex and promotes mitotic transition. J. Cell Biol. ***185***, 827-839.

Zhu Q., Yasumoto H., Tsai R.Y. (2006) Nucleostemin delays cellular senescence and negatively regulates TRF1 protein stability. Mol. Cell. Biol. ***26***, 9279-9290.

CHAPTER 3

KINETIC ANALYSIS OF PARKIN PHOSPHORYLATION BY PINK1

3.1 Introduction

3.1.1 Mitochondrial quality control and Parkinson's disease

Parkinsonism is a common degenerative disorder of the central nervous system that is characterized by progressive motor dysfunction. The disease can either be sporadic or familial. Symptoms of Parkinson's disease include muscle stiffness, tremor at rest, slowness of movement, postural instability, poor balance, and eventual muscle immobility (Jankovic 2008; Fox et al. 2011). Parkinson's disease can also give rise to non-motor symptoms such as cognitive impairments, sensory deficits, and difficulty sleeping (Fox et al. 2011; Jankovic 2008).

A growing body of evidence indicates that mitochondrial dysfunction and oxidative stress are involved in the development of Parkinson's disease. Research using animal models suggests that the physical symptoms of Parkinson's disease may result from a decline in dopamine levels in the brain (Greenamyre and Hastings 2004). Damaged mitochondria can negatively influence dopamine producing neurons, causing a decline in dopamine levels (Schapira et al. 1990; Keeney et al. 2006). In fact, several mitochondrial mutations have been linked to Parkinson's disease (Bonifati et al. 2003; Kitada et al. 1998; Valente et al. 2004).

Mitochondrial dysfunction can be either acquired or hereditary. For instance, mitochondrial mutations can result from exposure to environmental toxins, infectious agents, or drugs. Mitochondrial mutations can also be inherited maternally. To add complexity, genetic components upstream of the mitochondria can also interfere with the molecular mechanisms that regulate its function.

Although there is no cure for Parkinson's disease, clinical treatments focused on improving mitochondrial function are showing signs of promise. For instance, compounds that mimic dopamine have been used to treat Parkinson's disease patients (Rilstone et al. 2013). Levodopa (L-3,4-dihydroxyphenylalanine), also known as $_{L}$-DOPA, is a compound that naturally occurs in the human body. $_{L}$-DOPA crosses the blood–brain barrier to function as a precursor to dopamine, noradrenaline, and epinephrine, and is the most commonly prescribed drug for treating Parkinson's disease. This treatment is usually combined with inhibitors of aromatic-L-amino-acid decarboxylase (DCC), monoamine oxidase B (MAO-B), or catechol-o-methyl transferase (COMT) – drugs that inhibit the breakdown of $_{L}$-DOPA. In the case of patients that do not respond to $_{L}$-DOPA, dopamine agonists such as pramipexole, ropinirole, bromocriptine, and rotigotine are routinely prescribed. Coenzyme Q10, known to boost mitochondrial function, has also shown promise (Shults et al. 2002). However, such treatments do not target the root cause of the disease, but only alleviate symptoms to increase patient life quality. Therefore, it is worthwhile to explore signaling pathways involved in mitochondrial regulation.

3.1.2 Clinical importance of PINK1 and Parkin

Over the last several decades, approximately 20 genes associated with Parkinson's disease have been discovered (Puschmann 2013). Among them is the PTEN (phosphatase and tensin homologue) induced kinase 1 (PINK1) gene, where mutations in the loci are known causes of early-onset Parkinson's disease that is characterized by its recessive hereditary nature (Valente et al. 2004). PINK1 is a 581 amino acid protein that contains an atypical N-terminal mitochondrial localization signal. PINK1 is homologous to serine/threonine kinases.

Overexpression and loss of function studies implicate the PINK1 protein in apoptosis, aberrant mitochondrial fission/fusion dynamics, dopamine release problems, and motor defects (Morais et al. 2009). The protein has also been implied in mitochondrial quality control and electron transport chain function (Dodson and Guo 2007; Schapira, 2008). These findings implicate that mitochondrial integrity may be a factor in PINK1 induced Parkinson's disease.

Mutations in the gene PARK2, which encodes the ubiquitin E3 ligase Parkin, are also linked to early-onset autosomal recessive Parkinson's disease (Kitada et al. 1998). Disease-relevant mutation sites span the entire length of the protein, which indicates the physiological importance of all Parkin domains. In humans, PINK1 and Parkin mutations both give rise to symptoms such as early development of $_{L}$-DOPA induced dyskinesia and dystonia (Khan et al. 2003; Lucking et al. 2000). In *Drosophila melanogaster*, PINK1 knockout flies and Parkin knockout flies both exhibit mitochondrial and neuronal defects - ultimately resulting in motor degeneration (Clark et al. 2006; Park et al. 2006; Yang et al 2006). These findings agree with previous studies that have implicated both PINK1 and Parkin in a common signaling pathway.

Moreover, studies indicate that Parkin is regulated by PINK1 from upstream. Overexpression of Parkin can rescue PINK1 knockout flies. Overexpression of PINK1, on the other hand, cannot rescue Parkin knockout flies. These studies suggest that Parkin functions downstream of PINK1 (Clark et al. 2006; Park et al. 2006; Yang et al 2006). Cellular studies show that PINK1 is required for recruiting Parkin to the mitochondria upon depolarization of the mitochondrial membrane potential (Geisler et al. 2010; Matsuda et al. 2010; Narendra et al. 2010; Vives-Bauza et al. 2010). Recently, it has been shown that PINK1 can phosphorylate Parkin at Ser^{65} (Kazlauskaite et al 2014; Kazlauskaite 2014).

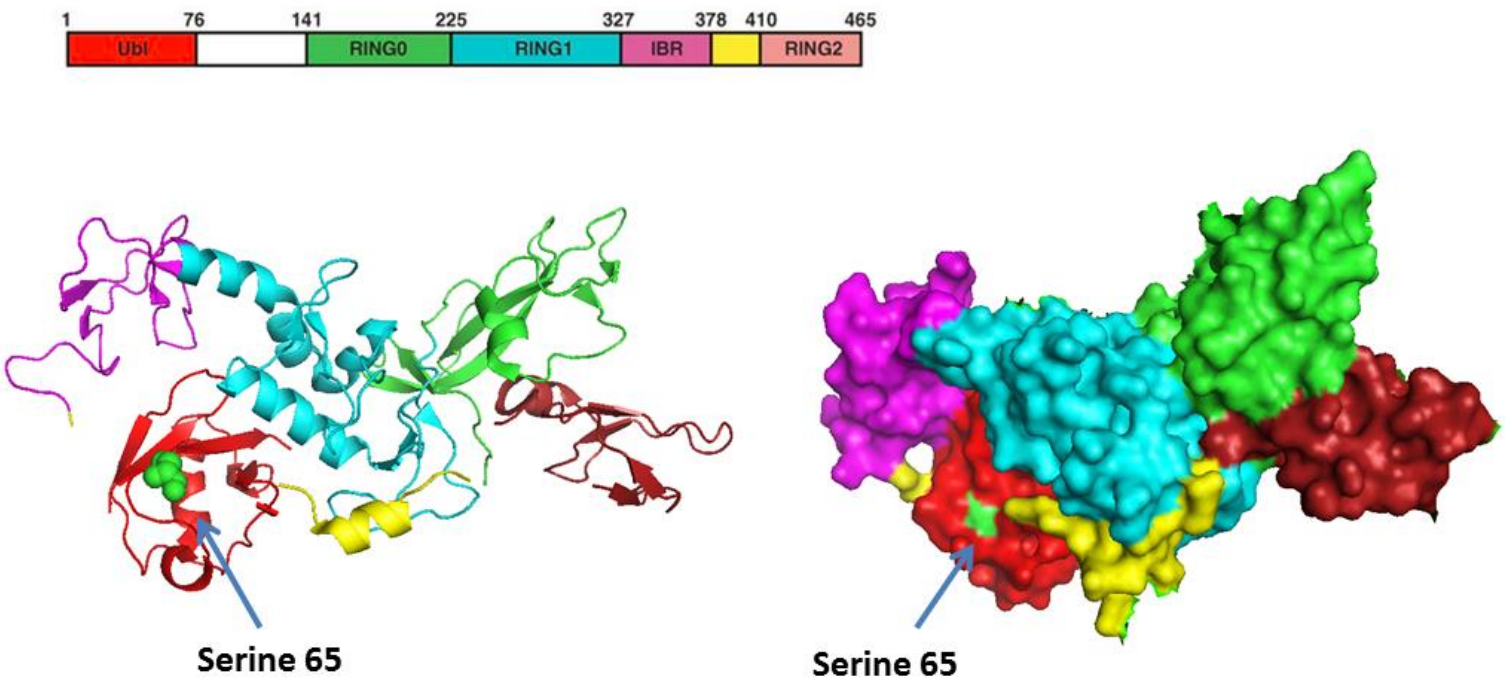

Figure 3.1: Parkin is phosphorylated by PINK1 at Ser^{65}. Pink1 activates Parkin E3 ligase activity by phosphorylating Ser^{65}. Ser^{65} (green) is located in the UBL domain (red) of Parkin.

3.1.3 PINK1-Parkin pathway promotes mitophagy

Mitophagy involves the engulfment of mitochondria by autophagosomes followed by degradation via lysosomes. In 1998, Lemasters et al. found that mitophagy occurs upon loss of mitochondrial membrane potential (Lemasters et al. 1998), suggesting mitophagy as a means of selective removal of defective mitochondria.

Studies indicate that PINK1 and Parkin play a pivotal role in selective autophagy (Geisler et al. 2010; Matsuda et al. 2010; Narendra et al. 2010; Vives-Bauzaet et al. 2010). Under steady-state conditions, PINK1 undergoes rapid constitutive degradation (Matsuda et al. 2010). When mitochondrial depolarization occurs, PINK1 stabilizes and accumulates on the outer membrane of the mitochondria (Matsuda et al. 2010). The accumulated PINK1 then recruits Parkin from the cytoplasm to the mitochondria, which allows Parkin to ubiquitinate proteins located in the outer mitochondrial membrane (Chan et al. 2011; Geisler et al. 2010; Matsuda et al. 2010; Poole et al. 2010; Wang et al. 2011; Ziviani et al. 2010). These series of events may ultimately lead to autophagic degradation of the mitochondria (Matsuda et al. 2010).

In fact, Parkin has been observed to selectively accumulate on damaged mitochondria (Narendra et al. 2008). It has been shown that overexpression of Parkin results in complete removal of mitochondria in cells, by mitophagy, upon mitochondrial depolarization (Narendra et al. 2008). Furthermore, Parkin mutant flies were shown to have a decreased rate of mitochondrial protein turnover, as is seen with drug-induced autophagy (Vincow et al. 2013).

In the case of PINK1, the protein is required for Parkin-mediated mitophagy in cells treated with mitochondrial depolarizing agents (Narendra et al. 2011; Vives-Bauza et al. 2010). These findings further corroborate the relationship between mitophagy, PINK1, and Parkin. Despite confirming that PINK1 phosphorylates Parkin at Ser^{65} (Kondapalli et al 2012;

Kazlauskaite et al. 2014), the catalytic efficiency of this process *in vitro* is not known. In this section, the *in vitro* phosphorylation of Parkin by PINK1 is investigated.

3.2 Materials and Methods

Protein expression and purification: Tc-PINK1 fused to an N-terminal maltoase-binding protein (MBP) was expressed in *E. coli*. For protein expression, *E. coli* cells were grown to an OD_{600} of 0.8 in Luria Broth at 37°C. After reducing the temperature to 16°C, protein expression was induced by addition of isopropyl-β-D-thiogalactopyranoside (IPTG; 0.1 mM). Cells were harvested by centrifugation (4000 *g*) after 16 hours of induction.

For purification of Tc-PINK1, the harvested cells were re-suspended in lysis buffer containing 50 mM Tris-HCl (pH 7.5), 150 mM NaCl, 1 mM DTT, 5% (v/v) glycerol, 1% (v/v) Triton X-100, and 0.1 mM PMSF. Cells were then lysed via sonication. The lysate was then clarified by centrifugation at 12 000 *g* for 30 min. The resulting supernatant was incubated with amylose resin (NEB) for 30 min. Afterwards, the resin was washed 3 times with a wash buffer containing 50 mM Tris-HCl (pH 7.5), 1 M NaCl, 1 mM DTT, 5% (v/v) glycerol, and 1% (v/v) Triton X-100. MBP-TcPINK1 was eluted using an elution buffer containing 40 mM maltose, 50 mM Tris-HCl (pH 7.5), 150 mM NaCl, 1 mM DTT.

Wild-type rParkin fused to an N-terminal GST-tag was expressed in BL21 (DE3) *E. coli* cells. The transformed *E. coli* cells were grown in Luria Broth supplemented with 200 µM zinc chloride at 37°C until reaching an OD_{600} of 0.6. Protein expression was induced by addition of a final concentration of 50 µM IPTG, and the cells were incubated for an additional 16 hours at 16°C before harvesting. The cells were harvested by low-speed centrifugation (4000 *g*, for 20 min), re-suspended in NETN buffer (Tris base, pH 7.5, 150 mM NaCl, 1 mM EDTA, 0.5 %

NP40, 1 mM DTT), and lysed through sonication. The cell debris was removed by centrifugation (15,000 *g*, for 30 min). The resulting supernatant was incubated with glutathione-Sepharose beads (Qiagen) for 30 min, before washing 3 times with NETN buffer. Wild-type rParkin was eluted off the beads using a buffer containing 20 mM glutathione, 25 mM Tris-HCl (pH 8.0), 100 mM NaCl, 0.5 mM DTT. Fractions containing pure protein, as determined by SDS-PAGE and Coomassie Brilliant Blue staining, were combined, dialyzed into a buffer containing 25 mM Tris pH, 8.0 and 100 mM NaCl, and concentrated using Vivaspin 20 concentrators (Sartorius Stedim Biotech). Proteins were stored in 20% glycerol at -80°C.

Kinase assay: For the *in vitro* kinase assays, wild-type rParkin was incubated with Tc-PINK1 in a buffer composed of Tris (50 mM, pH 8.0), $MgCl_2$ (10 mM), ATP, and [γ-^{32}P]-ATP. Reactions were carried out in a volume of 10 µL at 30°C, and stopped by addition of 4× Laemmli sample buffer containing 100 mM EDTA, before heating at 95°C for 7 min. The proteins were separated via 12% SDS-PAGE, and the resulting gels were dried prior to phosphorimaging analysis.

Kinetic studies: Tc-PINK1 concentration was varied from 0.5 nM to 500 nM to confirm that reaction rates scaled linearly. 40 nM PINK1 was used to determine k_{cat} and K_M for ATP. Time course experiments were performed to determine the linear range of the reaction. Time points of 0 min, 5 min, and 10 min were selected to yield linear initial kinase reaction rates. The concentration of ATP was varied from 12.5 µM to 3.2 mM at a constant, saturating concentration of 5 µM wild-type rParkin to determine the steady state rate constants. The velocity at each concentration was determined using (linear) least-squares methods, and the reactions were carried out in triplicates. The velocity data were fit using nonlinear least squares methods to the Michaelis-Menten equation ($V = V_{max}[S]/(K_M+[S])$), where V is the measured reaction velocity, [S] is the ATP concentration, and K_M is the Michaelis constant.

To determine k_{cat} and K_M for rParkin, 40 nM PINK1 was used. Once again, time course experiments were performed to determine the linear range. Time points of 0 min, 5 min, and 10 min were selected to yield linear initial rates. The concentration of wild-type rParkin was varied from 12.5 nM to 3.2 μM at a constant, saturating concentration of 3 mM ATP to determine steady state rate constants k_{cat} and K_M. Once again, the velocity at each concentration was determined using (linear) least-squares methods, and the reactions were performed in triplicates. Data were fit to the Michaelis-Menten equation ($V = V_{max}[S]/(K_M+[S])$), where V is the measured reaction velocity, K_M is the Michaelis constant, and [S] is the wild-type rParkin concentration. Data sets were fit using Sigma Plot 5.0 software (SPSS Inc.). The amounts of phosphorylated wild-type rParkin were determined by densitometry using ImageJ. Calibration curves were obtained to allow quantification. Calibration curves were prepared by spotting known amounts of ATP to filter paper before subjecting it to phosphorimaging analysis.

3.3 Results

3.3.1 PINK1 phosphorylates Parkin *in vitro*

The phosphorylation reaction of human Parkin by human PINK1 has not been reconstituted *in vitro* up to this date. We suspect that the challenge is due to a high degree of protein mis-folding and/or overall protein instability (Beilina et al. 2005). However, it has been determined that TcPINK1 has robust phosphorylation activity against full length wild-type GST-rParkin *in vitro*. When Ser^{65} of Parkin is mutated into an alanine residue, TcPINK1 can no longer phosphorylate Parkin. The kinase-inactive TcPINK1 exhibits no phosphorylation activity (Conggang Zhang; Woodroof et al. 2011; Kondapalli et al. 2014).

A)

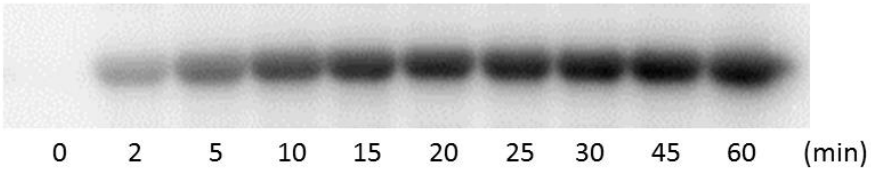

B)

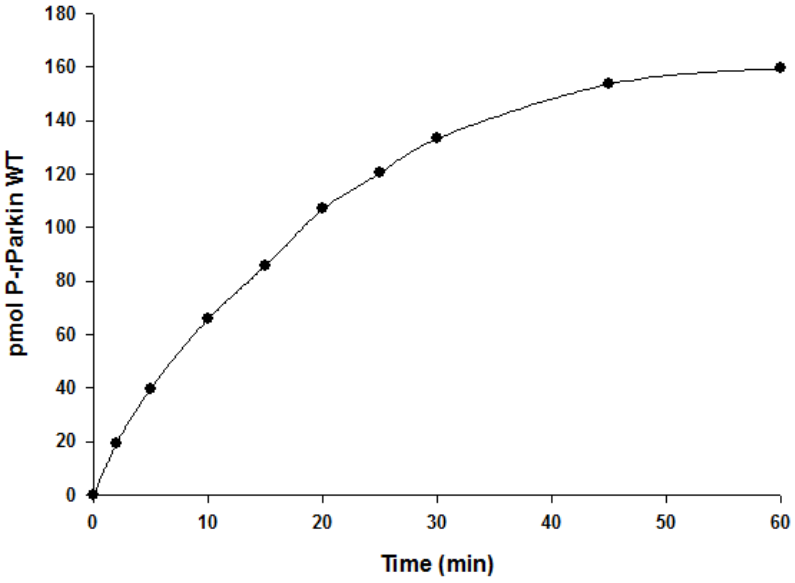

Figure 3.2: Time course experiment. 5 μM wild-type rParkin was phosphorylated in the presence of 25 μM ATP, $MgCl_2$, and 40 nM TcPINK1 for the indicated times in a reaction volume of 10 μL at 30°C. pmol P-rParkin WT was plotted as a function of time.

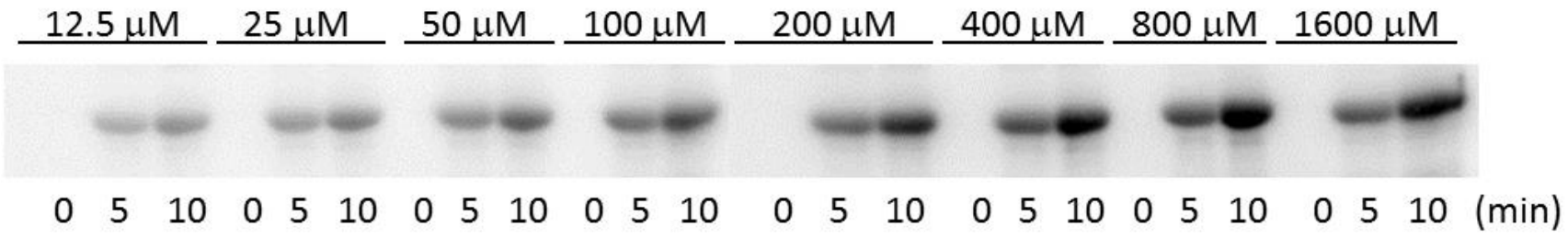

Figure 3.3: Michaelis-Menten kinetics experiment to determine k_{cat} and K_M for substrate ATP. ATP concentrations were varied between 12.5 and 1600 µM. Wild-type rParkin concentration was kept constant at 5 µM. These reactions were carried out at 30°C.

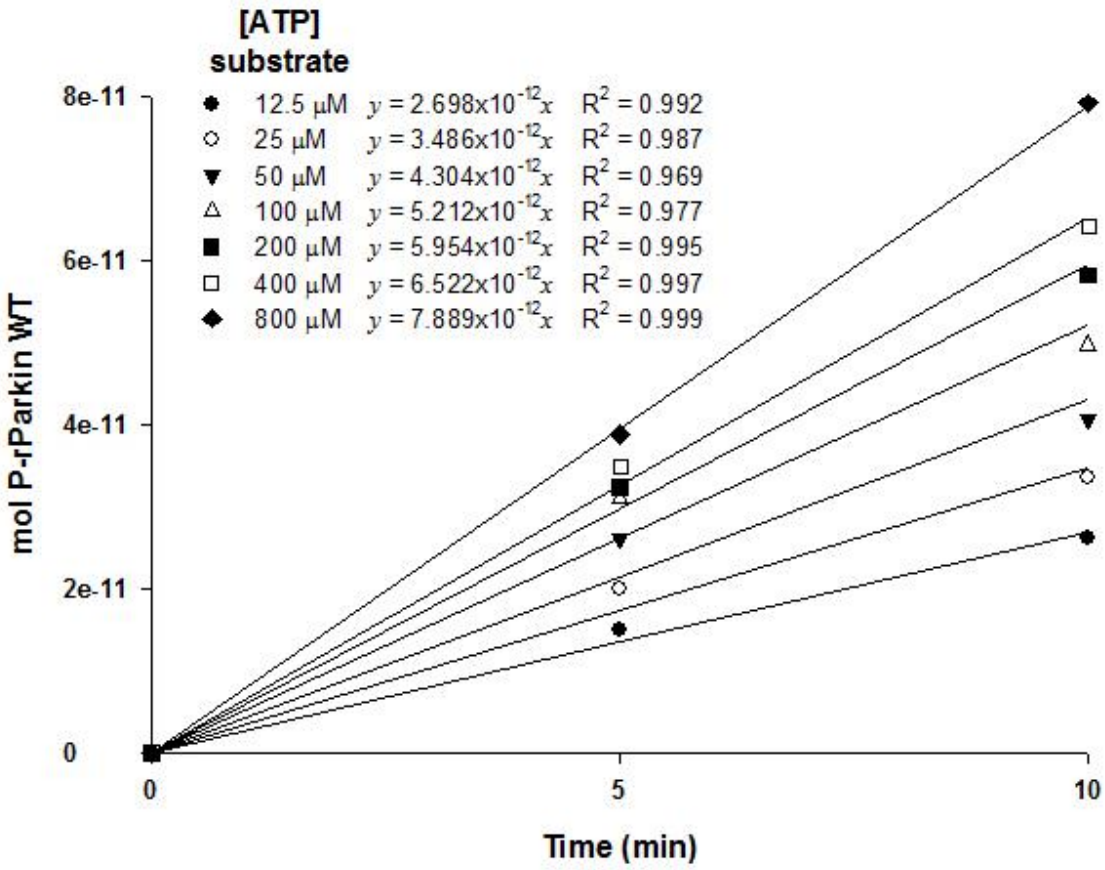

Figure 3.4: Data analysis. Data sets were fitted using Sigma Plot 5.0 software. Plots were generated to determine initial rates.

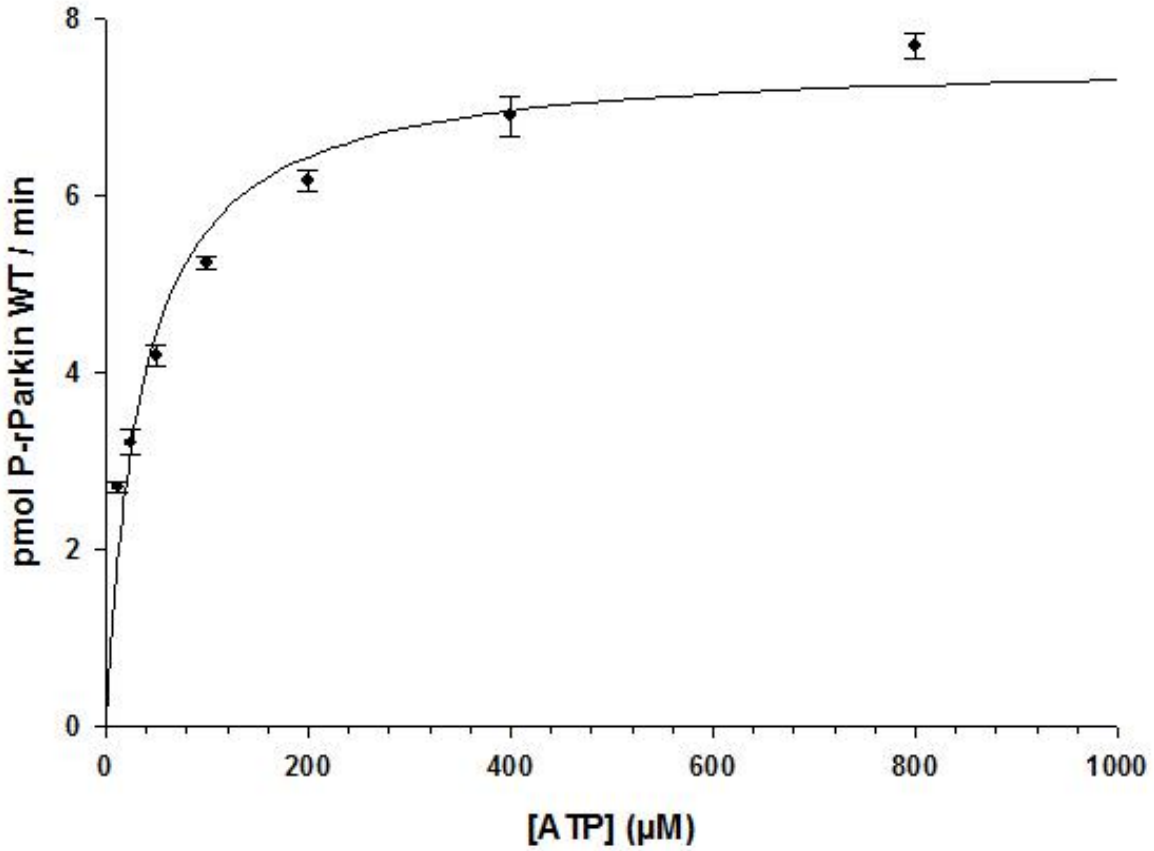

Figure 3.5: TcPINK1 phosphorylates wild-type rParkin using ATP as a substrate. The results of experiments (n=3) shown in Figure 3.3 were quantified to determine the kinetic parameters of phosphorylation of wild-type rParkin by TcPINK1. Error bars represent the standard deviation of the mean. Data sets were fit to the Michaelis-Menten equation with Sigma Plot 5.0 software.

3.3.2 Kinetic studies of Parkin phosphorylation by PINK1

Time course experiments were first carried out to establish initial velocity conditions. Figure 3.2 shows that TcPINK1 phosphorylates wild-type GST-rParkin in a time dependent manner. In addition, the initial segment (0 to 10 min) demonstrates linearity at saturating conditions of wild-type GST-rParkin (5 μM).

Steady state kinetics of TcPINK1 as a function of ATP is shown in Figure 3.5. Parameters derived from these experiments are summarized in Table 3.1. Kinetic analysis was conducted by plotting the initial velocities of phosphorylated wild-type GST-rParkin formation against ATP concentrations ranging from 12.5 μM to 1600 μM. The enzyme exhibited a hyperbolic response to ATP. k_{cat}, or turnover number, is the number of substrate molecules each enzyme active site converts to product per time unit (second). The k_{cat} of TcPINK1 with regard to ATP was 0.315 ± 0.006 s^{-1}. K_M is defined as the substrate concentration at which the reaction reaches half-maximal velocity. The K_M was determined to be 35.0 ± 3.2 μM. k_{cat}/K_M, a ratio often referred to as the specificity constant, describes how efficiently an enzyme converts its substrate to product. k_{cat}/K_M of TcPINK1 with regard to ATP was determined to be 9.00 x 10^3 $M^{-1}s^{-1}$.

A time course experiment using saturating concentrations ATP (3000 μM) was performed as well (Figure 3.6). This experiment also demonstrates that TcPINK1 phosphorylates wild-type GST-rParkin in a time dependent manner at the concentration range examined. Under saturating concentrations of ATP, phosphorylated wild-type GST-rParkin levels also increases linearly over the time scale of 0 to 10 min.

Steady state kinetics of TcPINK1 as a function of wild-type GST-rParkin is shown in Figure 3.9. The parameters derived from these experiments are summarized in Table 3.1 as well.

A)

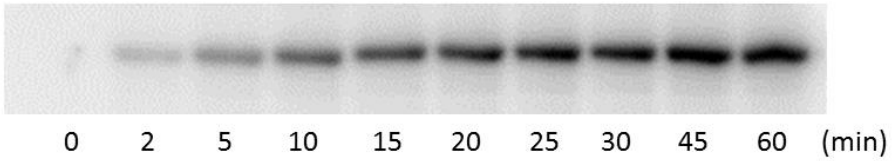

B)

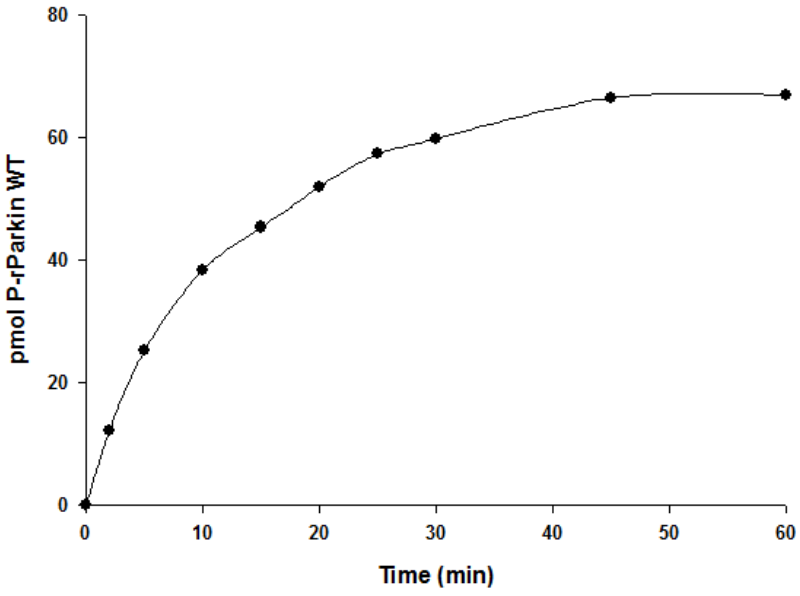

Figure 3.6: Time course experiment. 800 nM wild-type rParkin was phosphorylated in the presence of 3000 μM ATP, $MgCl_2$, and 40 nM TcPINK1 for the indicated times in a reaction volume of 10 μL at 30°C. pmol P-rParkin WT was plotted as a function of time.

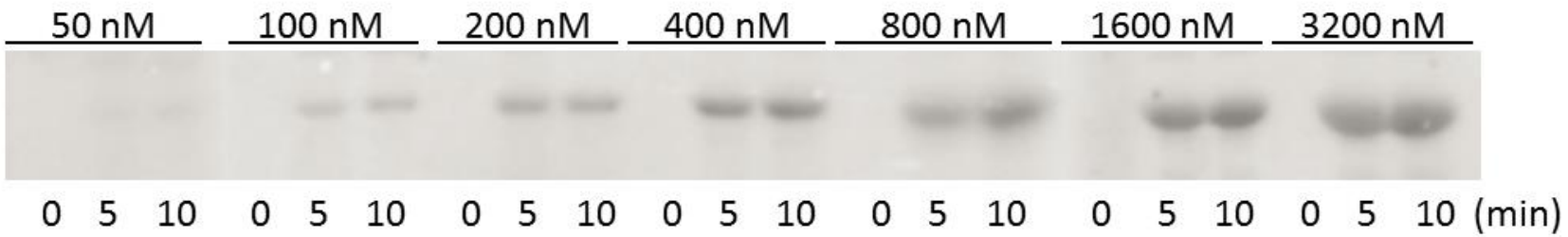

Figure 3.7: Michaelis-Menten kinetics experiment to determine k_{cat} and K_M for substrate wild-type rParkin. Wild-type rParkin concentrations were varied from 50 nM to 3200 nM. ATP concentration was kept constant at 3000 μM. These reactions were carried out at 30°C.

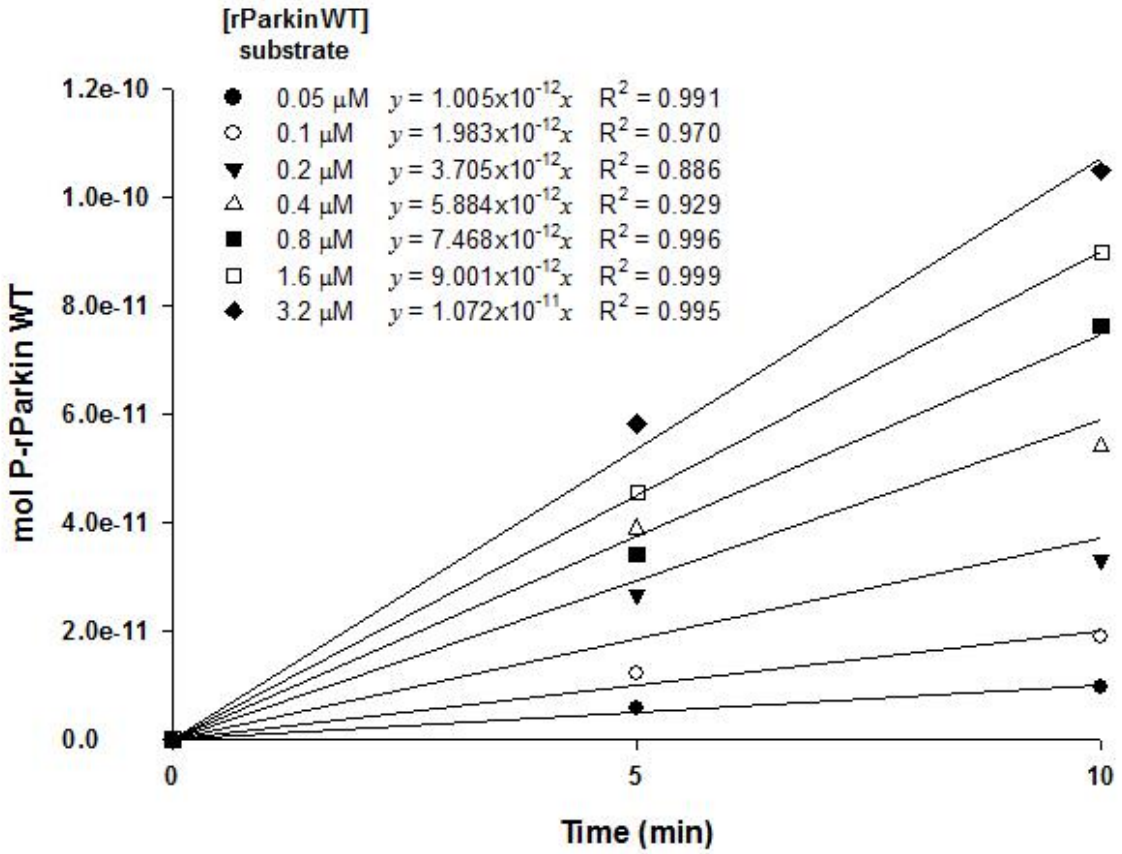

Figure 3.8: Data analysis. Data sets were fitted using Sigma Plot 5.0 software. Plots were generated to determine initial rates.

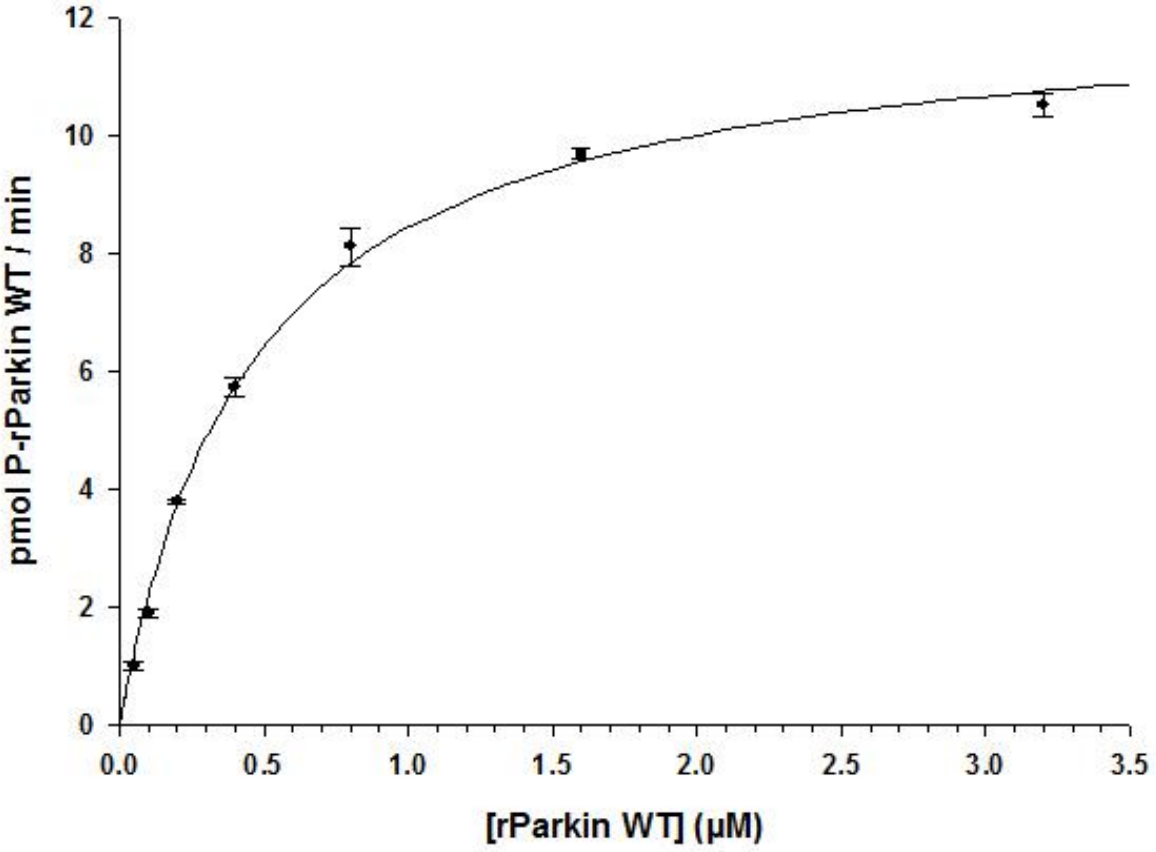

Figure 3.9: TcPINK1 phosphorylates wild-type rParkin. The results from Figure 3.7 were quantified to determine the kinetic parameters of phosphorylation of wild-type rParkin by TcPINK1. Error bars represent the standard deviation of the mean. Triplicate data sets were averaged and fitted to the Michaelis-Menten equation using Sigma Plot 5.0 software.

Kinetic analysis was conducted by plotting initial velocities of phosphorylated wild-type GST-rParkin formation against wild-type GST-rParkin concentrations ranging from 50 nM to 3200 nM. Rates increase hyperbolically with respect to concentration increases of wild-type rParkin. The k_{cat} of TcPINK1 determined by varying wild-type GST-rParkin concentrations is 1.02 ± 0.02 s^{-1}. The K_M of TcPINK1 with regard to wild-type GST-rParkin is 0.46 ± 0.03 μM. k_{cat}/K_M, or the specificity constant, is 2.25 x 10^6 $M^{-1}s^{-1}$.

3.4 Discussion

We determined the kinetics parameters of TcPINK1. The affinity (K_M) of TcPINK1 for its substrate ATP was measured to be 35.0 ± 3.2 μM *in vitro*. Hertz et al. has shown that the K_M value of human PINK1 for ATP is 74.6 ± 13.2 μM (Hertz et al. 2013). As mentioned previously, human PINK1 is highly unstable. To optimize the expression of human PINK1, Hertz et al. purified a truncated C-terminal $FLAG_3$ tagged version from baculovirus infected SF21 insect cells. The protein was co-expressed with TRAP1 to enhance its stability (Hertz et al. 2013). TcPINK, on the other hand, was highly stable and did not require expression optimization protocols.

Only a two-fold difference can be seen between the K_M values of the two species specific but highly conserved enzymes. When a substrate is sufficiently abundant, discriminating it against promiscuous substrates becomes less of an issue. In cells, ATP exists at high concentrations (> 100 μM). In fact, ATP is one of the most abundant metabolites in the cell. The kinase TcPINK1 exhibits a K_M value that is in the micromolar range, which indicates that ATP is a relatively weak binder to TcPINK. This finding is consistent with the aforementioned

notion that TcPINK1 can afford to have a high K_M for its substrate ATP, due to the high cellular concentrations of ATP.

The K_M of TcPINK1 for the substrate wild-type GST-rParkin is 0.46 ± 0.03 μM. The K_M value of TcPINK1 for wild-type rParkin indicates that TcPINK1 has a higher affinity for wild-type GST-rParkin over ATP. PINK1's affinity for ATP is weaker than its affinity for GST-rParkin by over 70-fold, which is not surprising when considering the fact that wild-type rParkin exists in cells at a much lower concentration.

The k_{cat} value for wild-type rParkin is ~3-fold larger than the k_{cat} value for ATP at 30°C. This indicates that in TcPINK1, the active site that interacts with wild-type rParkin is 3 times more processive than the active site that interacts with ATP. The k_{cat}/K_M values for ATP (9.00 x 10^3 $M^{-1}s^{-1}$) and wild-type rParkin (2.25 x 10^6 $M^{-1}s^{-1}$) are both smaller than the diffusion-controlled limit of 10^8 to 10^9. In summary, the kinetics data supports that TcPINK1 is an effective enzyme that selectively phosphorylates wild-type rParkin.

A number of diseases result from inactive kinases. Both the inactivation of death-associated protein kinase (DAPK) and LKB1 tumor-suppressor kinase cause cancer (Gao et al. 2011; Kissil et al. 1997). Diabetes results from desensitization of the insulin receptor kinase (Kulkarni et al. 1999). However, there are no clinically approved drugs that enhance kinase activity up to this date. Recently, therapeutic approaches that increase the activity of the PINK1 kinase have been considered. Kinetin, a blood-brain barrier crossing precursor to the ATP analog kinetin triphosphate, has been shown to restore the catalytic activity of mutant PINK1 to near-wild-type levels *in vitro* and *in vivo* (Hertz et al. 2013), in addition to enhancing the activity of wild-type PINK1. This raises the possibility that kinetin may be used to treat Parkinson's patients who harbor PINK1 mutations. In fact, increasing PINK1 activity above endogenous

	k_{cat}, s^{-1}	K_M, μM	k_{cat}/K_M, $M^{-1}s^{-1}$
ATP	0.315 ± 0.006	35.0 ± 3.2	9.00×10^3
rParkin WT	1.02 ± 0.02	0.46 ± 0.03	2.25×10^6

Table 3.1: Kinetic parameters for TcPINK1. k_{cat} and K_M values were determined from *in vitro* kinase assays. All experiments were performed in triplicates.

levels is known to protect cells against apoptotic stressors (Klinkenberg et al. 2010; Petit et al. 2005; Pridgeon et al. 2007). Therefore, there is also the possibility that enhancing PINK1 activity can benefit sporadic Parkinson's disease patients.

To our knowledge, we have determined the kinetics parameters of full-length wild-type PINK1 for the first time. The significance of this study lies in the fact that such parameters can serve as a valuable reference point when developing small molecule or peptide therapeutics using either *in vivo* or *in vitro* methods.

3.5 References

Beilina A, Van Der Brug M, Ahmad R, Kesavapany S, Miller DW, Petsko GA, Cookson MR. (2005) Mutations in PTEN-induced putative kinase 1 associated with recessive parkinsonism have differential effects on protein stability. Proc. Natl. Acad. Sci. USA ***102***, 5703-5708.

Bonifati V., Rizzu P., van Baren M.J., Schaap O., Breedveld G.J., Krieger E., Dekker M.C., Squitieri F., Ibanez P., Joosse M., van Dongen J.W., Vanacore N., van Swieten J.C., Brice A., Meco G., van Duijn C.M., Oostra B.A., Heutink P. (2003) Mutations in the DJ-1 gene associated with autosomal recessive early-onset parkinsonism. Science ***299***, 256-259.

Chan N.C., Salazar A.M., Pham A.H., Sweredoski M.J., Kolawa N.J., Graham R.L., Hess S., Chan D.C. (2011) Broad activation of the ubiquitin-proteasome system by Parkin is critical for mitophagy. Hum. Mol. Genet. ***20***, 1726-1737.

Clark I.E., Dodson M.W., Jiang C., Cao J.H., Huh J.R., Seol J.H., Yoo S.J., Hay B.A., Guo M. (2006) Drosophila pink1 is required for mitochondrial function and interacts genetically with parkin. Nature ***441***, 1162-1166.

Dodson M.W., Guo M. (2007) Pink1, Parkin, DJ-1 and mitochondrial dysfunction in Parkinson's disease. Curr. Opin. Neurobiol. ***17***, 331-337.

Fox S.H., Katzenschlager R., Lim S.Y., Ravina B., Seppi K., Coelho M., Poewe W., Rascol O., Goetz C.G., Sampaio C. (2011) The Movement Disorder Society Evidence-Based Medicine Review Update: Treatments for the motor symptoms of Parkinson's disease. Mov. Disord. ***3***, S2-S41.

Gao Y., Ge G., Ji H. (2011) LKB1 in lung cancerigenesis: a serine/threonine kinase as tumor suppressor. Protein Cell. ***2***, 99-107.

Geisler S., Holmström K.M., Skujat D., Fiesel F.C., Rothfuss O.C., Kahle P.J., Springer W. (2010) PINK1/Parkin-mediated mitophagy is dependent on VDAC1 and p62/SQSTM1. Nat. Cell Biol. ***12***, 119-131.

Greenamre J.T., Hastings T.G. (2004) Parkinson's – divergent causes, convergent mechanism. Science. ***304***, 1120-1122.

Hertz N.T., Berthet A., Sos M.L., Thorn K.S., Burlingame A.L., Nakamura K., Shokat K.M. (2013) A neo-substrate that amplifies catalytic activity of parkinson's-disease-related kinase PINK1. Cell ***154***, 737-747.

Jankovic J. (2008) Parkinson's disease: clinical features and diagnosis. J. Neurol. Neurosurg. Psychiatry ***79***, 368-376.

Kazlauskaite A., Kelly V., Johnson C., Baillie C., Hastie C.J., Peggie M., Macartney T., Woodroof H.I., Alessi D.R., Pedrioli P.G., Muqit M.M. (2014) Phosphorylation of Parkin at

Serine^{65} is essential for activation: elaboration of a Miro1 substrate-based assay of Parkin E3 ligase activity. Open Biol. ***4***, 130213.

Kazlauskaite A., Kondapalli C., Gourlay R., Campbell D.G., Ritorto M.S., Hofmann K., Alessi D.R., Knebel A., Trost M., Muqit M.M. (2014) Parkin is activated by PINK1-dependent phosphorylation of ubiquitin at Serine^{65}. Biochem. J. [Epub ahead of print]

Keeney P.M., Xie J., Capaldi R.A., Bennett J.P. Jr. (2006) Parkinson's disease brain mitochondrial complex I has oxidatively damaged subunits and is functionally impaired and misassembled. J. Neurosci. ***26***, 5256-5264.

Khan N.L., Graham E., Critchley P., Schrag A.E., Wood N.W., Lees A.J., Bhatia K.P., Quinn N. (2003) Parkin disease: a phenotypic study of a large case series. Brain ***126***, 1279-1292.

Kissil J.L., Feinstein E., Cohen O., Jones P.A., Tsai Y.C., Knowles M.A., Eydmann M.E., Kimchi A. (1997) DAP-kinase loss of expression in various carcinoma and B-cell lymphoma cell lines: possible implications for role as tumor suppressor gene. Oncogene ***15***, 403-407.

Kitada T., Asakawa S., Hattori N., Matsumine H., Yamamura Y., Minoshima S., Yokochi M., Mizuno Y., Shimizu N. (1998) Mutations in the Parkin gene cause autosomal recessive juvenile parkinsonism. Nature ***392***, 605-608.

Klinkenberg M., Thurow N., Gispert S., Ricciardi F., Eich F., Prehn J.H., Auburger G., Kögel D. (2010) Enhanced vulnerability of PARK6 patient skin fibroblasts to apoptosis induced by proteasomal stress. Neuroscience ***166***, 422-434.

Kulkarni R.N., Brüning J.C., Winnay J.N., Postic C., Magnuson M.A., Kahn C.R. (1999) Tissue-specific knockout of the insulin receptor in pancreatic beta cells creates an insulin secretory defect similar to that in type 2 diabetes. Cell ***96***, 329-339.

Lemasters J.J., Nieminen A.L., Qian T., Trost L.C., Elmore S.P., Nishimura Y., Crowe R.A., Cascio W.E., Bradham C.A., Brenner D.A., Herman B. (1998) The mitochondrial permeability transition in cell death: a common mechanism in necrosis, apoptosis and autophagy. Biochim. Biophys. Acta. ***1366***, 177-196.

Lücking C.B., Dürr A., Bonifati V., Vaughan J., De Michele G., Gasser T., Harhangi B.S., Meco G., Denèfle P., Wood N.W., Agid Y., Brice A. (2000) Association between early-onset Parkinson's disease and mutations in the parkin gene.
N. Engl. J. Med. *342*, 1560-1567.

Matsuda N., Sato S., Shiba K., Okatsu K., Saisho K., Gautier C.A., Sou Y.S., Saiki S., Kawajiri S., Sato F., Kimura M., Komatsu M., Hattori N., Tanaka K. (2010) PINK1 stabilized by mitochondrial depolarization recruits Parkin to damaged mitochondria and activates latent Parkin for mitophagy. J. Cell Biol. ***189***, 211-221.

Morais V.A., Verstreken P., Roethig A., Smet J., Snellinx A., Vanbrabant M., Haddad D., Frezza C., Mandemakers W., Vogt-Weisenhorn D., Van Coster R., Wurst W.,.Scorrano L., De Strooper B. (2009) Parkinson's disease mutations in PINK1 result in decreased Complex I activity and deficient synaptic function. EMBO Mol. Med. ***1***, 99-111.

Narendra D.P., Jin S.M., Tanaka A., Suen D.F., Gautier C.A., Shen J., Cookson M.R., Youle R.J. (2010) PINK1 is selectively stabilized on impaired mitochondria to activate Parkin. PLoS Biol. ***8***, e1000298.

Park J., Lee S.B., Lee S., Kim Y., Song S., Kim S., Bae E., Kim J., Shong M., Kim J.M., Chung J. (2006) Mitochondrial dysfunction in Drosophila PINK1 mutants is complemented by parkin. Nature ***441***, 1157-1161.

Pattingre S., Tassa A., Qu X., Garuti R., Liang X.H., Mizushima N., Packer M., Schneider M.D., Levine B. (2005) Bcl-2 antiapoptotic proteins inhibit Beclin 1-dependent autophagy. Cell *122*, 927-939.

Petit A., Kawarai T., Paitel E., Sanjo N., Maj M., Scheid M., Chen F., Gu Y., Hasegawa H., Salehi-Rad S., Wang L., Rogaeva E., Fraser P., Robinson B., St George-Hyslop P., Tandon A. (2005) Wild-type PINK1 prevents basal and induced neuronal apoptosis, a protective effect abrogated by Parkinson disease-related mutations. J. Biol. Chem. ***280***, 34025-34032.

Poole A.C., Thomas R.E., Yu S., Vincow E.S., Pallanck L. (2010) The mitochondrial fusion-promoting factor mitofusin is a substrate of the PINK1/parkin pathway. PLoS One ***5***, e10054.

Pridgeon J.W., Olzmann J.A., Chin L.S., Li L. (2007) PINK1 protects against oxidative stress by phosphorylating mitochondrial chaperone TRAP1. PLoS Biol. ***5***, e172.

Puschmann A. (2013) Monogenic Parkinson's disease and Parkinsonism: clinical phenotypes and frequencies of known mutations. Parkinsonism Relat. Disord. ***19***, 407-415.

Rilstone J.J., Alkhater R.A., Minassian B.A. (2013) Brain dopamine-serotonin vesicular transport disease and its treatment. N. Engl. J. Med. ***368***, 543-550.

Schapira A.H. (2008) Mitochondria in the aetiology and pathogenesis of Parkinson's disease. Lancet Neurol. ***7***, 97-109.

Schapira A.H., Cooper J.M., Dexter D., Clark J.B., Jenner P., Marsden C.D. (1990) Mitochondrial complex I deficiency in Parkinson's disease. J. Neurochem. ***54***, 823–827.

Shults C.W., Oakes D., Kieburtz K., Beal M.F., Haas R., Plumb S., Juncos J.L., Nutt J., Shoulson I., Carter J., Kompoliti K., Perlmutter J.S., Reich S., Stern M., Watts R.L.,Kurlan R., Molho E., Harrison M., Lew M. (2002) Effects of coenzyme Q_{10} in early Parkinson disease: evidence of slowing of the functional decline. Arch. Neurol. ***59***, 1541-1550.

Valente E.M., Abou-Sleiman P.M., Caputo V., Muqit M.M., Harvey K., Gispert S., Ali Z., Del Turco D., Bentivoglio A.R., Healy D.G., Albanese A., Nussbaum R., González-Maldonado R., Deller T., Salvi S., Cortelli P., Gilks W.P., Latchman D.S., Harvey R.J., Dallapiccola B., Auburger G., Wood N.W. (2004) Hereditary early-onset Parkinson's disease caused by mutations in PINK1. Science ***304***, 1158-1160.

Vincow E.S., Merrihew G., Thomas R.E., Shulman N.J., Beyer R.P., MacCoss M.J., Pallanck L.J. (2013) The PINK1-Parkin pathway promotes both mitophagy and selective respiratory chain turnover *in vivo*. Proc. Natl. Acad. Sci. USA ***110***, 6400-6405.

Vives-Bauza C., Zhou C., Huang Y., Cui M., de Vries R.L., Kim J., May J., Tocilescu M.A., Liu W., Ko H.S., Magrané J., Moore D.J., Dawson V.L., Grailhe R., Dawson T.M., Li C., Tieu K., Przedborski S. (2010) PINK1-dependent recruitment of Parkin to mitochondria in mitophagy. Proc. Natl. Acad. Sci. USA ***107***, 378-383.

Wang X., Winter D., Ashrafi G., Schlehe J., Wong Y.L., Selkoe D., Rice S., Steen J., LaVoie M.J., Schwarz T.L. (2011) PINK1 and Parkin target Miro for phosphorylation and degradation to arrest mitochondrial motility. Cell ***147***, 893-906.

Woodroof H.I., Pogson J.H., Begley M., Cantley L.C., Deak M., Campbell D.G., van Aalten D.M., Whitworth A.J., Alessi D.R., Muqit M.M. (2011) Discovery of catalytically active orthologues of the Parkinson's disease kinase PINK1: analysis of substrate specificity and impact of mutations. Open Biol. ***1***, 110012.

Yang Y., Gehrke S., Imai Y., Huang Z., Ouyang Y., Wang J.W., Yang L., Beal M.F., Vogel H., Lu B. (2006) Mitochondrial pathology and muscle and dopaminergic neuron degeneration caused by inactivation of Drosophila Pink1is rescued by Parkin. Proc. Natl. Acad. Sci. USA ***103***, 10793-10798.

Ziviani E., Tao R.N., Whitworth A.J. (2010) Drosophila parkin requires PINK1 for mitochondrial translocation and ubiquitinates mitofusin. Proc. Natl. Acad. Sci. USA ***107***, 5018-5023.

CHAPTER 4

PHOSPHORYLATION CAUSES ALLOSTERIC ACTIVATION OF PARKIN

4.1 Introduction

4.1.1 Role of Parkin in Parkinson's disease

Parkinson's disease is the second most common neurodegenerative disorder, behind only Alzheimer's disease. As mentioned in the previous section, the cause of Parkinson's disease can be either sporadic or genetic. The term "familial Parkinson's disease" is used to discern genetic Parkinson's disease from idiopathic Parkinson's disease. Autosomal recessive juvenile onset Parkinsonism (AR-JP) is one of the most common forms of hereditary Parkinson's disease that is characterized by an early-onset and slow progression. The clinical features of AR-JP are indistinguishable from the late-onset idiopathic form of Parkinson's disease. Mutations in several genes account for AR-JP. Among these genes, the E3 ubiquitin ligase Parkin is the most commonly mutated (Hardy 2010; Kitada et al. 1998; Lucking et al. 1998; Martin et al. 2011; Quadri et al. 2013). There are currently an excess of 100 reported clinically relevant mutations in the PARK2 gene (Bekris et al. 2010). Deletion mutations, rearrangements, duplications, missense and nonsense point mutations are commonly detected in the PARK2 gene of AR-JP patients. These pathogenic mutations span the entire length of the PARK2 gene. In fact, mutations in Parkin account for fifty percent of all AR-JP cases. In recent years, heterozygous Parkin mutations have also been discovered in patients with late-onset Parkinson's disease, indicating that Parkin may also play a role in the pathogenesis of sporadic Parkinsonism (Oliveira et al. 2003).

4.1.2 Parkin is a RING-between-RING E3 ligase

Studies of PARK2 gene mutations found in AR-JP patients have revealed that the molecular basis of AR-JP is the loss of Parkin E3 ligase activity (Chung et al. 2001; Imai et al. 2001; Shimura et al. 2001). Parkin is a 52-kDa protein that consists of 465 amino acids and 5 domains (Trempe et al. 2013). Parkin is classified as a member of the RING-between-RING family (RBR) of E3 ubiquitin ligases, where the transfer of ubiquitin from E2 to substrate involves a thioester intermediate at the E3 active-site cysteine (Imai et al., 2000; Shimura et al., 2000; Zhang et al., 2000). Parkin is capable of mono-ubiquitination, multiple mono-ubiquitination, and polyubiquitination (Doss-Pepe et al. 2005; Hample et al. 2006; Lim et al. 2005; Matsuda et al. 2006; Moore et al. 2008).

The 2.8 Å low resolution crystal structure of full-length rat Parkin determined by Trempe et al. reveals that the E2 binding site is located on the RING1 domain of Parkin (Trempe et al. 2013). The N-terminal ubiquitin-like (UBL) domain, which shares 30% sequence identity with human ubiquitin, is not directly involved in interacting with E2, but has been shown to be necessary for ligase activity *in vivo* (Henn et al. 2005; Sato et al. 2006; Shimura et al. 2000; Shimura et al. 2005). However, the UBL domain is not necessary for the ligase activity *in vitro* (Matsuda et al. 2006). The UBL domain also mediates Parkin auto-inhibition (Chaugule et al. 2011). Parkin also contains an in between domain that separates the RING1 and RING2 domains (IBR) and a zinc co-ordinating motif termed RING0 (Kitada et al. 1998).

As mentioned above, it has been shown that the UBL domain of wild-type Parkin acts as an auto-inhibitory domain by binding to C-terminus of the protein (Chaugule et al. 2011). Due to the fact that Ser^{65} is located in the UBL domain of Parkin, our laboratory and other in the

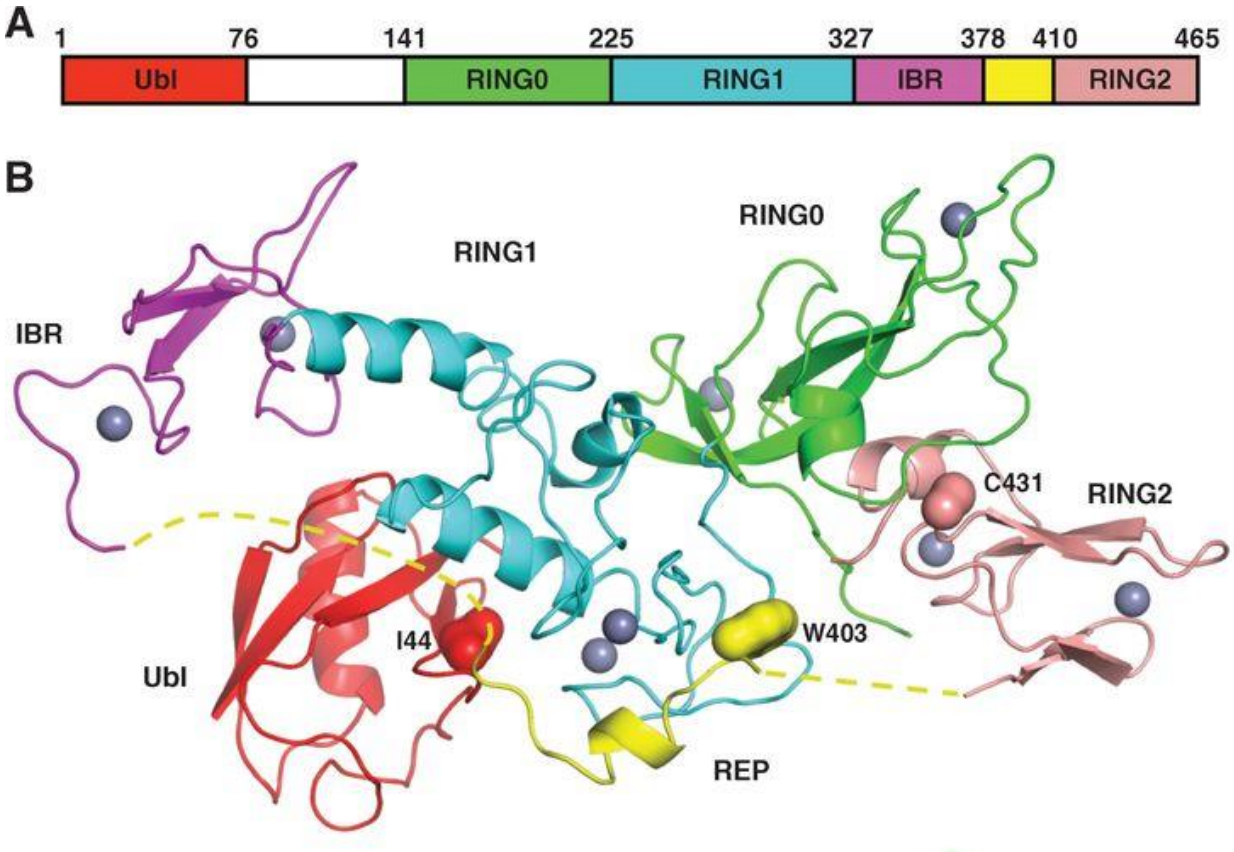

Figure 4.1: Domain organization of Parkin. The UBL domain interacts with the 26S proteasome. The RING-box recruits (E2) ubiquitin conjugating enzymes (Trempe et al. 2013).

field have hypothesized that phosphorylation of Ser^{65} will abolish auto-inhibition, thereby activating the E3 ligase (Kazlauskaite et al. 2014).

Parkin is susceptible to auto-ubiquitination. There are three classes of Parkin mutations (Trempe et al. 2013). The first class of mutations disrupts protein folding or coordination of zinc. The second class causes changes in the catalytic site. The third class of mutations changes protein contacts. As mentioned previously, wild-type Parkin is auto-inhibited, and therefore, has indiscernible auto-ubiquitiation activity. However, results by Trempe et al. show that introducing point mutations such as W403A, C457S, and F463A activate Parkin's ability to self-ubiquitinate. N-terminal tags also activate Parkin E3 ubiquitin ligase activity by disrupting its auto-inhibited conformation (Burchell et al. 2012; Chaugule et al. 2011). Lastly, our laboratory and others in the field have demonstrated that Parkin can trans-ubiquitinate substrates such as Bcl2, Mcl1, and Miro1 *in vitro* (Kazlauskaite et al. 2014).

4.1.3 Interaction partners of Parkin

Parkin interacts with a wide variety of proteins. Parkin interacts with the ubiquitin conjugating enzymes Ubc4, Ubc7, UbcH7, UbcH8, and the UbcH13/Uev1a (Olzmann et al. 2007; Shimura et al. 2000; Zhang et al. 2000). Parkin interacts with Rpn10 - a subunit of the 26S proteosome complex (Sakata et al. 2003). Parkin has been reported to interact with the 20S proteasome (Dachsel et al. 2005). Parkin also associates with synphilin1 – an α-synuclein binding protein. This interaction plays a role in cytosolic inclusion body formation (Chung et al. 2001; Lim 2005). CASK/LIN-2 plays a role in localizing Parkin at synapses (Fallon et al. 2002). Research by Staropoli et al. suggests that Parkin may function as part of a SCF (Skp1-Cullin-F-box protein) - like complex involving cullin1 and Fbox/WD (Staropoli et al. 2003). Parkin

association with the mutated DJ-1 protein or BAG5, on the other hand, results in inhibition of Parkin ubiquitin E3 ligase activity (Kalia et al. 2004; Moore et al. 2005; Sato et al. 2006).

Various target substrates of Parkin have been identified *in vivo* up to this date. For instance, both the endothelin receptor type B-like G protein coupled receptor (GPR37) and the p38 subunit of the aminoacyl-tRNA synthetase complex are substrates of Parkin (Corti et al. 2003; Imai et al. 2001; Ko et al. 2005). CDcrel-1, a nucleotide binding protein involved in regulating the cytoskeleton, is a substrate of Parkin as well (Zhang et al. 2000). Cyclin E (Staropoli et al., 2003), RanBP2 (Um et al. 2006), Eps15 (Fallon et al. 2006), SEPT5_v2 (Choi et al. 2003), Synaptotagmin XI (Huynh et al. 2003), and α– and β– tubulin (Ren et al. 2003), and far upstream sequence element-binding protein 1 (Ko et al. 2006) are also substrates of Parkin.

4.1.4 Parkin, Bcl2, mitophagy, and cellular autophagy

Cytosolic cytochrome c is necessary for the initiation of apoptosis. Bcl2 is known as an anti-apoptotic protein, primarily located on the outer mitochondrial membrane, which prevents the efflux of cytochrome c from the mitochondrial intermembrane space. In fact, over expression of Bcl2 prevents cells from going into apoptosis (Yang et al. 1997). The primary function of Parkin, on the other hand, is that of an E3 ubiquitin ligase. Parkin is found in the cytosol (Shimura et al. 1999), but also located in the mitochondria (Darios et al. 2003). Parkin is predominantly cytosolic under steady state conditions. In proliferating cells, Parkin plays a role in the biogenesis of the mitochondria (Kuroda et al. 2006). As described in previous sections, Parkin promotes turnover of damaged mitochondria (Geisler et al. 2010; Jin and Youle 2012; Narenda et al. 2008; Poole et al. 2008). It has been shown that treating Parkin over-expressing cells with the mitochondrial uncoupler CCCP (carbonyl cyanide m-chlorophenylhydrazone)

results in rapid localization of Parkin to the mitochondria, followed by significant mitochondrial loss. Autophagic proteins are necessary in this process.

Apart from mitochondria specific autophagy (mitophagy), it has been shown that Parkin can also inhibit cellular autophagy by mono-ubiquitinating Bcl2 (Chen et al. 2010). Co-immunoprecipitation studies show that Parkin directly interacts with the C-terminal end of Bcl2. Interestingly, Chen et al. demonstrate that Bcl2 is stabilized upon mono-ubiquitination, which leads to an increase in Bcl2 levels. A subsequent increase in binding between Beclin1 and Bcl2 is observed when Bcl2 levels increase. Beclin1 is a known inducer of autophagy (Kang et al. 2011). Under normal conditions, Bcl2 inhibits autophagy by binding to Beclin1 (Pattingre et al. 2005). Upon cellular stress, Bcl2 dissociates from Beclin1, Vps34 is activated, and autophagy is initiated (Pattingre et al. 2005). The BH3 domain in Beclin1 binds to a hydrophobic groove in Bcl2 proteins (Maiuri 2007; Oberstein 2007).

The Beclin1-Bcl2 interaction has been shown to be Parkin dependent, where overexpression of Parkin increases Bcl2 binding to Beclin1 (Chen et al. 2000). However, when E3 ligase activity-defective mutants are overexpressed, increases in Bcl2 binding to Beclin1 are not seen. In addition, several E3 ligase activity-defective disease-linked mutants failed to inhibit autophagy (Chen et al. 2010). To summarize, Parkin induces mitophagy while inhibiting autophagy. The mechanism behind these findings will most likely depend on Parkin localization. As mentioned previously, damaged mitochondria will target Parkin to the mitochondria. Global cellular stress, on the other hand, may cause Parkin to remain in the cytosol - preventing autophagy (Chen et al. 2010; Decuypere et al. 2012).

Protein aggregates are cleared via autophagy, and alterations in the lysosomal pathway are oftentimes suggested in neuro-degenerating diseases such as Parkinson's. It has been shown

that selective deletion of autophagy genes in the central nervous system leads to neuronal damage (Hara et al. 2006; Komatsu et al. 2006). In fact, autophagosomes are known to accumulate in the brain tissues of Parkinson's disease patients (Williams et al. 2006). Such studies provide a link between autophagy and Parkinson's disease. Interestingly, neuronal cultures from Parkin-knockout mice showed an increase in autophagy markers (Casarejos et al. 2009). Autophagy is induced in Parkin knockout cells, whereas Parkin overexpression represses autophagy (Chen et al. 2010). Collectively, these results confirm that Parkin down-regulation induces autophagy. The fact that Parkin induces mitophagy while inhibiting autophagy is ironic. Mitophagy may play a role in preventing the development of Parkinson's disease by removing damaged mitochondria that can negatively affect dopamine neurons. Autophagy, on the other hand, may contribute to pathogenic neuronal death – selective death of dopamine neurons is a known cause of Parkinson's disease. The full role Parkin plays in Parkinson's disease remains a mystery, but the complete mechanism may very well be a delicate balancing act. Further understanding of the Parkin - Bcl2 - Beclin1 regulation will prove to be crucial.

4.2 Materials and Methods

Expression and purification of proteins: Point mutants in the UBL domain (W403A and C431S) were generated using Site Directed Mutagenesis (Stratagene). *E. coli* strains BL21 (DE3) were transformed with plasmids containing genes for GST-E1, wild-type GST-Parkin, GST-Parkin GST-W403A, and GST-Parkin W403A-C431S. The cells were grown at 37°C in Luria Broth supplemented with 200 µM zinc chloride until reaching an OD_{600} of 0.8. The cells were then induced with 50 µM IPTG at 16 °C for 16 hours, harvested via centrifugation, and lysed by sonication. The soluble fraction was separated from the non-soluble by centrifugation at 15 000

g for 30 min. The resulting supernatant was incubated with GST beads for 30 min at 4°C. The beads then were washed with NETN buffer 3 times and eluted with 20 mM GSH. The eluted proteins were dialyzed into a buffer containing 25mM Tris pH, 8.0 100mM NaCl, and 0.5 mM DTT.

All His_6-tagged constructs were transformed into either *E. coli* BL21 (DE3) or *E. coli* BL21 (DE3) pLysS stains (Promega). His_6-ubiquitin, His_6-Bcl2, and His_6-ppERK2 (pLysS) were grown in Luria Broth at 37°C, and induced with 100 μM ITPG at OD_{600} for 16 hours at 16°C. Cells were then harvested via centrifugation. Harvested cells were sonicated in a lysis buffer containing 50 mM Tris-HCl pH 8.0, 250 mM NaCl, 10 mM imidazole, and 1 mM DTT. Following sonication, the supernatant was clarified by centrifugation at 15 000 *g*. The resulting supernatant was incubated with Ni-NTA beads (Qiagen). Beads were then washed using a buffer containing 50 mM Tris-HCl pH 8.0, 1 M NaCl, 20 mM imidazole, and 1 mM DTT. The protein was eluted using a buffer containing 50 mM Tris-HCl pH 8.0, 250 mM NaCl, 250 mM imidazole, and 1 mM DTT.

For expression of His_6-UbcH7, cells were grown in Luria Broth at 37°C to an OD_{600} of 0.8 and induced with 100 μM ITPG for 16 hours at 16°C. Cells were once again harvested via centrifugation (4000 *g*), and lysed by sonication. His_6-UbcH7 was initially purified using Nickel-affinity chromatography methods. The resulting fractions containing His_6-UbcH7 were pooled and further purified via ion exchange chromatography (Mono S). After washing the column, the bound protein was eluted using a NaCl gradient from 0 to 1 M in (25 mM Tris-HCl pH 6.0, 1 mM DTT). Once the proteins were purified to apparent homogeneity, they were flash frozen at −80°C in a buffer containing, 50 mM Tris pH 8, 200 mM NaCl, 1 mM DTT, and 10%

glycerol. To confirm the purity, all proteins were analyzed via SDS-PAGE followed by Coomassie blue staining.

***In vitro* ubiquitination assays:** Bcl2 was labeled using [γ-^{32}P]-ATP and pp-ERK2 as the kinase. The kinase reactions were incubated for 1 hour at 30°C. The trans-ubiquitination reaction mixtures typically contained, in a final volume of 15 µL, phosphorylated Bcl2, 5 µM GST-E1 ubiquitin-activating ligase, 5 µM His_6-UbcH7 conjugating E2 ligase, 1 µM Parkin, and 25 µM ubiquitin. The reactions were carried out in buffers containing 4 mM ATP, 10 mM $MgCl_2$, 50 mM Tris-HCl pH 8.0 at 37°C. The auto-ubiquitination reaction mixtures typically contained, in a final volume of 15 µL, 5 µM GST-E1 ubiquitin-activating ligase, 5 µM His_6-UbcH7 conjugating E2 ligase, 1 µM Parkin, and 25 µM ubiquitin. The reactions were terminated by addition of SDS sample buffer supplemented with 2 mM EDTA followed by boiling at 95°C for 4 min. The reaction mixtures were analyzed by separation through 12% SDS-PAGE and phosphorimaging.

Single turnover UbcH7~Ub discharge assays: The substrate was generated by charging UbcH7 with ubiquitin at 37°C for 2 hours in a reaction mixture containing 5 µM E1, 0.5 mM ATP, 5 µM ubiquitin, 0.2 mM $MgCl_2$, and 50 mM Tris pH 8.0. The reaction was stopped by adding 2 mM EDTA. Single turnover discharge assays for Parkin variants were carried out in the presence of 50 mM Tris pH 8.0, 50 mM NaCl. Reactions were stopped using a 6× loading buffer, and proteins were separated on 16% SDS-PAGE gels. Proteins were then electrophoretically transferred to a nitrocellulose membrane. The resulting membrane was blocked for 1 hour, followed by incubation with rabbit anti-UbcH7 antibody (1:5000 dilution) in

Table 4.1: List of Proteins Used in this Study.

Protein	Construct	Strain	Expression	Purification
ppERK2	pET-His_6-ppERK2 (R4F)	Homo sapiens	E. coli	Ni-NTA, Mono Q
Bcl2	pET-His_6-Bcl2	Mus musculus	E. coli	Ni-NTA
E1	BEVS-GST-E1	Homo sapiens	sf9 cells	GST, S200
UbcH7	pET-His_6-UbcH7	Homo sapiens	E. coli	Ni-NTA, Mono S
PINK1	pMAL-MBP-PINK1	Tribolium Castaneum	E. coli	MBP
Parkin wild-type	pGEX-Parkin	Rattus Norvegicus	E. coli	GST
Parkin W403A	pGEX-Parkin-W403A	Rattus Norvegicus	E. coli	GST
Parkin W403A-C431S	pGEX-Parkin-W403A-C431S	Rattus Norvegicus	E. coli	GST
His-Ubiquitin	pET-His_6-Ubiquitin	Homo sapiens	E. coli	Ni-NTA

blocking buffer (5% BSA in PBS-T). Following extensive washing using PBS-T, the membrane was incubated with horseradish peroxidase-conjugated goat anti-rabbit IgG (1:10 000 dilution in blocking buffer; Pierce). After extensive washing using PBS-T, the membrane was incubated in SuperSignal West Femto Maximum Sensitivity Substrate (Pierce). The secondary antibody was detected using chemiluminescence film (Amersham Biosciences, Buckinghamshire, UK). All incubations and washes were performed at room temperature. ImageJ (National institutes of Health) was used to quantify the individual bands via densitometry.

4.3 Results

4.3.1 Reconstitution of *in vitro* ubiquitination assays using non-phosphorylated Parkin

Sufficient quantities of recombinant proteins were purified to homogeneity as shown in Figure 4.2, which allowed the reconstitution of Parkin self-ubiquitination *in vitro*, in addition to the development of an *in vitro* assay where Parkin catalyzes conjugation of ubiquitin to its substrate Bcl2. The development of these assays made it possible to evaluate the catalytic mechanism of the E3 ligase Parkin as demonstrated in the following sections.

Initially, we employed both tagged (His_6-SUMO) and untagged human Parkin to test its E3 ligase activity. However, human Parkin had limited self-ubiquitination activity in our hands. Recently, Trempe et al. have determined the crystal structure of Rattus norvegicus Parkin (Trempe et al. 2013). This led us to test the activity of wild-type rParkin. Untagged rParkin showed no activity - much like its human counterpart. GST-tagged wild-type rParkin, on the other hand, showed moderate auto-ubiquitination activity in our hands.

The crystal structure of rParkin suggests that the E2 binding site located on the RING1 domain is blocked by the repressor element of Parkin (REP). The REP consists of a two-turn

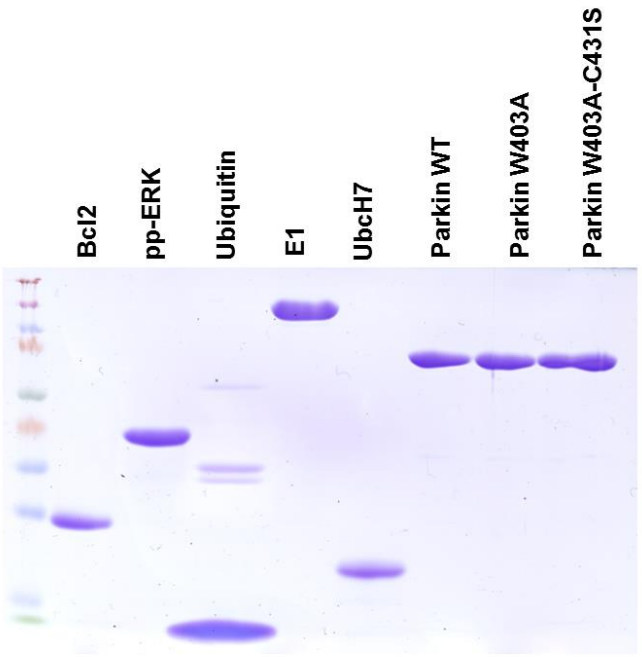

Figure 4.2: Proteins involved in ubiquitination *in vitro*. Proteins were purified to homogeneity and analyzed by SDS-PAGE using a 12% gel. The resulting gel was stained with Coomassie blue. Spectra™ multicolor broad range protein ladder (Thermo Scientific) was used to determine the molecular weights of proteins.

helix that is stabilized by a tryptophan residue (Trp^{403}). The stabilization occurs by inserting the Trp^{403} indole group into a pocket located on the RING1 domain (Trempe et al. 2013). Previous studies have shown that mutating the Trp^{403} residue into an alanine disrupts the RING1-REP interface, thereby increasing rParkin self-ubiquitination.

While GST-tagged rParkin W403A showed enhanced auto-ubiquitination activity, converting the highly conserved catalytic cysteine residue to a serine (GST-tagged rParkin W403A-C431S) abolished Parkin auto-ubiquitination activity. As mentioned in the previous section, Parkin exhibits HECT-like characteristics, where a catalytic cysteine residue located in the RING2 domain (Cys^{431}) acts as a ubiquitin acceptor that forms a thiosester intermediate (Wenzel et al. 2011).

The simplest model for Parkin auto-ubiquitination is that ubiquitination results from an intramolecular transfer of ubiquitin from Parkin's active site cysteine to one of the 22 lysine residues on the same molecule. However, it is also conceivable that Parkin auto-ubiquitination is not exclusively an intramolecular reaction. It is quite possible that Parkin auto-ubiquitination results from an intermolecular reaction where ubiquitin transfers from one Parkin molecule to another.

After confirming that the W403A mutant rParkin exhibits a rate enhancement in self-ubiquitination, we investigated if the mutation also induces a catalytic enhancement in *trans*-ubiquitination. As mentioned previously, Bcl2 is an anti-apoptotic, autophagy inhibiting protein that directly binds to the C-terminus of Parkin. Thus, we hypothesized that Bcl2 would act as a Parkin substrate *in vitro*. We reconstituted rParkin dependent Bcl2 ubiquitination by incubating P^{32} labeled Bcl2 with E1, UbcH7, wild-type GST-rParkin, ubiquitin, and ATP. Analysis of the reaction mixture by SDS-PAGE and subsequent phosphorimaging revealed a faint band that

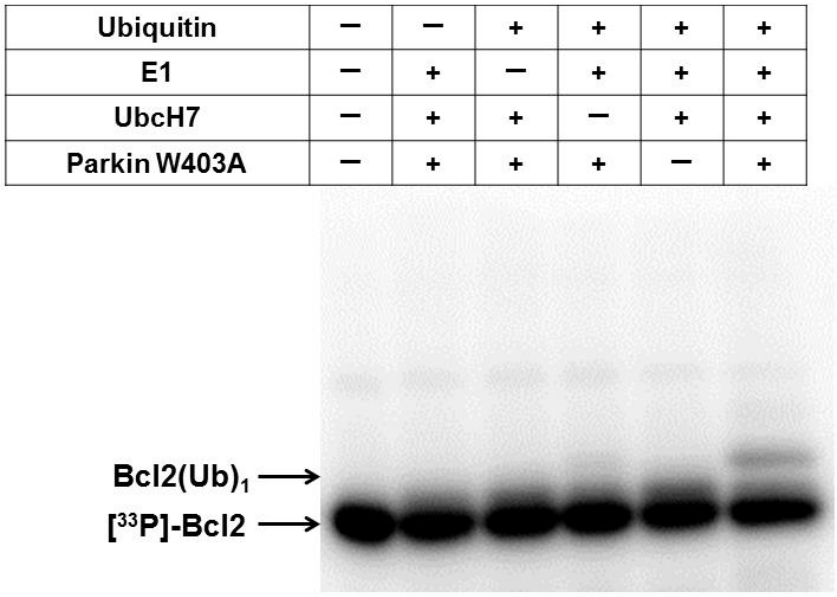

Figure 4.3: ***In vitro*** **ubiquitination of Bcl2.** Bcl2 was phosphorylated by pp-ERK2 in the presence of [γ–^{33}P]-ATP. [^{33}P]-Bcl2 ubiquitination reaction mixtures were incubated at 37°C for 3 hours and subsequently quenched with 6× SDS loading buffer. The resulting samples were analyzed by SDS-PAGE and phosphorimaging. Reactions were performed using 5 μM Parkin W403A.

A)

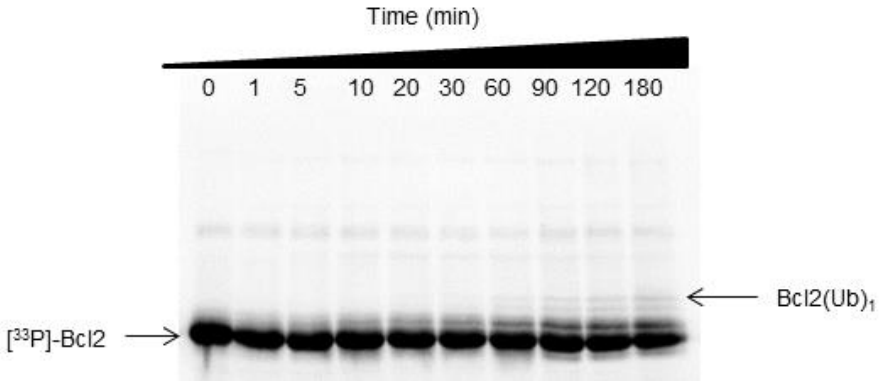

Parkin WT

B)

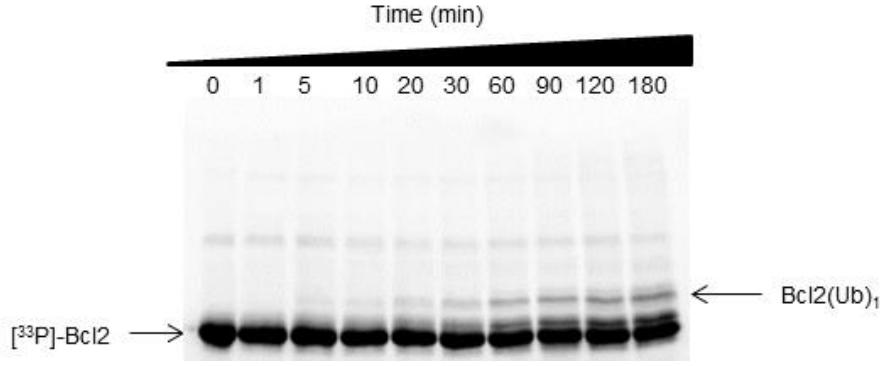

Parkin W403A

C)

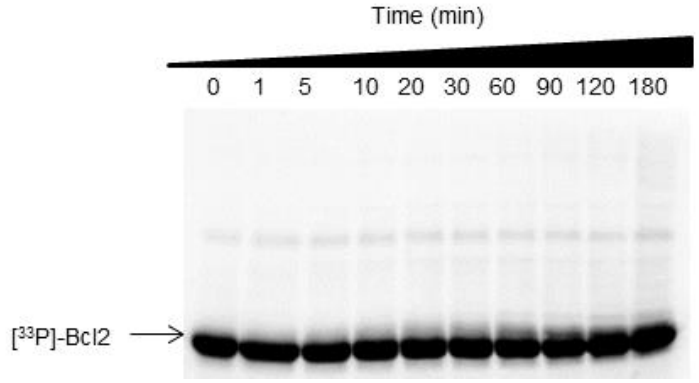

Parkin W403A-C431S

D)

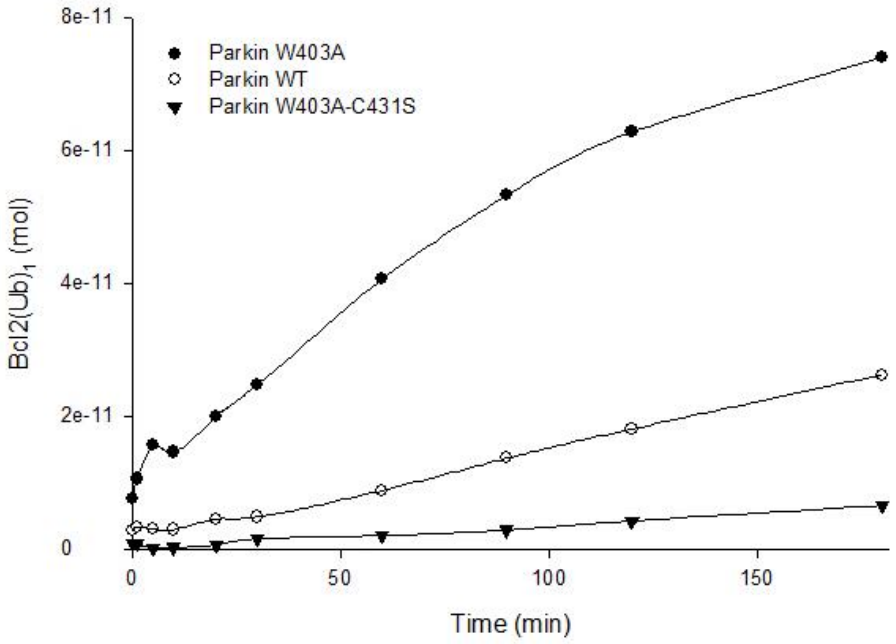

Figure 4.4: Time dependent ubiquitination of Bcl2. Times course experiments were performed by quenching the reaction mixtures with 6× SDS loading buffer at indicated times. Reactions were performed using 2.5 μM wild-type Parkin, Parkin W403A, and Parkin W403A-C431S.

represents mono-ubiquitination of Bcl2. Removing any one of the components necessary for ubiquitin transfer abrogated mono-ubiquitination of Bcl2. This allowed us to conclude that mono-ubiquitination of Bcl2 is Parkin dependent.

To see if the W403A mutation enhances *trans*-ubiquitination, we substituted wild-type GST-rParkin with GST-rParkin W403A in our *in vitro* ubiqutination assay. The substitution resulted in increased production of mono-ubiquitinated Bcl2. Omitting any one of the components necessary for ubiquitin transfer abrogated mono-ubiquitination of Bcl2 in this case as well (Figure 4.3). This led us to conclude that mutating Trp^{403} into an alanine results in a rate enhancement for *trans*-ubiquitination.

Parkin auto-ubiquitination activity was abolished upon converting the catalytic cysteine residue to a serine. We speculated that mutating Cys^{431} to serine would have a similar effect in the case of *trans*-ubiquitination. Time courses were run at intervals between 0 and 3 hours using Bcl2 as substrate and wild-type GST-rParkin, GST-rParkin W403A, GST-rParkin W403A-C431S as E3 ligase (Figure 4.4). The time course experiments in Figure 4.4 demonstrate that while GST-tagged rParkin W403A causes in increase in *trans*-ubiquitination activity, converting the highly conserved catalytic cysteine residue to a serine abrogates Parkin *trans*-ubiquitination activity.

4.3.2 Phosphorylation of Parkin results in its allosteric activation in *cis*

The E3 ligase activity of untagged Parkin is repressed through auto-inhibition (Chaugule et al. 2011; Matsuda et al. 2010; Riley et al 2013; Trempe et al 2013; Wauer and Komander2013). Untagged wild-type rParkin showed no apparent activity. Adding an N-

A)

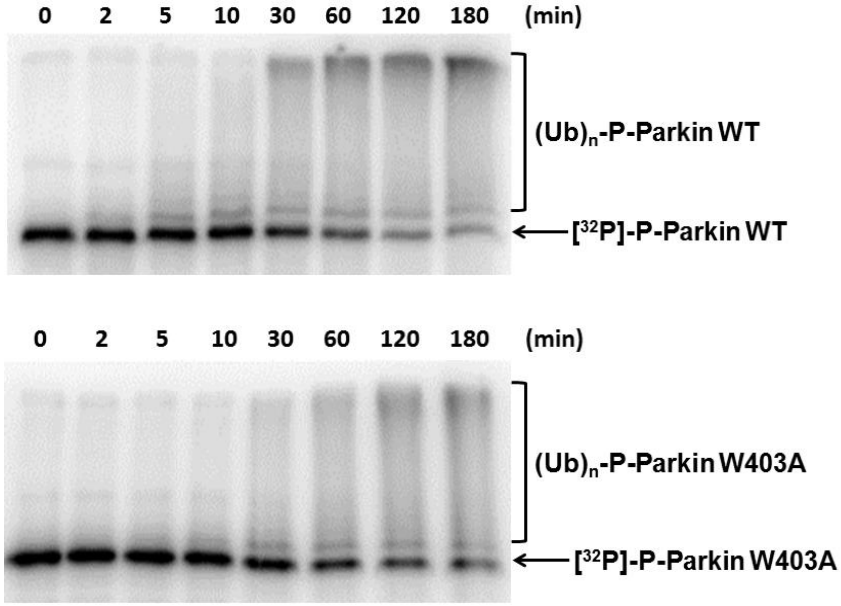

B)

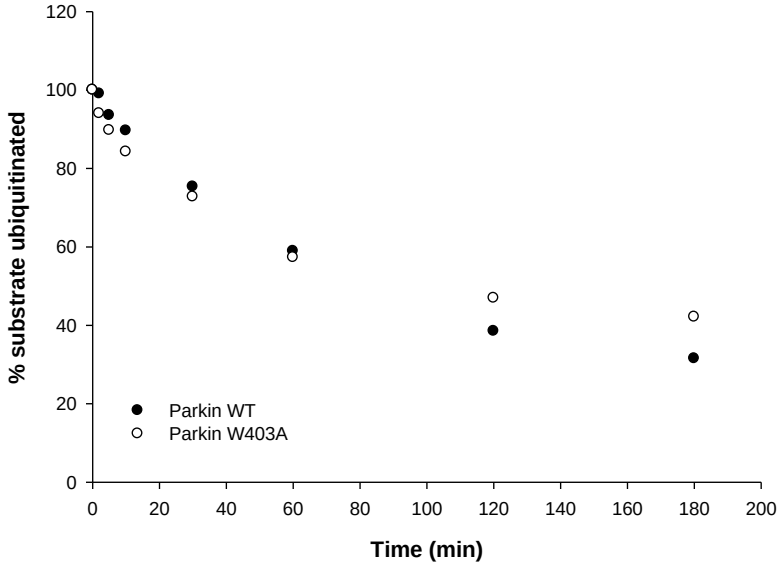

Figure 4.5: Time course of auto-ubiquitination of Parkin *in vitro*. (A) P^{32}-labeled recombinant wild-type and W403A Parkin were incubated with wild-type ubiquitin. Reactions were separated using SDS-PAGE followed by phosphorimaging analysis. (B) Individual bands were quantified using ImageJ.

A)

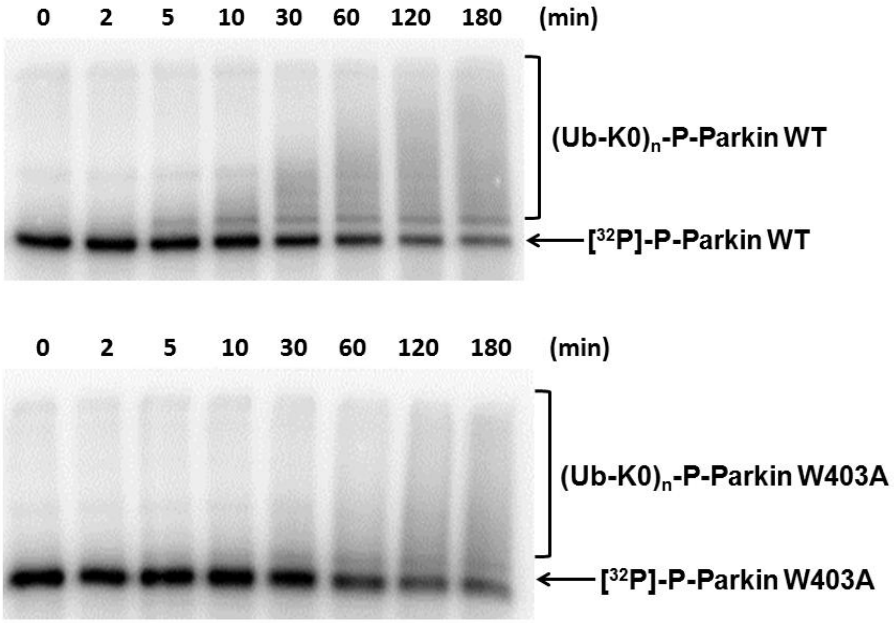

B)

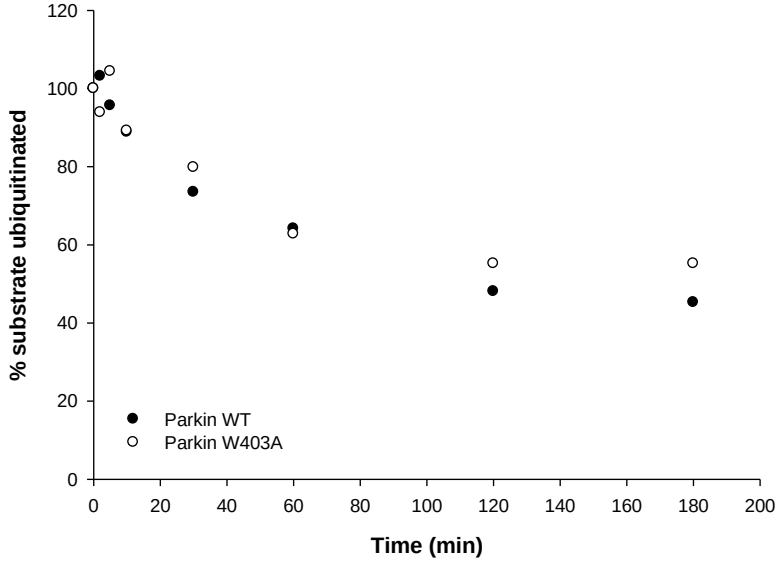

Figure 4.6: Time course of auto-ubiquitination of Parkin *in vitro*. (A) P^{32}-labeled recombinant wild-type and W403A Parkin were incubated with lysine-less ubiquitin (K0). Reaction mixtures were resolved via SDS-PAGE followed by phosphorimaging analysis. (B) Individual bands were quantified using ImageJ.

terminal tag such as GST induces a conformational change in Parkin that also changes its stability (Chaugule et al. 2011). It has been demonstrated that GST-tagged Parkin exhibits low but clear basal activity.

Previously, we have quantitatively demonstrated that PINK1 phosphorylates Parkin. It has recently been shown that Parkin is activated by PINK1-dependent phosphorylation of ubiquitin at Ser^{65} (Kazlauskaite et al. 2014). In this section, we hypothesize that phosphorylation of Parkin will activate the E3 ligase, thereby causing a rate increase in Parkin auto-ubiquitination activity. To test this hypothesis, GST-rParkin auto-ubiquitination time course experiments were carried out using phosphorylated GST-rParkin. Figures 4.5 and 4.6 show auto-ubiquitination time course experiments of phosphorylated wild-type and W403A GST-rParkin in the presence of wild-type or lysine-less ubiquitin (K0). In Figure 4.5, distinct high molecular weight poly-ubiquitination bands can be observed for both wild-type and W403A GST-rParkin when using wild-type ubiquitin. There was a shift in ubiquitination patterns when the reaction was carried out in the presence of ubiquitin-K0 for both wild-type GST-rParkin and GST-rParkin W403A. As expected, the high molecular weight poly-ubiquitination bands all but disappeared when only lysine-less ubiquitin was present in the reaction mixture. Wild-type Parkin contains 22 lysine residues. Since lysine-less ubiquitin cannot be poly-ubiquitinated, the higher molecular weight bands represent mono-ubiquitination at one or more separate lysine sites (Figure 4.6).

The overall disappearance rate of phosphorylated GST-rParkin was similar for both wild-type and W403A variants (Figure 4.5). This is not the case when using non-phosphorylated GST-rParkin variants. As a matter of fact, it has been shown that non-phosphorylated GST-tagged rParkin W403A self-ubiquitinates at an accelerated rate compared to non-phosphorylated GST-tagged wild-type rParkin (Trempe et al. 2013). The rate of disappearance of

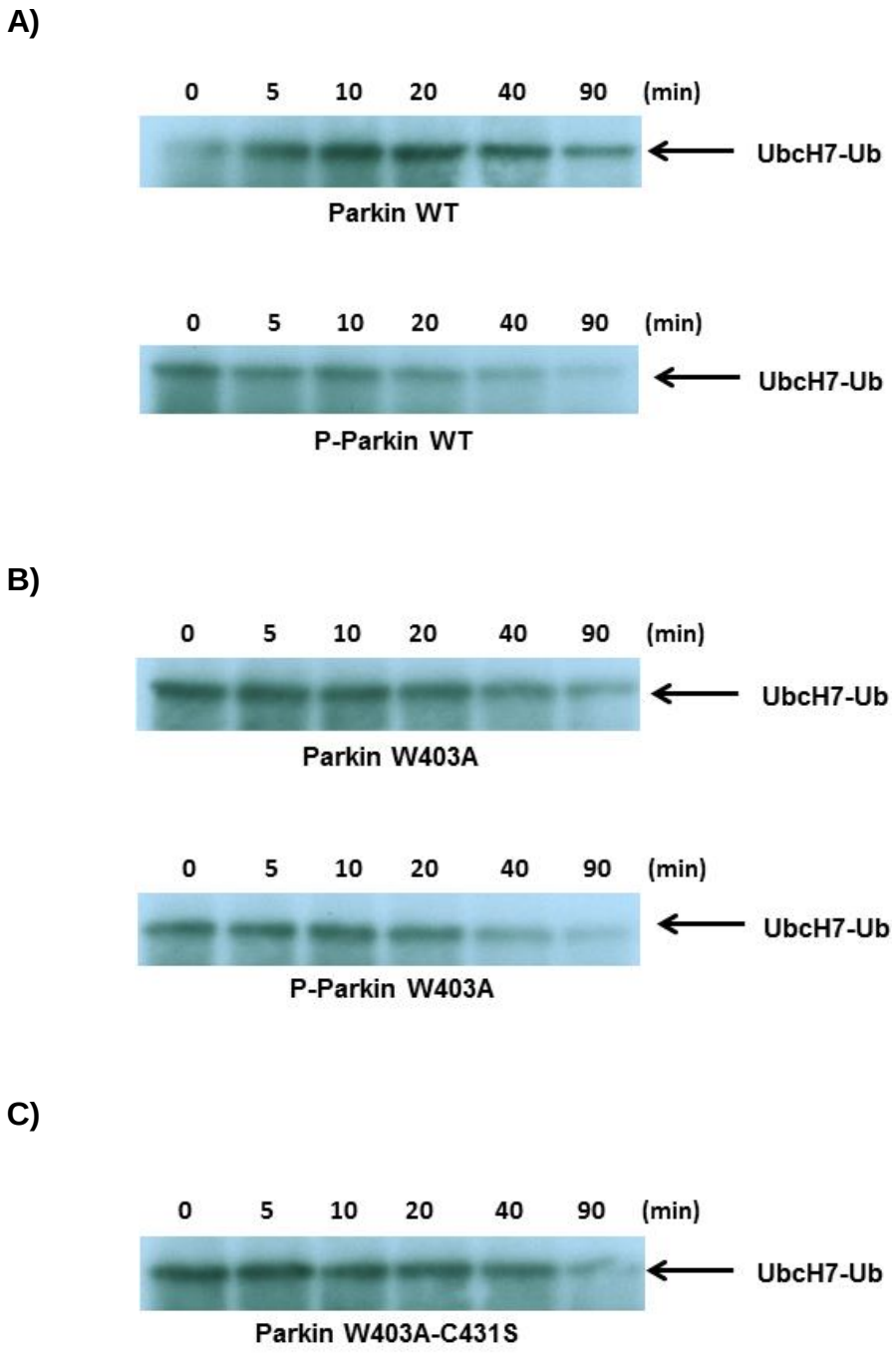

Figure 4.7: UbcH7~Ub thioester discharge assays. UbcH7 was charged with ubiquitin. Reactions were quenched using 10 mM EDTA. Parkin variants were added to the quenched reaction mixtures. Samples were analyzed using western blot analysis using anti-UbcH7 antibody.

phosphorylated GST-rParkin was similar between wild-type and W403A rParkin when using ubiquitin K0 as well.

We hypothesized that phosphorylation of wild-type GST-rParkin causes a conformational change in wild-type GST-rParkin that exposes the E2 binding site located on the RING1 domain, thereby making it more assessable to the E2 enzyme. To test this hypothesis, UbcH7~Ub thioester discharge assays were conducted using phosphorylated and non-phosphorylated versions of GST-rParkin wild-type, W403A, and W403A-C431S. The results in Figure 4.7 indicate that phosphorylating GST-rParkin accelerates the discharge of the thioester conjugate formed between ubiquitin and UbcH7 when using wild-type GST-rParkin or the W403A mutant. The levels of UbcH7~Ub remained constant when using GST-rParkin W403A-C431S as the E3 ligase. These findings further corroborate the hypothesis that phosphorylation of GST-rParkin causes the E2 binding site located on the RING1 domain to be exposed.

4.3.3 Phosphorylation of Parkin results in its allosteric activation in *trans*

To investigate the possibility that phosphorylation of GST-rParkin increases the rate of *trans*-ubiquitination, we ubiquitinated P^{32}-labeled Bcl2 using phosphorylated and non-phosphorylated GST-rParkin variants. In Figure 4.8, we can see that phosphorylation of wild-type GST-rParkin increases the levels of mono-ubiquitinated Bcl2 species produced. Phosphorylation of GST-rParkin W403A also causes an increase in mono-ubiquitinated Bcl2 species compared to when non-phosphorylated GST-rParkin W403A is used as the E3 ligase. The results allow us to conclude that, in the case of trans-ubiqutination, the effects of mutating Trp^{403} into an alanine and phosphorylating GST-rParkin are additive. The results suggest that in addition to making the E2 binding site on GST-rParkin more accessible, phosphorylation of

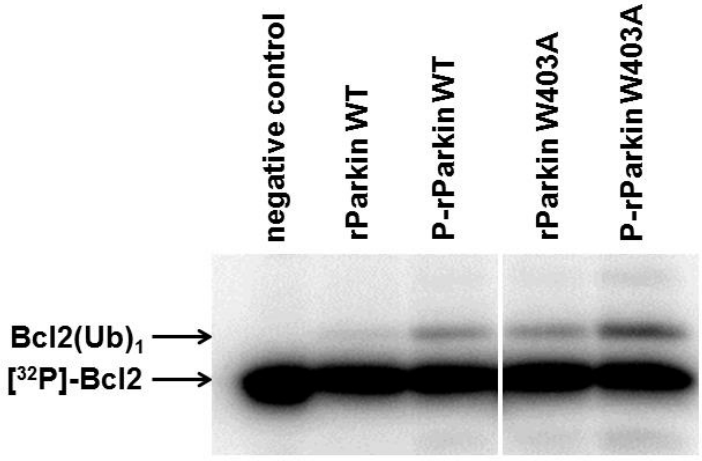

Figure 4.8: *In vitro* ubiquitination of Bcl2 using phosphorylated Parkin species. Bcl2 was phosphorylated by pp-ERK2 in the presence of [γ–^{33}P]-ATP. [^{33}P]-Bcl2 ubiquitination reaction mixtures were incubated at 37°C for 3 hours and subsequently quenched with 6× SDS loading buffer. The resulting samples were analyzed by SDS-PAGE and phosphorimaging. Reactions were performed using 5 μM rParkin variants.

GST-rParkin causes an allosteric shift in the ligase that enables it to interact with its substrate Bcl2 in a more effective manner.

4.4 Discussion

Phosphorylation is one of the most common posttranslational modifications. In both prokaryotic and eukaryotic cells, this modification causes enzymes and cell surface receptors to undergo global conformational changes. Phosphorylation oftentimes serves as a regulatory mechanism that causes proteins to become activated or deactivated, thereby altering their function and activity (Gallagher et al. 2006; Smith et al. 2009).

Since the discovery that Parkin exists in an auto-inhibited state, the question of how Parkin is activated has been under investigation. In the present study, we have demonstrated that phosphorylation of Parkin unlocks the auto-inhibited state of the E3 ligase, allowing both self-ubiquitination of Parkin and mono-ubiquitination of its substrate Bcl2. The crystal structure of rParkin determined by Trempe et al. shows that the REP domain blocks the Parkin E2 binding site (Trempe et al. 2013). Similar to the mutations that disrupt the interaction between the aforementioned sites, we believe that phosphorylation of the UBL domain increases the rate of ubiquitination at least in part by relieving steric hindrance imposed by the non-phosphorylated UBL domain and exposing the E2 binding site. In fact, our UbcH7~Ub thioester discharge assay results indeed provide evidence that phosphorylation of Parkin exposes its E2 binding site, which makes it more assessable to E2 ubiquitin-conjugating enzymes. We suspect that the change in Parkin activity is due to allosteric changes that occur upon phosphorylation of the protein. Clarifying the molecular mechanisms of Parkin activation will allow us to further understand the role Parkin plays in both familial and sporadic Parkinson's disease progression.

Cases have been reported where Parkin-mediated ubiquitination of substrates results in the substrates adapting degradation independent roles (Choi et al. 2003; Lim et al. 2005; Moore et al. 2008). Understanding such degradation independent roles may be crucial for the development of therapeutics that target Parkin dependent Parkinson's disease. At the present moment, the exact function Parkin mediated mono-ubiquitination of Bcl2 plays in Parkinson's disease remains a mystery.

4.5 References

Bekris L.M., Mata I.F., and Zabetian C.P. (2010) The genetics of Parkinson's disease. J. Geriatr. Psychiatry Neurol. ***23***, 228–242.

Burchell L., Chaugule V.K., Walden H. (2012) Small, N-terminal tags activate Parkin E3 ubiquitin ligase activity by disrupting its autoinhibited conformation. PLoS One. ***7***, e34748.

Casarejos M.J., Solano R.M., Rodriguez-Navarro J.A., Gómez A., Perucho J., Castaño J.G., García de Yébenes J., Mena M.A. (2009) Parkin deficiency increases the resistance of midbrain neurons and glia to mild proteasome inhibition: the role of autophagy and glutathione homeostasis. J. Neurochem. ***110***, 1523-1537.

Chaugule V.K., Burchell L., Barber K.R., Sidhu A., Leslie S.J., Shaw G.S., Walden H. (2011) Autoregulation of Parkin activity through its ubiquitin-like domain. EMBO J. ***30***, 2853-2867.

Chen D., Gao F., Li B., Wang H., Xu Y., Zhu C., Wang G. (2010) Parkin mono-ubiquitinates Bcl-2 and regulates autophagy. J. Biol. Chem. ***285***, 38214-38223.

Chin L.S., Olzmann J.A., Li L. (2010) Parkin-mediated ubiquitin signaling in aggresome formation and autophagy. Biochem. Soc. Trans. ***38***, 144-149.

Choi P., Snyder H., Petrucelli L., Theisler C., Chong M., Zhang Y., Lim K., Chung K.K., Kehoe K., D'Adamio L., Lee J.M., Cochran E., Bowser R., Dawson T.M., Wolozin B. (2003) SEPT5_v2 is a parkin-binding protein. Brain Res. Mol. Brain Res. ***117***, 179-189.

Chung K.K., Zhang Y., Lim K.L., Tanaka Y., Huang H., Gao J., Ross C.A., Dawson V.L., Dawson T.M. (2001) Parkin ubiquitinates the alpha-synuclein-interacting protein, synphilin-1: implications for Lewy-body formation in Parkinson disease. Nat. Med. ***7***, 1144-1150.

Corti O., Hampe C., Koutnikova H., Darios F., Jacquier S., Prigent A., Robinson J.C., Pradier L, Ruberg M, Mirande M, Hirsch E, Rooney T, Fournier A, Brice A. (2003) The p38 subunit of the aminoacyl-tRNA synthetase complex is a Parkin substrate: linking protein biosynthesis and neurodegeneration. Hum. Mol. Genet. ***12***, 1427-1437.

Dächsel J.C., Lücking C.B., Deeg S., Schultz E., Lalowski M, Casademunt E, Corti O, Hampe C, Patenge N, Vaupel K, Yamamoto A, Dichgans M, Brice A, Wanker EE, Kahle PJ, Gasser T. (2005) Parkin interacts with the proteasome subunit alpha4. FEBS Lett. ***579***, 3913-3919.

Darios F., Corti O., Lücking C.B., Hampe C., Muriel M.P., Abbas N., Gu W.J., Hirsch E.C., Rooney T., Ruberg M., Brice A. (2003) Parkin prevents mitochondrial swelling and cytochrome c release in mitochondria-dependent cell death. Hum. Mol. Genet. ***12***, 517-526.

Decuypere J.P., Parys J.B., Bultynck G. (2012) Regulation of the Autophagic Bcl-2/Beclin 1 Interaction. Cells ***1***, 284-312

Doss-Pepe E.W., Chen L., Madura K. (2005) Alpha-synuclein and parkin contribute to the assembly of ubiquitin lysine 63-linked multiubiquitin chains. J. Biol. Chem. ***280***, 16619-16624.

Fallon L., Bélanger C.M., Corera A.T., Kontogiannea M., Regan-Klapisz E., Moreau F., Voortman J., Haber M., Rouleau G., Thorarinsdottir T., Brice A., van Bergen En Henegouwen P.M., Fon E.A. (2006) A regulated interaction with the UIM protein Eps15 implicates parkin in EGF receptor trafficking and PI(3)K-Akt signalling. Nat. Cell Biol. ***8***, 834-842.

Fallon L., Moreau F., Croft B.G., Labib N., Gu W.J., Fon E.A. (2002) Parkin and CASK/LIN-2 associate via a PDZ-mediated interaction and are co-localized in lipid rafts and postsynaptic densities in brain. J. Biol. Chem. ***277***, 486-491.

Gallagher E., Gao M., Liu Y.C., Karin M. (2006) Activation of the E3 ubiquitin ligase Itch through a phosphorylation-induced conformational change. Proc. Natl. Acad. Sci. USA ***103***, 1717-1722.

Geisler S., Holmström K.M., Skujat D., Fiesel F.C., Rothfuss O.C., Kahle P.J., Springer W. (2010) PINK1/Parkin-mediated mitophagy is dependent on VDAC1 and p62/SQSTM1. Nat. Cell Biol. ***12***, 119-131.

Hampe C., Ardila-Osorio H., Fournier M., Brice A., Corti O. (2006) Biochemical analysis of Parkinson's disease-causing variants of Parkin, an E3 ubiquitin-protein ligase with monoubiquitylation capacity. Hum. Mol. Genet. ***15***, 2059-2075.

Hara T., Nakamura K., Matsui M., Yamamoto A., Nakahara Y., Suzuki-Migishima R., Yokoyama M., Mishima K., Saito I., Okano H., Mizushima N. (2006) Suppression of basal autophagy in neural cells causes neurodegenerative disease in mice. Nature ***441***, 885-889.

Hardy J. (2010) Genetic analysis of pathways to Parkinson disease. Neuron ***68***, 201–206.

Henn I.H., Gostner J.M., Lackner P., Tatzelt J., Winklhofer K.F. (2005) Pathogenic mutations inactivate parkin by distinct mechanisms. J. Neurochem. ***92***, 114-122.

Hristova V.A., Beasley S.A., Rylett R.J., Shaw G.S. (2009) Identification of a novel Zn2+-binding domain in the autosomal recessive juvenile Parkinson-related E3 ligaseparkin. J. Biol. Chem. ***284***, 14978-14986.

Huynh D.P., Scoles D.R., Nguyen D., Pulst S.M. (2003) The autosomal recessive juvenile Parkinson disease gene product, parkin, interacts with and ubiquitinates synaptotagmin XI. Hum. Mol. Genet. ***12***, 2587-2597.

Imai Y., Soda M., Inoue H., Hattori N., Mizuno Y., Takahashi R. (2001) An unfolded putative transmembrane polypeptide, which can lead to endoplasmic reticulum stress, is a substrate of Parkin. Cell ***105***, 891-902.

Jin S.M., Youle R.J. (2012) Pink1- and parkin-mediated mitophagy at a glance. J. Cell Sci. ***125***, 795-799.

Kalia S.K., Lee S., Smith P.D., Liu L., Crocker S.J., Thorarinsdottir T.E., Glover J.R., Fon E.A., Park D.S., Lozano A.M. (2004) BAG5 inhibits parkin and enhances dopaminergic neuron degeneration. Neuron ***44***, 931-945.

Kang R., Zeh H.J., Lotze M.T., Tang D. (2011) The Beclin 1 network regulates autophagy and apoptosis. Cell Death Differ. ***18***, 571-580.

Kazlauskaite A., Kondapalli C., Gourlay R., Campbell D.G., Ritorto M.S., Hofmann K., Alessi D.R., Knebel A., Trost M., Muqit M.M. (2014) Parkin is activated by PINK1-dependent phosphorylation of ubiquitin at Ser^{65}. Biochem. J. ***460***, 127-139.

Kitada T., Asakawa S., Hattori N., Matsumine H., Yamamura Y., Minoshima S., Yokochi M., Mizuno Y., Shimizu N. (1998) Mutations in the Parkin gene cause autosomal recessive juvenile parkinsonism. Nature ***392***, 605-608.

Ko H.S., von Coelln R., Sriram S.R., Kim S.W., Chung K.K., Pletnikova O., Troncoso J., Johnson B., Saffary R., Goh E.L., Song H., Park B.J., Kim M.J., Kim S., Dawson V.L., Dawson T.M. (2005) Accumulation of the authentic parkin substrate aminoacyl-tRNA synthetase cofactor, p38/JTV-1, leads to catecholaminergic cell death. J. Neurosci. ***25***, 7968-7978.

Ko H.S., Kim S.W., Sriram S.R., Dawson V.L., Dawson T.M. (2006) Identification of far upstream element-binding protein-1 as an authentic Parkin substrate. J. Biol. Chem. ***281***, 16193-16196.

Komatsu M., Waguri S., Chiba T., Murata S., Iwata J., Tanida I., Ueno T., Koike M., Uchiyama Y., Kominami E., Tanaka K. (2006) Loss of autophagy in the central nervous system causes neurodegeneration in mice. Nature ***441***, 880-884.

Kondapalli C., Kazlauskaite A., Zhang N., Woodroof H.I., Campbell D.G., Gourlay R., Burchell L., Walden H., Macartney T.J., Deak M., Knebel A., Alessi D.R., Muqit MM. (2012) PINK1 is activated by mitochondrial membrane potential depolarization and stimulates Prkin E3 ligase activity by phosphorylating $Serine^{65}$. Open Biol. ***2***, 120080.

Kuroda Y., Mitsui T., Kunishige M., Shono M., Akaike M., Azuma H., Matsumoto T. (2006) Parkin enhances mitochondrial biogenesis in proliferating cells. Hum. Mol. Genet. ***15***, 883-895.

Lim K.L., Chew K.C., Tan J.M., Wang C., Chung K.K., Zhang Y., Tanaka Y., Smith W., Engelender S., Ross C.A., Dawson V.L., Dawson T.M. (2005) Parkin mediates nonclassical,

proteasomal-independent ubiquitination of synphilin-1: implications for Lewy body formation. J. Neurosci. ***25***, 2002-2009.

Lucking C.B., Abbas N., Durr A., Bonifati V., Bonnet A.M., de Broucker T., de Michele G., Wood N.W., Agid Y., Brice A. (1998) Homozygous deletions in parkin gene in European and North African families with autosomal recessive juvenile parkinsonism. The European Consortium on Genetic Susceptibility in Parkinson's Disease and the French Parkinson's Disease Genetics Study Group. Lancet ***352***, 1355–1356.

Maiuri M.C., Le Toumelin G., Criollo A., Rain, J.C., Gautier, F., Juin P., Tasdemir E., Pierron G., Troulinaki K., Tavernarakis N., Hickman J.A., Geneste O., Kroemer G. (2007) Functional and physical interaction between Bcl-x(L) and a BH3-like domain in Beclin-1. EMBO J. ***26***, 2527-2539.

Martin I., Dawson V.L., Dawson T.M. (2011) Recent advances in the genetics of Parkinson's disease. Annu. Rev. Genomics Hum. Genet. ***12***, 301–325.

Matsuda N., Kitami T., Suzuki T., Mizuno Y., Hattori N., Tanaka K. (2006) Diverse effects of pathogenic mutations of Parkin that catalyze multiple monoubiquitylation *in vitro*. J. Biol Chem. ***281***, 3204-3209.

Matsuda N., Sato S., Shiba K., Okatsu K., Saisho K., Gautier C.A., Sou Y.S., Saiki S., Kawajiri S., Sato F., Kimura M., Komatsu M., Hattori N., Tanaka K. (2010) PINK1 stabilized by mitochondrial depolarization recruits Parkin to damaged mitochondria and activates latent Parkin for mitophagy. J. Cell Biol. ***189***, 211-221.

Moore D.J., West A.B., Dikeman D.A., Dawson V.L., Dawson T.M. (2008) Parkin mediates the degradation-independent ubiquitination of Hsp70. J. Neurochem. ***105***, 1806-1819.

Moore D.J., Zhang L., Troncoso J., Lee M.K., Hattori N., Mizuno Y., Dawson T.M., Dawson V.L. (2005) Association of DJ-1 and parkin mediated by pathogenic DJ-1 mutations and oxidative stress. Hum. Mol. Genet. ***14***, 71-84.

Narendra D., Kane L.A., Hauser D.N., Fearnley I.M., Youle R.J. (2010) p62/SQSTM1 is required for Parkin-induced mitochondrial clustering but not mitophagy; VDAC1 is dispensable for both. Autophagy ***6***, 1090–1106.

Narendra D., Tanaka A., Suen D.F., Youle R.J. (2008) Parkin is recruited selectively to impaired mitochondria and promotes their autophagy. J. Cell Biol. ***183***, 795–803.

Oberstein A., Jeffrey P.D., Shi Y. (2007) Crystal structure of the Bcl-xL-Beclin 1 peptide complex: Beclin 1 is a novel BH3-only protein. J. Biol. Chem. ***282***, 13123-13132.

Oliveira S.A., Scott W.K., Martin E.R., Nance M.A., Watts R.L., Hubble J.P., Koller W.C., Pahwa R., Stern M.B., Hiner B.C., Ondo W.G., Allen F.H. Jr, Scott B.L., Goetz

C.G., Small G.W., Mastaglia F., Stajich J.M., Zhang F., Booze M.W., Winn M.P., Middleton L.T., Haines J.L., Pericak-Vance M.A., Vance J.M. (2003) Parkin mutations and susceptibility alleles in late-onset Parkinson's disease. Ann. Neurol. ***53***, 624-629.

Olzmann J.A., Li L., Chudaev M.V., Chen J., Perez F.A., Palmiter R.D., Chin L.S. (2007) Parkin-mediated K63-linked polyubiquitination targets misfolded DJ-1 to aggresomes via binding to HDAC6. J. Cell Biol. ***178***, 1025-1038.

Pattingre S., Tassa A., Qu X., Garuti R., Liang X.H., Mizushima N., Packer M., Schneider M.D., Levine B. (2005) Bcl-2 antiapoptotic proteins inhibit Beclin 1-dependent autophagy. Cell ***122***, 927-939.

Poole A.C., Thomas R.E., Andrews L.A., McBride H.M., Whitworth A.J., Pallanck L.J. (2008) The PINK1/Parkin pathway regulates mitochondrial morphology. Proc. Natl. Acad. Sci. USA ***105***, 1638-1643.

Quadri M., Fang M., Picillo M., Olgiati S., Breedveld G.J., Graafland J., Wu B., Xu F., Erro R., Amboni M., Pappatà S., Quarantelli M., Annesi G., Quattrone A., Chien H.F., Barbosa E.R., Oostra B.A., Barone P., Wang J., Bonifati V. (2013) Mutation in the SYNJ1 gene associated with autosomal recessive, early-onset Parkinsonism. Hum. Mutat. ***34***, 1208-1215.

Ren Y., Zhao J., Feng J. (2003) Parkin binds to alpha/beta tubulin and increases their ubiquitination and degradation. J. Neurosci. ***23***, 3316-3324.

Riley B.E., Lougheed J.C., Callaway K., Velasquez M., Brecht E., Nguyen L., Shaler T., Walker D., Yang Y., Regnstrom K., Diep L., Zhang Z., Chiou S., Bova M., Artis D.R., Yao N., Baker J., Yednock T., Johnston J.A. (2013) Structure and function of Parkin E3 ubiquitin ligase reveals aspects of RING and HECT ligases. Nat. Commun. ***4***, 1982.

Sakata E., Yamaguchi Y., Kurimoto E., Kikuchi J., Yokoyama S., Yamada S., Kawahara H., Yokosawa H., Hattori N., Mizuno Y., Tanaka K., Kato K. (2003) Parkin binds the Rpn10 subunit of 26S proteasomes through its ubiquitin-like domain. EMBO ***4***, 301-306.

Sato S., Chiba T., Sakata E., Kato K., Mizuno Y., Hattori N., Tanaka K. (2006) 14-3-3eta is a novel regulator of parkin ubiquitin ligase. EMBO J. ***25***, 211-221.

Shimura H., Hattori N., Kubo S., Mizuno Y., Asakawa S., Minoshima S., Shimizu N., Iwai K., Chiba T., Tanaka K., Suzuki T. (2000) Familial Parkinson disease gene product, parkin, is a ubiquitin-protein ligase. Nat. Genet. ***25***, 302–305.

Shimura H., Hattori N., Kubo S., Yoshikawa M., Kitada T., Matsumine H., Asakawa S., Minoshima S., Yamamura Y., Shimizu N., Mizuno Y. (1999) Immunohistochemical and subcellular localization of Parkin protein: absence of protein in autosomal recessive juvenile parkinsonism patients. Ann. Neurol. ***45***, 668-672.

Shimura H., Schlossmacher M.G., Hattori N., Frosch M.P., Trockenbacher A., Schneider R., Mizuno Y., Kosik K.S., Selkoe D.J. (2001) Ubiquitination of a new form of alpha-synuclein by parkin from human brain: implications for Parkinson's disease. Science ***293***, 263-269.

Smith H., Peggie M., Campbell D.G., Vandermoere F., Carrick E., Cohen P. (2009) Identification of the phosphorylation sites on the E3 ubiquitin ligase Pellino that are critical for activation by IRAK1 and IRAK4. Proc. Natl. Acad. Sci. USA ***106***, 4584-4590.

Staropoli J.F., McDermott C., Martinat C., Schulman B., Demireva E., Abeliovich A. (2003) Parkin is a component of an SCF-like ubiquitin ligase complex and protects postmitotic neurons from kainate excitotoxicity. Neuron ***37***, 735-749.

Trempe J.F., Sauve V., Grenier K., Serafi M., Tang M.Y., Menade M., Al-Abdul-Wahid S., Krett J., Wong K., Kozlov G., Nagar B., Fon E.A., and Gehring K. (2013) Structure of parkin reveals mechanisms for ubiquitin ligase activation. Science ***340***, 1451-1455.

Um J.W., Min D.S., Rhim H., Kim J., Paik S.R., Chung K.C. (2006) Parkin ubiquitinates and promotes the degradation of RanBP2. J. Biol. Chem. ***281***, 3595-3603.

Wauer T., Komander D. (2013) Structure of the human Parkin ligase domain in an autoinhibited state. EMBO J. ***32***, 2099-2112.

Wenzel D.M., Lissounov A., Brzovic P.S., Klevit R.E. (2011) UBCH7 reactivity profile reveals parkin and HHARI to be RING/HECT hybrids. Nature ***474***, 105-108.

Williams A, Jahreiss L, Sarkar S, Saiki S, Menzies FM, Ravikumar B, Rubinsztein DC. (2006) Aggregate-prone proteins are cleared from the cytosol by autophagy: therapeutic implications. Curr. Top. Dev. Biol. ***76***, 89-101.

Yang J., Liu X., Bhalla K., Kim C.N., Ibrado A.M., Cai J., Peng T.I., Jones D.P., Wang X. (1997) Prevention of apoptosis by Bcl-2: release of cytochrome c from mitochondria blocked. Science. ***275***, 1129-1132.

Zhang Y., Gao J., Chung K.K., Huang H., Dawson V.L., Dawson T.M. (2000) Parkin functions as an E2-dependent ubiquitin- protein ligase and promotes the degradation of the synaptic vesicle-associated protein, CDCrel-1. Proc. Natl. Acad. Sci. USA ***97***, 13354–13359.

CHAPTER 5

CONCLUSIONS AND FUTURE DIRECTIONS

Parkinson's disease occurs from the premature death of dopamine neurons. Cancer results from inappropriate cell survival. Therefore, one would expect their pathogenic mechanisms to differ greatly, but this is not the case. Despite their striking differences, overlapping pathways are involved in cancer and Parkinson's disease. In particular, genetic studies of familial Parkinson's disease have shed light to the fact that the involved genes are also linked to cancer. This may be a direct result of cancer cells being prone to accumulating mutations. However, it is difficult to overlook the functional roles of the overlapping genes. In the case of the PARK2 gene, recessive mutations cause autosomal recessive Parkinson's disease. Mutations in the same gene have also been found in glioblastoma, colorectal and lung cancer (Veeriah et al. 2010). Such areas of convergence will provide insights into both diseases.

In recent years, a study performed by Martin et al. advocates the development of PINK1 inhibitors to treat colorectal cancer carrying mutations in the mismatch repair genes MSH2, MLH1 and MSH6 (Martin et al. 2011). The primary issue with such treatment options is the likelihood of the inhibitor inducing Parkinson's disease. However, literature in the field suggests that short periods of exposure to such compounds would carry only a small risk as opposed to long term drug administration (Woodroof et al. 2011).

In this thesis, we reconstituted *in vitro* ubiquitination assays involving the E3 ligases SCF^{Fbx4} and Parkin. We are the first in the field to generate structure-based computationally derived peptide inhibitors that disrupt the binding interface between SCF^{Fbx4} and it substrate

TRF1. Our studies on Parkin, on the other hand, provide insight into how post-translational modifications such as phosphorylation can affect E3 ubiquitin ligase activity.

It has been established that Parkin plays a large and complex role in the physiology of the cell. Up to date, a large number of Parkin substrates have been discovered and the list is constantly growing. We expect that studying such substrates in Parkin or PINK1 knockout cells will provide crucial insight into the pathogenesis of Parkinson's disease. It may also be worthwhile to identify substrates of phosphorylated Parkin *in vivo*. Investigating which of these substrates are most commonly defective in Parkinson's patients may help us prioritize pathways for therapeutic targeting.

In Chapter 4, we have demonstrated that phosphorylation at Ser^{65} causes allosteric activation of Parkin. Given the fact that loss-of-function mutations of Parkin cause Parkinson's disease, as a treatment strategy, it may even be possible to screen for small molecules that activate Parkin by mimicking phosphorylation-dependent conformational changes upon the compound binding to Ser^{65}. In addition, it would also be interesting to investigate whether or not Bcl2 can be poly-ubiquitinated *in vivo* by E3 ubiquitin ligases other than Parkin. It may very well be that mono-ubiquitination of Bcl2 targets the protein for poly-ubiquitination by other E3 ubiquitin ligases.

Ubiquitination reactions are largely mediated via protein-protein interactions. Traditionally, drug targets have been enzyme-substrate interactions that involve deep binding pockets. In the last decade, protein-protein interactions with large binding interfaces have emerged as important targets for drug development and design. Peptides are promising candidates in targeting these large binding interfaces due to their relatively large size compared

to traditional small molecule drugs. In addition, peptides can serve as valuable therapeutic leads that can be modified to increase specificity and potency.

However, peptide drugs have weaknesses such as high cost and short half-life resulting from proteolysis in a biological setting. In the past, peptidomimetics have been used to mimic structural elements of proteins (Craik et al. 2013). Peptidomimetics oftentimes involve changes to peptides such as altered backbones and incorporation of non-natural amino acids. Such changes result in potent inhibitors that are stable *in vivo*. In several instances, chemical staples have been used to stabilize peptides to prevent the proteolytic cleavage of promising leads. Furthermore, peptide inhibitors such as those described in Chapter 2 can be used to study protein-protein interactions. For instance, crosslinking peptide inhibitors with their protein binding sites will allow us to isolate and characterize peptide-protein complexes. Such studies will provide clues for future small molecule inhibitor design.

It is important to note that most compounds that block protein-protein interactions do so at relatively high concentrations. Therefore, it may also be worthwhile to simultaneously target elements of ubiquitination associated pathways. For instance, proteins that require ATP, such as Nae1 (Nedd8 activating enzyme), may prove to be a good targets - given the success of targeting kinases (Garber et al. 2005). The caveat is that targeting such proteins may turn out to be a less specific approach than targeting E3 ligases.

The ubiquitination pathway plays a regulatory role in virtually all mammalian cells. Recent advances in the field have enhanced our understanding of the innate complexity of the ubiquitination pathway. Structural information on ubiquitin ligases and their substrates is becoming more abundant than ever before, which makes selective targeting of ubiquitin E3 ligases and their substrates a promising and potentially abundant avenue for drug development -

not to mention that a better understanding of ubiquitin E3 ligases and their substrates will provide crucial insight into the natural progression of common and rare diseases alike. With numerous areas of the ubiquitination class of signaling pathways still unexplored, an important goal is to discover new correlations between the ubiquitination pathway and human illnesses.

The outlook for utilizing the ubiquitination pathway is optimistic. The most pressing issue is to develop highly specific anti-cancer drugs, and the clinical benefits must outweigh the side effects. However, to achieve such goals, we must thoroughly understand how ubiquitination controls protein function, activity, and localization - in addition to how the signal is propagated to regulate downstream cellular events. With similarities to phosphorylation, ubiquitination is emerging as an underexploited mechanism. In the age of molecular-targeted therapies for cancer, Parkinson's, and numerous other diseases, designing drugs against components of the ubiquitin system seems more feasible than ever.

5.2 References

Craik D.J., Fairlie D.P., Liras S., Price D. (2013) The future of peptide-based drugs. Chem. Biol. Drug Des. ***81,*** 136-147.

Garber K. (2005) Missing the target: ubiquitin ligase drugs stall. J. Natl. Cancer Inst. ***97,*** 166-167.

Martin S.A., Hewish M., Sims D., Lord C.J., Ashworth A. (2011) Parallel high-throughput RNA interference screens identify PINK1 as a potential therapeutic target for the treatment of DNA mismatch repair-deficient cancers. Cancer Res. ***71***, 1836-1848.

Veeriah S., Taylor B.S., Meng S., Fang F., Yilmaz E., Vivanco I., Janakiraman M., Schultz N., Hanrahan A.J., Pao W., Ladanyi M., Sander C., Heguy A., Holland E.C., Paty P.B., Mischel P.S., Liau L., Cloughesy T.F., Mellinghoff I.K., Solit D.B., Chan T.A. (2010) Somatic mutations of the Parkinson's disease-associated gene PARK2 in glioblastoma and other human malignancies. Nat. Genet. ***42***, 77-82.

Woodroof H.I., Pogson J.H., Begley M., Cantley L.C., Deak M., Campbell D.G., van Aalten D.M., Whitworth A.J., Alessi D.R., Muqit M.M. (2011) Discovery of catalytically active orthologues of the Parkinson's disease kinase PINK1: analysis of substrate specificity and impact of mutations. Open Biol. ***1***, 110012.

APPENDIX

CHARACTERIZATION OF SMALL MOLECULE INHIBITORS THAT DISRUPT THE SKP2-CKS1 INTERACTION

A.1 Introduction

Decreased levels of the cell cycle inhibitor $p27^{Kip1}$ are observed in a variety of human tumor cells. In fact, $p27^{Kip1}$ levels can serve as a therapeutic marker for cancer survival, where low levels of $p27^{Kip1}$ indicate poor prognosis in patients (Benmaamar 2003; Chu et al. 2008; Pagano and Hiramatsu et al. 2006; Slingerland and Pagano 2000). Decreased levels of $p27^{Kip1}$ can be caused by excessive degradation of $p27^{Kip1}$. Re-expressing $p27^{Kip1}$ in tumor cells has been shown to induce their apoptosis (Chen et al. 1996; Craig et al. 1997). Therefore, increasing $p27^{Kip1}$ levels may serve as an effective route of therapeutic intervention to suppress tumor growth.

$p27^{Kip}$ ubiquitination and subsequent degradation is regulated by the E3 ligase SCF^{Skp2}. SCF^{Skp2} recognizes and targets T187-phosphorylated $p27^{Kip1}$ to the proteasome for degradation (Nakayama and Nakayama 2006). Contact with CDK2/cyclin E or CDK2/cyclin A is also required for $p27^{Kip1}$ ubiquitination to occur (Montagnoli et al. 1999; Ungermannova et al. 2005). $p27^{Kip1}$ is unique in that it requires the accessory protein Cks1 to be recognized and ubiquitinated by its E3 ligase SCF^{Skp2}. As a matter of fact, Cks1 functions as the central adaptor protein that binds to the CDK/Cyclin complex, phosphorylated $p27^{Kip}$, and Skp2 (Hao et al. 2005; Sitry et al. 2002; Wang et al. 2004). Therefore, perturbation of the Skp1-Cks1 interaction may prove to be an effective anti-cancer strategy. Here we use a high-throughput AlphaScreen (PerkinElmer) assay to discover small molecule inhibitors that disrupt the Skp2-Cks1 binding interaction.

A)

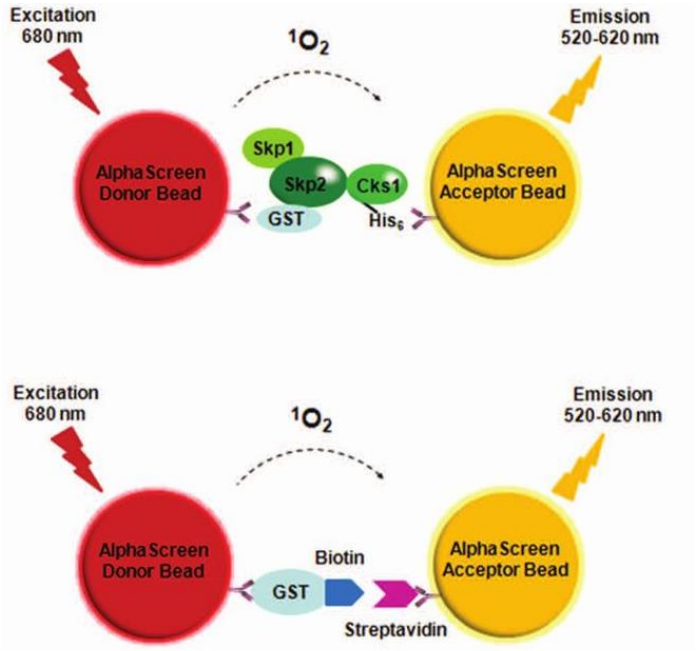

B)

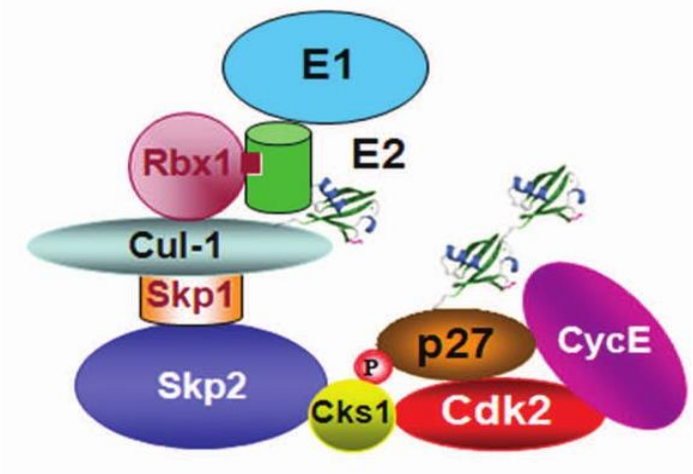

Figure A.1: AlphaScreen assay to detect Skp2-Cks1 interactions. (A) Beads are brought together when GST–Skp2/Skp2 binds to His_6-Cks1. Donor beads generate singlet oxygen molecules upon excitation at 680 nm. The singlet oxygen molecules then diffuse to the acceptor beads, generating chemiluminescence. For the counterscreen assay, donor beads conjugated to GST-biotin served as the interacting partner for streptavidin-conjugated acceptor beads (B) Schematic diagram of the SCF^{Skp2}-dependent p27 ubiquitination pathway.

A.2 Materials and Methods

AlphaScreen assays were carried out using OptiPlate-384 (PerkinElmer) plates in a total volume of 25 μL per well. All dilutions were made in 1X AlphaScreen assay buffer containing 50 mM Tris (pH 7.4), 150 mM NaCl, 0.05% bovine serum albumin (BSA), 0.02% Tween, and 1 mM DTT. After mixing GST-Skp2/Skp1 with His_6-Cks1, the assay plate was incubated at room temperature for 1 hour. Subsequently, glutathione donor beads and nickel chelate acceptor beads were added to each well (20 μg/mL working concentration for each bead). Plates were then sealed and incubated while shaking in the dark at room temperature. After a 2.5 hour incubation, the beads were excited at a wavelength of 680 nm, with emission detected at 520 to 620 nm using a EnVision 2102 Multilabel Reader (PerkinElmer). IC_{50} values of the small molecule inhibitors were determined by adding final concentrations of 20 nM GST-Skp2/Skp1 and 200 nM His_6-Cks1 to each well. Curves were fit using SigmaPlot 5.0 software (SPSS Inc.). Since signal suppression can occur from on-target events or false positives, a counterscreening assay was performed to validate the hits from the primary screen. This assay was carried out using GST-biotin conjugated to donor beads and streptavidin-conjugated acceptor beads (Figure A.1).

A.3 Results

Two structurally related compounds (NSC689857 and NSC681152) that disrupt the Skp2-Cks1 interaction were identified by Dana Ungermannova. Several analogues of NSC689857 (857) were generated by Dr. Gan Zhang to identify the pharmacophore - quinone (Q857), two oxidation-blocking analogues that were generated by nonselective methylation (E857, A857), methylhydroquinone (MHQ), and 1,4-benzoquinone (BQ). I tested the analogues

Compound	Structure	Inhibition of Skp2-Cks1 IC_{50} (μM)
857	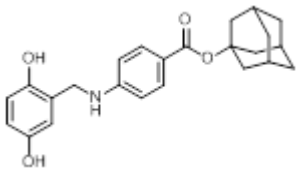	36 ± 6.2
Q857	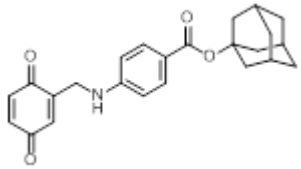	71 ± 4.4
A857	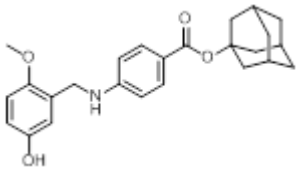	1090 ± 189
E857	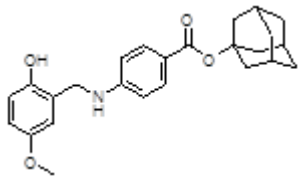	8311 ± 1458
MHQ	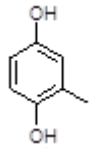	434 ± 39.5
BQ		626 ± 65.7
NSC681152	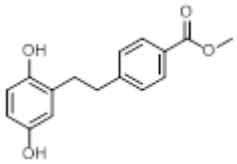	75.6 ± 6.8

BQ, 1,4-benzoquinone; MHQ, methylhydroquinone.

Table A.1: Structure activity relationship of Skp2-Cks1 inhibitors. IC_{50} values were determined from AlphaScreen assays. All experiments were performed in triplicates.

using the AlphaScreen assay developed for the Skp1-Cks1 interaction, in addition to the counterscreening assay.

NSC681152, NSC689857, and its quinone derivative (Q857) were found to disrupt the Skp2-Cks1 interaction at low μM concentrations (Table A.1). Modifications of either hydroxyl group by methylation abrogated the inhibitory activity. BQ and MHQ had little if any effect on disrupting the Skp2-Cks1 interaction. These findings suggest that the specific structures of NSC681152 and NSC689857, rather than quinone functionality, are necessary for disrupting the Skp2-Cks1 interaction. The dihydrophenol ring configuration and the linker are likely to be critical elements.

Both NSC689857 and NSC681152 are hydroquinones. Therefore, we tested if hydroquinones and quinones had the ability to indiscriminately interfere with the AlphaScreen assay. When the counterscreening assay was performed using the same concentration (10 μM) for each compound, we did not observe a dramatic reduction in signal (Figure A.2).

A.4 Discussion

NSC689857 and NSC681152 are known antitumor agents. The two compounds were originally generated for the structure-activity relationship studies of AG957 - an inhibitor of the epidermal growth factor receptor and tyrosine kinases. The exact mechanism of inhibition by this class of molecules is still remains a mystery. The results in this study suggest that they may also play a role in disrupting the interaction between Skp2-Cks1 and subsequent degradation of p27. The dual action nature of these inhibitors may play a synergistic role in their antitumor activity. Future *in vivo* studies should be performed to further elucidate their mechanism of action.

In summary, a high-throughput AlphaScreen assay was used to discover inhibitors of p27 proteolysis. The strength of the assay lies in its robustness, reproducibility, cost-effectiveness, and its high dynamic range. In the future, more potent inhibitors will be screened for using larger libraries. We are also interested in testing NSC689857 and NSC681152 in animal models.

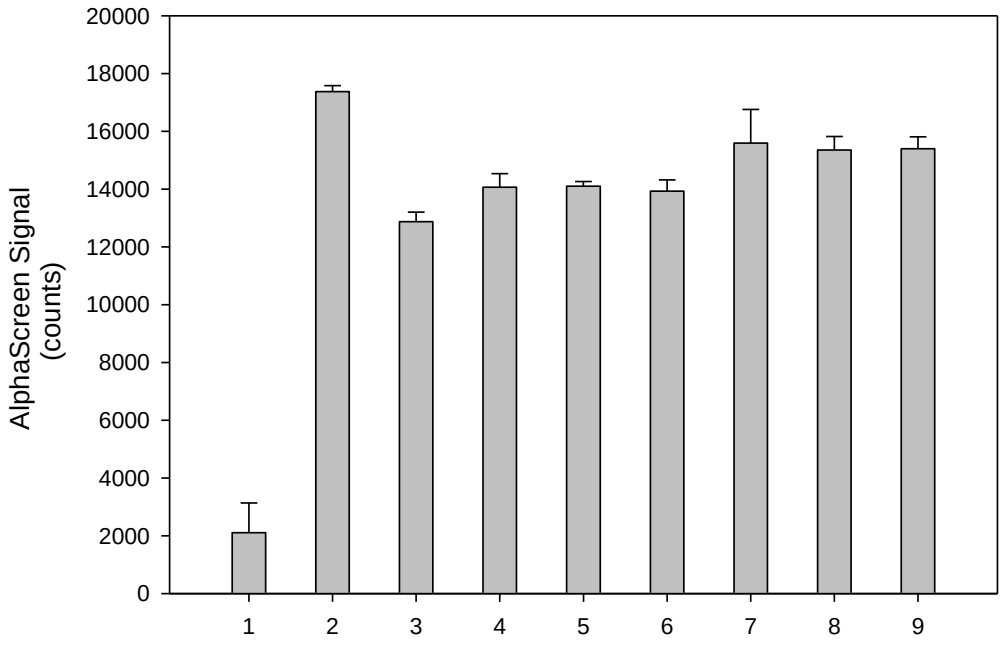

1: A/D beads
2: Biotinylated-GST + A/D beads
3: 857 + Biotinylated-GST + A/D beads
4: Q857 + Biotinylated-GST + A/D beads
5: A857 + Biotinylated-GST + A/D beads
6: E857 + Biotinylated-GST + A/D beads
7: MHQ + Biotinylated-GST + A/D beads
8: BQ + Biotinylated-GST + A/D beads
9: NSC681152 + Biotinylated-GST + A/D beads

Figure A.2: Counterscreen of hits identified by the primary screen. 0.5 nM of biotinlyated GST and a mixture of donor/acceptor beads (20 μg/mL final concentration) were added into each well in a reaction volume of 25 μL with 10 μM of each compound. The effect of NSC689857 and its analogs on a biotinlyated GST control that artificially brings donor and acceptor beads together. Data are presented in mean +/- SD form. Each experiment was performed in triplicate.

A.5 References

Chen J., Willingham T., Shuford M., Nisen P.D. (1996) Tumor suppression and inhibition of aneuploid cell accumulation in human brain tumor cells by ectopic overexpression of the cyclin-dependent kinase inhibitor $p27^{KIP1}$. J. Clin. Invest. ***97***, 1983-1988.

Chu I.M., Hengst L., Slingerland J.M. (2008) The Cdk inhibitor p27 in human cancer: prognostic potential and relevance to anticancer therapy. Nat. Rev. Cancer. ***8***, 253-267.

Craig C., Wersto R., Kim M., Ohri E., Li Z., Katayose D., Lee S.J., Trepel J., Cowan K., Seth P. (1997) A recombinant adenovirus expressing $p27^{Kip1}$ induces cell cycle arrest and loss of cyclin-Cdk activity in human breast cancer cells. Oncogene 1997 ***14***, 2283-2289.

Hao B., Zheng N., Schulman B.A., Wu G., Miller J.J., Pagano M., Pavletich N.P. (2005) Structural basis of the Cks1-dependent recognition of p27(Kip1) by the SCF(Skp2) ubiquitin ligase. Mol. Cell. ***20***, 9-19.

Hiramatsu Y., Kitagawa K., Suzuki T., Uchida C., Hattori T., Kikuchi H., Oda T., Hatakeyama S., Nakayama K.I., Yamamoto T., Konno H., Kitagawa M. (2006) Degradation of Tob1 mediated by SCF^{Skp2}-dependent ubiquitination. Cancer Res. ***66***, 8477-8483.

Montagnoli A., Fiore F., Eytan E., Carrano A.C., Draetta G.F., Hershko A., Pagano M. (1999) Ubiquitination of p27 is regulated by Cdk-dependent phosphorylation and trimeric complex formation. Genes Dev. ***13***, 1181–1189.

Nakayama K.I., Nakayama K. (2006) Ubiquitin ligases: cell-cycle control and cancer. Nat. Rev. Cancer ***6***, 369-381.

Pagano M., Benmaamar R. (2003) When protein destruction runs amok, malignancy is on the loose. Cancer Cell. ***4***, 251-256.

Sitry D., Seeliger M.A., Ko T.K., Ganoth D., Breward S.E., Itzhaki L.S., Pagano M., Hershko A. (2002) Three different binding sites of Cks1 are required for p27-ubiquitin ligation. J. Biol. Chem. ***277***, 42233-42240.

Slingerland J., Pagano M. (2000) Regulation of the cdk inhibitor p27 and its deregulation in cancer. J. Cell Physiol. ***183***, 10-17.

Ungermannova D., Gao Y., Liu X. (2005) Ubiquitination of p27Kip1 requires physical interaction with cyclin E and probable phosphate recognition by SKP2. J. Biol. Chem. ***280***, 30301-30309.

Wang W., Ungermannova D., Chen L., Liu X. (2004) Molecular and biochemical characterization of the Skp2-Cks1 binding interface. J. Biol. Chem. ***279***, 51362-51369.